A comparative study on the fabrication and assessment of anticorrosive marine coatings

By

Sehrish Kanwal

Department of Chemistry

Quaid-i-Azam University

Islamabad 45320 Pakistan August, 2017

A comparative study on the fabrication and assessment of anticorrosive marine coatings

A dissertation submitted to the Department of Chemistry, Quaid-i-Azam University, Islamabad, in partial fulfillment of the requirements for the degree

of

Master of Philosophy

In

Analytical/Inorganic Chemistry

By

Sehrish Kanwal

Department of Chemistry

Quaid-i-Azam University

Islamabad 45320, Pakistan (August, 2017)


بسم الله الرحمن الرحيم

DEDICATED

TO

My beloved parents

ACKNOWLEDGEMENTS

First of all thanks to **ALLAH ALMIGHTY** for giving me the strength to carry out this project. I express my gratitude and respect to the ***Holy Prophet Hazrat Mohammad (S.A.W)***, the symbol of guidance for the whole of humanity.

I would like to take this opprotunity to thank my supervisor **Prof. Dr.** ***Zareen Akhter***, for her excellent supervision, substantive guidance and enthusiastic encouragement throughout this M.phil project. Many thanks to **Dr.** ***Naveed Zafar Ali***, senior scientific officer, National Centre for Physics (NCP), Islamabad for his help and advice on instrumentation and data interpretation actually he was the driving force who directed me into this fascinating field with his continuous encouragement, support and motivation.

I also feel the need to extend thanks to **Prof. Dr.** ***Muhammad Siddiq,*** Chairman, Department of Chemistry, Quaid-i-Azam University (QAU) for providing all research facilities. I am also obliged to **Prof.Dr.** ***Amin Badshah,*** Dean of Inorganic/Analytical Section, Department of Chemistry, QAU for providing the laboratory facilities. Many thanks to the technical staff of Chemistry Department, QAU and NCP for their assistance.

Thanks to my friends, all lab fellows, seniors, ***Adeel Bhai, Iram, Uzma, Shandana, Ambreen, Alia*** and juniors ***Samina and Maida*** for their helping attitude and constant nagging and a very special thanks to my friends ***Shaista, Madiha and Humera*** for the memorable time we spent together.

Last but not the least, I would like to thank my family especially parents, for their love and wholehearted support, without their support, I would not be able to go this far.

Sehrish Kanwal

FOREWORD

The work described in this dissertation concerns the fabrication and assessment of corrosion inhibitors and three broad categories of anticorrosive marine coatings. Firstly, nine eco-friendly corrosion inhibitors were synthesized via microwave assisted irradiation.

Secondly, three types of diverse anticorrosive coatings; namely sulphonate based conducting polymer coatings, adduct modified clay based composite coatings and self-healing smart coatings were synthesized using various polymerization techniques and coating methodologies. The aim of this work was to study anticorrosion behavior of these exotic materials against artificial marine environment.

The entire work is summarized into three chapters. A brief introduction of marine corrosion, along with corrosion inhibitors and coatings, their properties, methods of synthesis and applications in seawater is presented in *Chapter 1*. Experimental details and synthetic methodologies are summed up in *Chapter 2*. Finally, *Chapter 3* comprises of results and discussions with focus on structure elucidation by various analytical techniques such as FTIR for functional group identification, XRD for phase composition and identification. SEM-EDX is used for particle size characterization and morphology. Thermal stability is analysed by using TGA and DSC techniques. Finally, the electrochemical studies (EIS, tafel) were performed to evaluate the anticorrosion properties of all the synthesized material and their coatings. The supplementary data is summarized in the appendix.

ABSTRACT

Carbohydrate graft copolymers were prepared by using microwave assissted irradiation in company with three different types of coatings; sulphonate doped conducting polymer coatings, adduct modified clay based composite coatings and smart functional poly-thiourea formaldehyde based self-healing coatings by using various polymerization methods, exploiting their eco-friendly nature. The synthesized material was characterized by different analytical techniques such as fourier transformed infrared spectroscopy (FT-IR) for functional group identification, X-ray powder diffraction (XRD) was used for phase composition and identification and the thermal properties of afore synthesized material were explored using thermogravimetric analysis (TGA) and differential scanning calorimetry (DSC). The synthesized graft copolymers were also run for electrochemical analysis (EIS and Tafel) in artificial seawater in order to check their corrosion inhibition properties. Coatings were also analyzed electrochemically using electrochemical impedance spectroscopy (EIS) along with tafel measurements. SEM-EDX was employed for particle characterization and surface morphology of coatings after electrochemical corrosion testing. The results showed that the synthesized corrosion inhibitors and coatings can be successfully employed against marine corrosion.

LIST OF ABBREVIATIONS

ASTM	American Society for Testing and Materials
APS	ammonium per sulphate
b.p	Boiling point
˚C	Degree celsius
CP	Conducting polymers
CAS	Cerium ammonium sulphate
CSA	Camphor sulphonic acid
CTAB	Cetyltriethylammoniumchloride
DSC	Differential scanning calorimetry
DCPD	Dicyclopentadiene
DETA	Diethylenetriamine
EPA	Environmental Protection Agency
%E	Percentage efficiency
%G	Percentage grafting
G	Gram
FT-IR	Fourier Transform Infrared
HNO_3	Nitric acid
HCl	Hydrochloric acid
HMDI	Hexamethylenediisocyanate
M	Molar
MMt	Clay montmorillonite
MMA	Methylmethacrylate
KPS	Potassium per sulphate
mins.	Minutes
MIC	Microbial induced corrosion
MDI	4,4-diphenylmethane diisocyanate
mL	Mililitre
OCP	Open circuit potential
p-TSA	Para toluene sulphonic acid
PRS	Panreacquimica
POTS	1H,1H`,2H,2H` perfluorooctyltriethoxysilane

PUF	Polyurea formaldehyde
RT	Room temperature
SSA	5-sulfosalicylic acid
SFA	Sulfamic acid
Tg	Glass transition temperature
TGA	Thermogravimetric analysis
Secs	Seconds
UV	Ultra violet
XRD	X-ray Diffraction

LIST OF FIGURES

LIST OF TABLES

LIST OF CODES

Gum Arabic	GA
Guar Gum	GG
Starch	ST
Cellulose	CL
Chitosan	CS
Polyacrylamide	PAM
Polyacrylic acid	PAA
Polyethylene glycol	PEG
Polymethylmethacrylate	PMMA
Polyacrylamide grafted gum arabic	PAM-g-GA
Polyacrylamide grafted guar gum	PAM-g-GG
Polyacrylamide grafted starch	PAM-g-ST
Polyacrylic acid grafted guar gum	PAA-g-GG
Polyacrylic acid grafted chitosan	PAA-g-CS
Polymethylmethacrylate grafted gum arabic	PMMA-g-GA
Polymethylmethacrylate grafted cellulose	PMMA-g-CL
Polyethylene glycol grafted chitosan	PEG-g-CS
Poly(acrylamide-co-acrylic acid) grafted guar gum	PAM-co-PAA-g-GG
Polyaniline	PANi
Polypyrrole	PPy
Polythiophene	PTH
Polyaniline doped para toluenesulphonic acid	PANi-TSA
Polyaniline doped camphorsulphonic acid	PANi-CSA
Polyaniline doped sulphamic acid	PANi-SFA

Polyaniline doped 5-sulfosalicylic acid	PANi-SSA
Polypyrrole doped para toluenesulphonic acid	PPy-TSA
Polypyrrole doped camphorsulphonic acid	PPy-CSA
Polypyrrole doped sulphamic acid	PPy-SFA
Polypyrrole doped 5-sulfosalicylic acid	PPy-SSA
Oleic acid	OA
Montmorillonite	Mt
Bentonite	Bt
Amberlite	Am
Adduct modified montmorillonite	OC-AMt
Adduct modified bentonite	OC-ABt
Adduct modified amberlite	OC-AAm
Adduct modified montmorillonite based PANi composite	Mt-PANi
Adduct modified bentonite based PANi composite	Bt-PANi
Adduct modified amberlite based PANi composite	Am-PANi
Adduct modified montmorillonite based PTH composite	Mt-PTH
Adduct modified bentonite based PTH composite	Bt-PTH
Adduct modified amberlite based PTH composite	Am-PTH
Polythiourea formaldehyde	PTF

The significant part of gross national product 3-4% has been estimated to be the cost of corrosion and it`s prevention in the Western world although exact number is still debatable. It can lead to dramatic consequences for the surroundings it affects, buildings, bridges, aircrafts and marine structures.

1.1 Corrosion

A physicochemical interface between metal and it's surrounding environment altering the properties of the metal.

1.2 Conditions of corrosion

1. An electrochemical reaction must occur at the metal-environment interface.
2. Potential gradient of the two adjoining areas.
3. Anode and cathode must have an electrical connection.
4. Exposure of an area to a common electrolyte (marine water).

1.3 Classification of environment

Metals are exposed to three different types of environments namely atmospheric, splash zone and immersion.

1.3.1 Atmospheric exposure

In atmospheric environments metals may stumble upon alternating conditions with reference to moisture, heat, UV radiation, salt and gas concentrations. The degree of corrosion may vary depending on point of climatic conditions, pollution and distance from the ocean for example rural environments are less corrosive compared with industrial and marine atmospheres. High content of chloride ions in seawater are aggressive towards metals causing pitting corrosion.

1.3.2 Splash zone

Splash zone constitute extremely aggressive environment due to continuous splashing of electrolytes from the sea by oxygen rich atmosphere near offshore plants and wind turbines. Decrepitude of anticorrosive materials is further accelerated by exposure to mechanical stress, ultraviolet radiations.

1.3.3 Immersion

Temperature, salinity, dissolved gases and pH contribute to the aggressiveness of environment leading to corrosion failures of structures buried in soil or immersed in water. It can be further divided on the basis of type of soil and water.[1] Sea water has elevated content of dissolved salts compared with freshwater counterparts. Bio-

fouling in marine environment also plays a key role. There are various types of corrosion here our focus would be on aqueous corrosion causing destruction of many structures, ships and other equipment used in sea water service.

1.4 Characteristics of sea water

Few characteristics of marine water are discussed below:

1.4.1 Seawater composition

Marine water is a complex solution of inorganic, organic, and biological components, combination of various salts including chlorides, sulfates and carbonates. The interaction of saline water often causes corrosion leading to the degradation of material affecting their properties.[2]

1.4.2 Specific conductance of seawater

Specific Conductance of seawater is it's ability to conduct electricity. This property implies to corrosion rates and cathodic protection[3]. It is a function of temperature and chlorinity whereas resistance reciprocates conductance.

1.4.3 Dissolved gases

All gases present in the atmosphere are also found in seawater but due to their limited solubility in water they are at relatively lower partial pressure. Nitrogen, oxygen and carbon dioxide are having significant role in corrosion together with ammonia, hydrogen sulfide, and hydrogen are also found to implicate the performance of materials.

1.4.4 Seawater pH

Seawater pH typically ranges from 7.8 to 8.4. The presence of cations; Ca, Mg, Na, K and carbonate equilibrium maintains this value which however fluctuates with fluctuations in temperature and pressure along with addition and removal of CO_2. It alters the calcareous deposits at metal cathode hence, affecting the rates of corrosion.

1.4.5 Seawater temperature

The surface water temperature is from -1.8 ˚C at poles to 30 ˚C at the equator.More constant temperature of about 4 ˚C was observed deep in the ocean, though thermal vents are active in the sea bed. Even higher temperatures will be found at desalination plants and heat exchangers[2]. Conductivity of seawater is enhanced when temperature is increased leading to decrease in the concentration of

oxygen affecting corrosion rates. A decline in temperature makes materials brittle leading to failures of steel structures whereas high temperature reduces the mechanical properties of thermoplastics.

1.4.6 Organic matter and biology

Abundance of marine organisms and organic matter in coastal areas have a huge impact on materials. Biological control is important in material selection due to microbial induced corrosion (MIC), biodegradation and bio-fouling.

1.5 Marine corrosion

Sea water corrosion, also called aqueous corrosion or marine corrosion, is an electrochemical process, which occurs due to the difference in potential at specific level of seawater (pH) at metal environment interface. Metallic components have been extensively deployed in water industry.It is the deterioration of material as a result of chemical interaction with environment. It includes degradation of plastics, wood, concrete along with metal which in most cases is Iron (as steel).[1]

1.5.1 Mechanism of marine corrosion

Corrosion may cause a noteworthy mutilation of the functionality of material. In a well knownupshot of corrosion ferrous oxide (rust) is formed when iron steel undergoes decrepitude, while many other metals corrode in a different way. Galvanic series of metals dictate the thermal stability and thermodynamic vulnerability of metals against corrosive environment[1] **Table 1.**

On metal surface some areas are cathodic while others are anodic respectively. Reduction of oxygen at catalytically active metal cathode occurs resulting in hydroxyl ion formation along with peroxides, superoxides, and radicals (1). Ferrous ions and electrons are formed at anodic end of the metal (2).

$$2H_2O_{(l)} + O_{2(g)} + 4e^- \rightarrow 4OH^-_{(aq)} \quad (1)$$

$$Fe_{(s)} \rightarrow Fe^{+2}_{(aq)} + 2e^- \quad (2)$$

Magnetite forms as a result of oxidation of Iron hydroxide into respective oxides and reverts back to $FeO.Fe_2O_3$.In the presence of oxygen it oxidizes to reddish brown hematite ($Fe_2O_3.2H_2O$) commonly called rust[4]. Therefore, largely the reaction is

$$6Fe_{(s)} + 4.5O_{2\,(aq)} + 3H_2O_{(l)} \rightarrow 3Fe_2O_3.H_2O_{(s)} \quad (3)$$

Table 1 Galvanic series in seawater (Passive refers to the natural layer of oxide formed on the metal surface whereas it is considered to be active when directly exposed to corrosive environment).

Anodic (Active)
Magnesium
Zinc
Aluminum
Mild Steel
Cast Iron
Stainless Steel (Active)
Copper
Stainless Steel (Passive)
Graphite
Gold
Platinum
Cathodic (Noble)

1.6 Factors affecting marine corrosion

There are many parameters that control the rate of corrosion some of them are mentioned below

1. Reactivity of metal
2. Presence of electrolytes in water
3. Presence of dissolved gases mainly carbon dioxide
4. Temperature, pH and UV light
5. Impurities mainly biological that accelerate the rate of corrosion

1.7 Corrosion control

1.7.1 Typical methods to avert corrosion

Corrosion rate can be reduced by taking following measures:

1. Barrier protection
2. Cathodic protection
3. Corrosion Inhibitors
4. Protective Coatings

Metal substrate is separated from the corrosive environment in **barrier protection** forming a thin layer that protects the metal alloys. In **cathodic protection**[5], corrosive attack is averted by making the structure to be sheltered by the cathode of the corrosion cell by either using sacrificial anode to protect expensive metal, an inert electrode or impressing a current using external source of power supply. Chemical compounds can also be injected that interfere with the corrosion process are called **corrosion inhibitors**[6], they are taken in minute quantities, reducing the corrosion rate of metal exposed to aggressive environment. They work either by oxygen scavenging, pH buffering or by producing barrier films on adsorption. Most prominent method used to combat corrosion is the use of **protective coatings**. Performance of coatings depend on the lifetime of coating, quality of whole system including, substrate (metal, metal alloys), surface pretreatment of metal, type of coating, method of application, curing procedure and external environment. Coatings may be **organic, inorganic** and **hybrid** depending on the type of fillers and matrix material used. With advancements in technology smart coatings with additional properties have also been employed a few of them are **self-healing coatings**, super hydrophobic coatings,scratch resistant coatings, composite coatings, abrasion resistant coatings, self-cleaning coatings, nanopolymer coatings and antifouling coatings etc. Some of the characteristic properties of smart functional coatings include: durability, reproducibility, easy application, cost effectiveness, tailored surface morphology and environmental friendliness.

1.8 Corrosion inhibitors

All living organisms contain polysaccharides from the tissues leaves of plants, in the bacterial cell walls, fungal extracellular fluidsand animal body fluids to the shell of crustaceans. Polysaccharides are plentiful and renewable and are well thought-out as reservoir for the production of high performance equipment. Native seed polysaccharides or those resulting from guar have been investigated for uses infood, cosmetic, textile, paper, and pharmaceutical industries. Amongst the preferred properties sought in carbohyratepolymer derivatives for effectual commercial utilization are flame retardance, adsorption and corrosion inhibition. Natural polysaccharides such as guar gum, xantham gum, alginates and starch are used as flocculants and coagulants, while upon modification (grafting) in their form they can be employed as water super sorbents. Modification of these materials can be carried

out all the way throughgrafting of polymeric chains, derivatization of functional groups and by hydrolytic or oxidative degradation[7].

1.8.1 Eco friendly grafted polysaccharides

Various ***natural polysaccharides*** have been widely graft tailored to obtain large-scale molecular materials superior to the basic polysaccharides, exhibiting better confrontation to abrasion, heat, mechanical strength, superior oil/water repellant behavior and antibacterial activity. Polysaccharides are useful as flocculants, impartially resistant to degradation but are susceptible to biodegradation. ***Synthetic polymers*** although suffer from meagre shear impervious properties can easily be tailored. In order to make them suitable for different applications having highly customizable hybrid properties both natural and synthetic polymers are modified by grafting. Most operative method to upsurge the compatibility between natural and synthetic polymers to acquire hybrid materials is **chemical grafting**[8]. Chemical grafting involves attachment of polymer chains (monomer) to the backbone polymer. Already utilized for commercial applications include various vinyl monomers such as such as acrylonitrile[9], acrylamide[10], methylmethacrylate, N-ter-butylacrylamide[11], and methacrylamide. Water sorbent and flocculating properties of vinyl monomers were improved to an extent by modification and dangling grafted chains of polysaccharides respectively. Themodified grafted productsof acrylamide based homopolymer and copolymers have found applications in petroleum, paper industries, pH sensitive drug delivery, stimuli dependent controlled drug release and in corrosion protection of alloys as biomaterials[12].

1.8.2 Conventional grafting procedures

Grafting of polymers can be done by using three main strategies:

1. Grafting through
2. Grafting on
3. Grafting from

In '*grafting through'* procedure pre-made vinyl functionalized material is copolymerized with diverse monomers. However, the '*grafting from'* technique which is the most extensively studied technique involves the development of grafts directly on the polysaccharide mainstays and radicals can be generated conveniently via chemical initiators. Grafted polymers were essentially synthesized employing free radicals, generated in situ by redox/radical initiators such as ceric ammonium

nitrate/ethylenediaminetetraacetic acid, potassium persulfate/ferrous ammonium sulfate, potassium persulfate (KPS)/ceric ammonium nitrate, /N,N,N,N-tetramethylethylenediamine and ascorbic acid. This method has gained substantial attention in recent years and has verified to be a productive method for the industrial production of tailored polysaccharides. However, radical-initiated functionalization necessitate inert working settings and are monotonous and time consuming along with homopolymer formation affecting yield. Now-a-days free radicals can also be generated through electron beam, rays, UV radiations and microwave irradiation. Meticulous radical polymerization in aqueous discrete media provides a gateway to across the board manufacture of products and frequently used techniques are nitroxide arbitrated polymerization, reversible addition fragmentation chain transfer techniques and atom transfer radical polymerization. By means of the same techniques, we can control the chemical composition, graft length and product topology along with reduction of dead polymer chains. Characterization of grafted polysaccharides poses various problems due to their rubbery texture and insolubility in most solvents. The evidence of grafting is in the gravimetric increase in the weight of the grafted product expressed as percentage grafting. Yield depends on the choice of certain organic solvents followed by careful and prolonged extraction which may lead to cross linking. Belligerent treatment methods such as sonication are also not ideal as they may bring about destruction of covalent bonds lowering the molecular weight of product.

1.8.3 Grafting under microwaves

Carbohydrate polymers are macromolecules having polar functional groups and they may be charged or electrically neutral, hydrophilic as well as hydrophobic. Properties of various synthetic and natural polysaccharides like guar gum, gum arabic, starch, cellulose and alginates have already been modified via grafting technique[13]. All it takes is aqueous reaction conditions, dielectric heating to polarize water for microwave absorption. Polarization and ionic conduction mechanisms are involved with inorganic salts enhancing the ability of water to convert microwave dynamism to heat energy. Extent of grafting depends on charge and functionality with bulky groups posing difficulty in migration and rotation of molecules. Grafting can be done under inert conditions using conventional heating, under atmospheric conditions using microwaves, in the attendance of initiators and crosslinkers (microwave assisted

grafting) providing relatively higher yields, least common but eco-friendly method involves grafting in the absence of any initiator (microwave initiated grafting)[14].

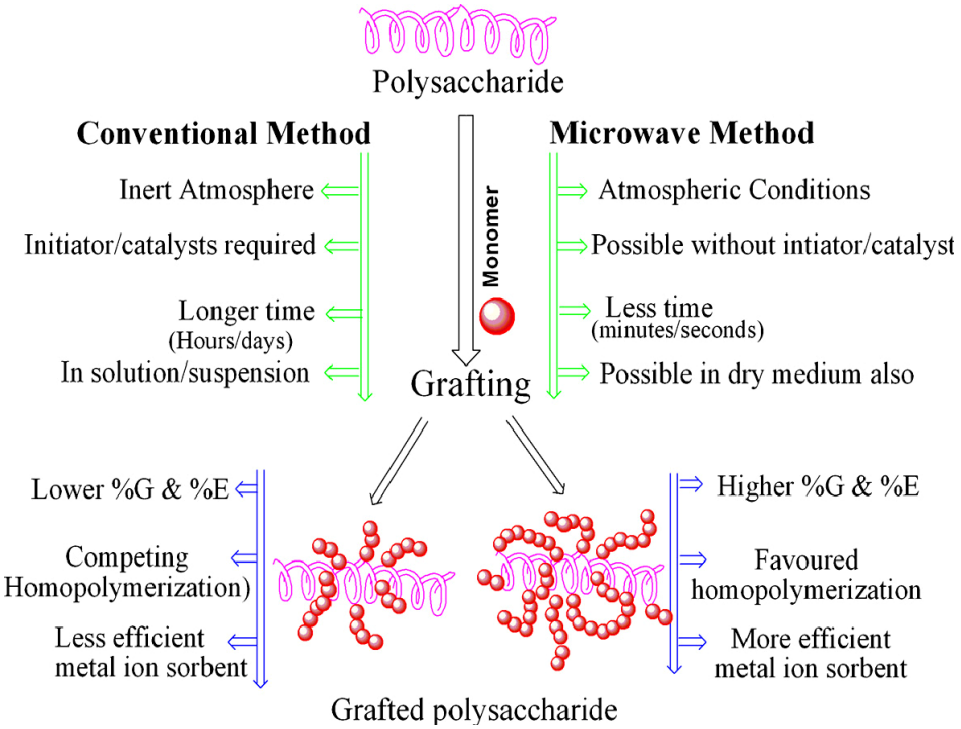

Fig.1.1 Comparison of conventional and microwave grafting methods

1.8.3.1 Microwaves

Generally, microwaves cover electromagnetic radiation in the frequency array of 300 MHz to 300 GHz. These waves incline to align charged or polar particles with electric field which reverses its direction at 2.4×10^9/s at 2.45 GHz microwave frequency. When these particles fail to align rapidly friction plays its part in heating the medium. Heating rate depends on dielectric field which is uttered as the dielectric loss tangent (tan), the ratio of ε (a measure of the efficacy with which electromagnetic field is transformed to heat) and ε.[15]

Dielectric loss tangent is the capacity of a medium to translate the electromagnetic energy to heat energy and its value hinge on the physical state and configuration of the medium besides being reliant on the microwave frequency and temperature. It generally decreases with temperature, yet for other solvents it depends on the frequency of the irradiation and the span of excitation. Penetration of microwaves in an absorbing medium may result in absorbance loss for which the beam intensity declines resulting in potential gradient of microwave energy also affecting the reaction frequency. Such reactions have been endeavored equally in solution as well as in parched medium[7]. Heterogeneous reactions proceed at quicker

rate compared to the traditional heating environments. Rate enhancement is credited to microwave effects in organic reactions. Kappe and coworkers[7] reported a figure of organic reactions when completed in pyrex glass or silicon carbide vials under alike conditions producing identical results in terms of purity profile, conversion, and product yields. Pyrex glass involves sincere microwave chemistry although silicon carbide vials comprise only microwave heating as it absorbs all the microwaves. Later, it was observed that SiC are very decent absorbers of microwaves[16]. Modern microwave reactors were planned for chemical synthesis leading to healthier reproducibility of the outcomes and are used in simplifying the synthesis of small organic molecules and polymers. The in-situ method of conversion has become an striking possibility for chemists, since it is possible to control material properties by controlling magnitude of dielectric assets of the reaction medium. Microwave grafting has made possible the convenient operation, reduction in usage of chemicals and reaction time with high consistency.

1.8.4 Polysaccharide grafting using microwaves

Microwave grafting reactions[8] have been endeavored by scientists by using three main methods.

(i) Under completely homogenous conditions with no phase separation in solution with full miscibility of reaction contents

(ii) Partial miscibility of reactants in suspension

(iii) Impregnation of monomer and polysaccharide on solid support

Microwave irradiation can be performed in exposed reaction vessels, with low solvent content leading to accomplishment of reaction.[17] Physiochemical stresses of predictable techniques are reduced. Instantaneous homogeneous heating, high yield of coploymeric product, short reaction time and controlled percentage of grafting and increased product selectivity instead of slow thermal heating and undesirable side reactions. **Fig.1.1** shows the comparison of conventional and microwave grafting methods.

1.8.4.1 Mechanism

Grafting depends on the efficiency of the “dielectric effect” i.e the interaction of molecules depending upon their polarity in a reaction mixture (catalyst, substrates, and solvents) with electromagnetic waves.[18] Low yields due to competing homopolymerization reactions in conventional grafting methods are replaced with

greater product selectivity using modern methods of grafting. The difference in yield is due to difference in heating rates. Water is used as solvent in most of the reactions due to the solubility of polysaccharides in water, it's polar nature, ease of absorption of microwaves, it's high heat capacity hence better performance at higher temperatures. Polysaccharides do not form true solutions and energy distribution and heat transfer during reaction is different at different domains Microwaves eliminates the use of initiator and consumes less time the true mechanism behind microwave grafting is not known but it is assumed that the sedentary free radicals that are formed by the blend of oxygen with the primary radicals are unstable and hence reverse back to the chief radicals for further proliferation of the grafting reaction taken place at higher temperature with shorter reaction time[8]. The measured temperature of reactions performed in domestic microwave oven after completion is 100◦C. In solvent free heterogeneous reactions, volumetric heating plays an important role as there is no likelihood of conductive heat transfer in solid supported grafting reactions as concentrations of reactants are high leading to super heating zones due to varied microwave absorbance. Depending upon reaction conditions two broad classifications of grafting are:

(1) grafting in aqueous solution and
(2) grafting at solid support

1.8.5 Grafting in aqueous solution

In aqueous medium carbohydrate polymer is in solution initiators, catalyst and monomers may be miscible or immiscible in the solutions. Some polysaccharides require heating to form homogeneous solutions while others form heterogeneous suspensions, the later proves to be useful due to it's facile grafting and better yield. Irradiation under aqueous media involves two mechanisms; polarization of water molecules and ionic conduction. The dielectric heating gives better selectivity at regular reaction temperatures compared to conventional means[19]. Reduction in dielectric constant of water due to increase in concentration of ionic product results in increase in solvating power towards organic molecules already reported in grafting of poly(carpolactone)[5] by tin octaoate catalyst. Two methods that have been used are:

(1) microwave assisted grafting and
(2) microwave initiated grafting

1.8.5.1 Microwave assisted grafting

In this practice microwave energy is converted to heat energy by the use of external redox initiators, producing ions.[17] This class involves dielectric heating, production of free radicals and initiators enabling grafting. Localized hot spot regions generate free radicals faster due to localized heating.

1.8.5.2 Microwave initiated grafting

Microwave initiated grafting eliminates the use of an initiator however it is considered that presence of a minute amount of inhibitor can potentially inhibit grafting. In this class lower %G and %E is observed although less time and less power is employed. Grafting is not a sufficient evidence of "microwave effect" as adventitious initiators might be the cause of grafting. Mechanism involves dielectric heating, dipolar separation of water and other reactants and discontinuous electric field of microwaves instigates heating[20]. No grafting without initiators upon simple heating supports the possibility of in situ radical formation in microwave irradiation due to microwave effect.

1.8.5.3 Grafting on solid support

Microwave fusion can also be done in solvent free conditions, where reactants are provided with microwave translucent support (silica, alumina, or clay) where either spotless or pre-adsorbed reagents were treated or inorganic support doped with catalysts or reagents. Main advantage of this method is the safe, clean, efficient and economical use of microwave ovens[21]. Inadequate mixing of reactants due to inhomogeneity in electric field creating super heating zones is actually responsible for accelerated rates of grafting.

Properties of valuable derivatives can be tailored by precise control over the graft polymers, that are in fact superior to derivatives synthesized conventionally. Dielectric heating provides cleaner and greener approach with greater control, higher reproducibility and mass production[22]. Other perks of microwave method includes, short reaction time, fast heating, solvent free and aqueous working conditions, high temperature chemistry with better selectivity.

1.8.6 Effect of polysaccharide type on grafting

It is not easy to simplify the parameters affecting the extent of grafting of various carbohydrate polymers[23]. Some of them are: reaction conditions, type of microwave oven used (power of domestic oven used), temperature, type of

polysaccharide used (Branched), ratio of the integral monosaccharide and the monomer type being grafted (%G). Following are some of the commonly employed polysaccharides.

1.8.6.1 Gum arabic

Gum arabic (GA) is a dirty, sticky, water soluble exudate obtained from acacia tree. An intricate arabinogalactan comprising a small quantity of proteinaceous materials, and has been catagorized as arabinogalactan protein complex. It has a highly capricious composition, physical and chemical properties reliant upon the source. It has already been employed as corrosion inhibitor for some metals in aqueous acid as well as alkaline media. From the literature, it is concluded that gum arabic has better inhibition efficiency for aluminum than mild steel however, it greatly depends on concentration, temperature, chemisorption mechanism along with substrate used[24].

1.8.6.2 Guar gum

A virtually uncharged, naturally occurring polymer with straight chain of mannose units merged by d-(1→4) linkages having d-galactopyranose units linked to the linear chain by (1 →6) linkages obtained from guar bean seeds is an effective corrosion inhibitor. Galactose to mannose ratio is informed to be 1:2, initially it`s water binding ability was harnessed in many industries like textile, mining, paper, petroleum, explosive and food where it is employed as flocculant. Itdegrades quickly in aqueous media and like gum arabic it's corrosion inhibition efficiency in aqueous acidic and alkaline media is concentration and temperature dependent. For introducing certain desired properties it is modified by grafting with hydrophilic as well as hydrophobic monomers like acrylamide, acrylonitrile, methylmeth acrylate. To get better yield, better %G and better %E, microwave initiated and microwave assisted grafting is used along with conventional techniques. **Fig.1.2** shows the structure of naturally occuring guar gum.

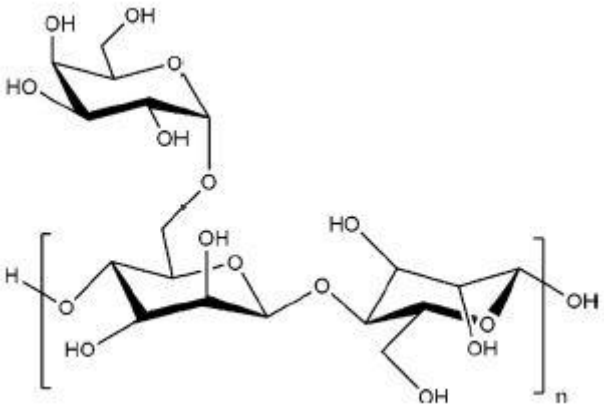

Fig.1.2 Structure of naturally occuring polysaccharide (Guar gum)

1.8.6.3 Starch

It is a cheap, abundant, renewable biopolymer[10], rudimentary form is a mixture of linear amylose (1,4-linked-d-glucopyranosyl units with molecular weight fluctuating from 10,000 to 60,000 g mole^{-1}) (25%) and branched amylopectin (d-glucopyranosyl residues connected together mainly by 1→4 linkages with 1→6 bonds at the branch sites with a high molecular weight, between 105 and 107 g mole^{-1}) (upto 95%) with gylcosidic bonds connecting it's units[25]. Starch and many of it's derivatives can be grafted quiet conveniently with various monomers using initiators like potassium persulfate.

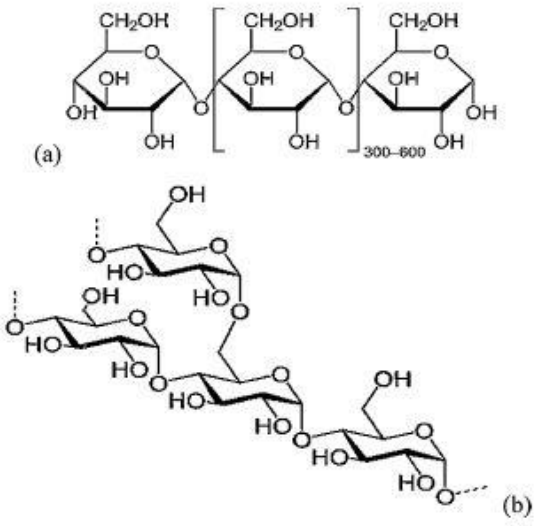

Fig.1.3 Structure of linear and branched starch. a) Structure of amylose
b) Structure of amylopectin

Microwave power effect the swelling ratio and product solubility. Starch is used as a source of energy, important constituent of human diet but has ability to fight against corrosion due to it`s unique structure, bearing electron rich OH groups coordinating with ferrous substrates by filling the empty and partially filled orbitals of iron [11]. **Fig.1.3** shows the structure of linear and branched starch. a) Structure of amylose b) Structure of amylopectin.

1.8.6.4 Cellulose

An organic compound , most abundant, naturally occurring, renewable polymer with the formulation $(C_6H_{10}O_5)_n$, comprising of a linear chain of several hundred to over ten thousand (1 → 4) linked d-glucose units. It has wide applications in biomedicines due to unique properties and insolubility in water. Microwave assisted grafting of immiscible cellulose carried out in dissipative manner under heterogeneous environments using initiator that generates free radicals easily. Unlike conventional heating methods this method requires less time but high temperature (>60◦C) and homoploymer being the only reaction product[18]. **Fig.1.4** Shows the structure of a derivative of cellulose, an insoluble polysaccharide

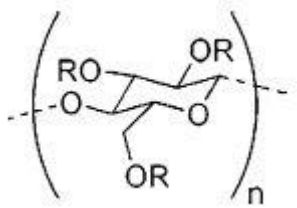

Fig.1.4 Structure of a derivative of cellulose, an insoluble polysaccharide

1.8.6.5 Chitosan

It's actually chitin that is converted to chitosan by deacetylation using a strong aqueous alkali solution. Hydrophillic chitosan is also naturally found in marine crustaceans, shrimps and crabs .It is also insoluble in water, brittle nature and can absorb moisture from the air. **Fig.1.5** shows the structure of chitosan. It has antibacterial activities along with applications in textile, paper and food industries.[5] Vinyl grafting makes it a suitable candidate for paper strengthening, flocculation, water sorbent, drug release by changing it`s morphology[11]. It is used as mixed type

inhibitor under acidic conditions and corrosion protection was enhanced in more highly grafted products via irradiation.

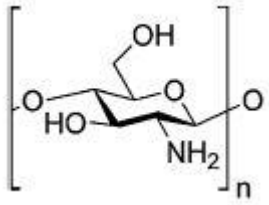

Fig.1.5 Structure of chitosan

1.9 Anticorrosion coatings

Effective methods to protect metals against aggressive environment also includes surface treatment i.e by applying protective coatings as they provide dual functionality by providing physical barrier against corrosive agents as well as electrical fence between environment /metal interface[6]. Common types of coatings include metallic, inorganic, and organic. However, these protective layers are prone to damage when exposed to external environment resulting in appearance of cracks that are sometimes invisible and are involved in acceleration in the rate of corrosion. From the past, few spans both organic and inorganic coverings have been employed for the protection of metals against corrosion. Despite advances in coating technologies, using various alloys long term protection of metal is still a huge problem for corrosion scientists. The complexity of substrate/coating system and numerous other aspects are responsible for the restricted number of high performance anticorrosion coating systems as well as decreasing their service life. Besides composition which includes binders, extenders, solvents and pigments several other parameters also affect the performance of coating such as coating thickness, curing, pretreatment of substrate, adhesion amid the coating layer and the substrate as well as environmental constraints. An effective coating must be intrinsically durable, have good adhesion to the substrate, flexible, tough enough to withstand cracking as well as preserve its appearance when exposed to mechanical abuse, stress and weathering. International and national legislation has vowed to mature the coating industry by undergoing continual change in technology, by plummeting the use of voltaic organic compounds, replacing them with powder coatings or water borne coatings leading to the better formulation of anticorrosive coatings[6]. Therefore, systematicinformation and

understanding of exchanges between different components of coatings is required in marine sector. The mechanisms (physical or chemical) responsible for the failure of coatings may offer a doorway to the best coating design.

1.9.1 Conducting polymer coatings

High strength metals and alloys when exposed to aggressive environments become thermodynamically unstable and undergo degradation. Enormous corrosion losses can be minimized by using organic coatings. Synthetic polymers have minimized the use of precious natural renewable petroleum resources. Nearly all corrosion inhibitors are detrimental to health and environment due to their carcinogenic nature. Similarly Chromium conversion coatings along with zinc and lead primers are injurious therefore made restrictive by Environmental Protection Agency (EPA)[4]. Several replacements have been proposed and one of them is the use of conducting polymers (CP) for the protection of expensive metals particularly steel and Aluminum. In order to enhance the efficacy of conducting polymers small concentration of inorganic pigments can be added as fillers. CP's can be synthesized quite easily by electro-deposition directly on the metal surface and via chemical oxidative polymerization.

CPs have the ability to conduct electric currents even without the addition of inorganic fillers. Some commercially available CPs include polyaniline (PANi), polypyrrole (PPy), polythiophene (PTH), polyindole and polycarbazole with intermediate electrical conductivity between metals and semi-conductors. According to the reported literature their conductivity ranges from 1- 1000 S/cm^2. Metals and metal alloys have found protection against corrosion using CPs since 1980[6]. Corrosion protection through CPs can be achieved by utilizing various methods:

1. Formulation of polymers with paints
2. Electro-deposition on metal surface
3. Direct addition into corrosive media as corrosion inhibitors

They can be easily synthesized using chemical and electrochemical oxidation. Convenient synthesis of conducting polymers can be made possible by making use of an initiator as oxidant to initiate polymerization .In-situ doping can be done by adding the doping agent during polymerization prior to the addition of an initiator. This method is called chemical oxidative polymerization. Effective coatings require the careful control of several factors such as type of substrate used, selection of a specific

CP, their composition along with chemical and physical properties, the type and amount of dopant used together with other active ingredients in the coating. Surface pre-treatment of the substrate is also considered for good adhesion of coatings. In our work we will be focusing on synthesis, protection mechanism and applications of following CPs.

Polyaniline (PANi)

Polypyrrole (PPy)

Polythiophene (PTH)

1.9.1.1 Polyaniline

The first ever commercialized CP having low cost, convenient and reproducible synthesis with high yield, electrical conductivity and has wide potential stability. It`s electrochemistry has revealed the generalized formula of polymer referring to its different oxidation states with terms 'leucoemeraldine', 'emeraldine' and 'pernigraniline' differentiating among them. Oxidation of the leucoemeraldine base and protonation of the emeraldine base may induce conductivity in PANi. Emeraldine base is nonconductive and can be made conductive via doping which refers to the insertion of charge carriers in the polymer chain by making use of chemical and electrochemical methods. Common method employed was the use of protonic acids to create charge carriers presently we have used HCL, p-toluene sulfonic acid, camphor sulfonic acid,sulfamic acid and 5-sulfo salicylic acid as dopants. Addition of dopants help determining the stability, conductivity and compatibility with the polymer matrix.

1.9.1.1.1 Mechanism of corrosion protection by PANi

The mechanism of corrosion protection is still not understood completely. Among the possibilities it is suggested that coating may form metal oxides on the surface shifting potential to passive state called **anodic protection mechanism**. In controlled **inhibitor release mechanism** the anion is released upon reduction by the deposited coating on metal surface in case of doped polymer it may be due to simple elimination of acid dopant. Electric field generated would limit the electron flow from metal to oxidizing species preventing the oxidation of metal. Dense, adherent and low porosity film of CP provides a **barrier effect** by lowering the transport rate of O_2 and H_2O into the polymer, shifting the reduction from Metal-coating interface to the coating-solution interface preventing the chances of cracking and delamination.

1.9.1.2 Polypyrrole

One the promising CP with high thermal stability, wide pH range, non-toxicity, high conductivity (δ >1S cm^{-2}), good mechanical properties and facile synthesis is the soft black powder called polypyrrole (PPy). Like polyaniline it can be synthesized by both chemical and electrochemical methods. One of it's major advantage is the facile synthesis on metal surface in a single step. Apart from corrosion protection other potential applications of polypyrrole include solid electrolytic capacitor, electrochromic windows, displays, biosensors, gas sensors, microactuators, wires, packaging, batteries, functional membranes, electronic devices and composites, etc. Electro-polymerization of polypyrrole on the surface of metal can be done by electrodeposition.[6]

1.9.1.2.1 Mechanism of corrosion protection

In case of PPy dualistic mechanisms have been anticipated: the **physical barrier effect**, and anodic protection. Polymer coating behave as a fence against penetration of destructive ions similar to paints. CPs with strong oxidative property acts as oxidant and shifts the potential of metal to passive state called **anodic protection**.

1.9.1.3 Polythiophene

Polymerization of thiophene gives rise to a stable polymer with striking electrical properties called polythiophene (PTH). It has wide applications related to it`s conductivity and resistance to oxidation in electrochemical sensors, electronic devices, electrochemical capacitors and electrochromic display devices. It can also be synthesized very easily by electropolymerization, metal catalyzed coupling reactions and via chemical oxidative polymerization according to the reported literature. It can be used as additive in paints along with it`s derivatives providing better protection against corrosion.

It is desired to replace hazardous coatings with CPs as corrosion protection layers as they have relatively positive potentials than aluminum and iron hence, providing protection comparable to chromate (VI) systems. Among the several strategies employed for better performance few of them are; copolymerization, use of multi-layer CPs, use of dopants, nanostructured CPs, composites and nanocomposites of CPs.

1.9.1.4 Doping

Doping agent or dopants are the materials added in minute quantities into the polymer matrix to enhance their properties. In conducting polymers although dopants do not aid in oxide layer formation but can decree the nature of thin film formed under intact areas of coating[26].

1.9.1.4.1 Doping of conducting polymers with sulphonic acids

Conducting polymers can be converted from insulating to conducting state for anodic protection of the metal surface. Doping techniques include electrochemical doping, organic doping by charge transmission, photo doping and also through charge inoculation at a metal-conducting polymer interface.[26]

1.9.2 Modified clay composite polymer coatings

A superior class of materials having exceptional physical properties leading to diverse applications such as sacrificial protection of metals are called composites. Protective coatings of conducting polymers reduce the rate of corrosion and semectic clays have the ability to encapsulate CPs in the interlayer spaces extraordinarily improving their electrical conductivity, physical properties like transparency, morphology, structural suitability, fast doping/dedoping mechanism. Better electromagnetic interference shielding of conductive textile composites is observed for PANi and PPy. Other applications of CPs include electrochromic displays, electrostatic materials, sensors, corrosion protection, batteries, printed circuit boards, and so on. The performance of composite coatings depends on electrochemical constraints such as current density and potential windows. Composite coating provides several functional properties for example wear and corrosion resistance etc. CPs are non-toxic[27]. Polyacetylene, polyaniline, polypyrrole and polythiophene have grown extensive theoretical curiosity and real-world applications in various grounds, especially in the fortification of metals counter to corrosion as they form dense, adherent films and maintains basic environment on substrate.

1.9.2.1 Bentonite

Clay containing montmorillonite, a cation exchanger, having stacks of negatively charged alumosilicate sheets and can easily disperse in epoxy resins. Bentonite has the intercalation ability and can be used as filler in polymer composites against corrosion.

1.9.2.2 Montmorillonite

MMT clay has small particle size (<10 μm) and ease of intercalation due to which it is adapted as a strong candidate for nanocomposites. Conducting polymer clay nanocomposite coatings have synergistic properties that cannot be attained individually by CPs, clay minerals reduce oxygen permeability and block products of corrosion. MMT has lamellar structure, high in plane strength and high aspect ratio. Clay minerals and ion exchange resins are widely used as fillers in coatings.

1.9.2.3 Adduct Modification of clays

Small defects in neat CP coatings may allow corrosive species to penetrate in metallic substrate. Nanoscale fillers are sometimes added polymer matrix to generate hybrid coatings. Complete dispersion or exfoliation of clays improve the physical, mechanical, thermal, chemical, flame retardant and solvent resistant properties of polymers. Exfoliation behavior of clays vary upon incorporation of polymers into interlayer spaces of organophillic clays. This dispersion increases the length of diffusion pathway of O_2 and H^+.

Perks of this method include

1. Better anticorrosion behavior even at high loading of modified clays (20 wt%)
2. Increase in barrier properties due to layer by layer self assembly
3. Simple adduct modification instead of using intercalating agent

1.9.2.4 Adduct modified clay based conducting polymer coatings

Inorganic clay based minerals forming nanocomposites with CPs provide a promising system because clays have high aspect ratio and plate like morphology. Such nanocomposites can boost physical properties, fire retardancy, mechanical strength, gas barrier of bulk polymers. Dispersion of nanolayers of clays and ion exchange resins into polymer matrix increase the tortuosity of the diffusion pathway of oxygen and water, can effectively enhance the corrosion protection ability of polymer[27]. Abundant, inexpensive clays with high mechanical strength and high chemical resistance enhance the barrier properties of polymeric coating, many scientists have used various kinds of additives such as extenders and inorganic pigments.

New emerging CPs for corrosion protection include polyindole, polycarbazole and their derivatives. CPs have replaced the hazardous conventional coatings due to

their good effectiveness and eco-friendly nature. In present work suitable dopant ions and modified clay fillers and ion exchange resins have been employed to enhance the corrosion protection efficiency of three widely used CPs namely polyaniline, polypyrrole and polythiophene. If the CPs are electroactive after doping self healing process operates, morphology of CPs influence their anticorrosion properties along with the controlled synthetic paths which is yet to be fully explored.

1.9.3 Self-healing coatings

Mimicking the self-healing ability of living organisms, a new class of smart materials having the ability to spontaneously and autonomously heal has emerged. The goal is to prolong the lifetime of coatings, making them cost effective by incorporation of innate properties of biological organisms to augment their operation efficiency by responding to external stimuli, imitating living systems. In a review, ‘‘Functional and Smart Coatings for Corrosion Protection: A Review of Recent Advances.’’ Montemor[28], has defined the self-healing term in two ways

1. Mending of defects occurring in polymer coating matrix by healing the scratched site.
2. Hindering the corrosion process by making use of chemical compounds called corrosion inhibitors.

1.9.3.1 Properties

1. Automatic healing
2. Ability to heal the damage of materials multiple times and does not require high energy
3. Ability to heal the materials with defects of any size
4. Reduced maintenance cost
5. Better self-healing performance in comparison to traditional materials

These multifunctional materials recover the following properties after the occurrence of damage; mechanical strength, conductivity, corrosion resistance and fracture toughness.

Moreover they are less expensive, can auto recover, can heal defects multiple times, heal cracks of any size, protect metallic components and have prolong service life.White *et al* proposed the first self-healing polymer in 2001.

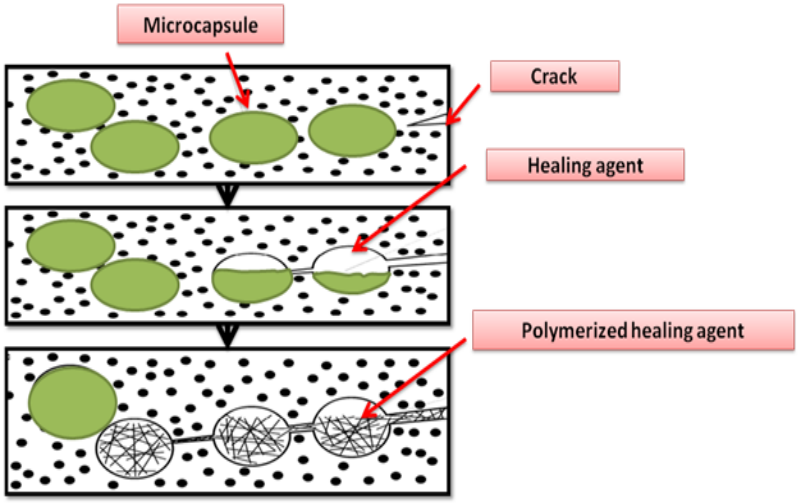

Fig.1.6 Self healing mechanism showing the appearance of crack in coating, the release of healing agent from microcapsules and consequently healing mechanism by catalytic polymerization.

Two categories of self-healing approach are autonomous and non-autonomous. **Autonomous healing** does not require any external intervention (temperature, UV light, pH change etc) while **non-autonomous healing** cannot be performed without these external stimuli. Healing polymers were classified as **thermoplastic** and **thermosetting** polymers by Wu *et al* thermoplastics are reconvertible whereas thermosetting becomes rigid upon reheating[29]. Blaiszik*et al*.[30] classified self-healing materials into **intrinsic** and **extrinsic**, subdivided into ***vascular*** and ***capsules based***. Materials heal cracks by themselves *intrinsically* as they possess pre-embedded healing agents and healing can be done either physically or chemically by bonding through reversible thermal reactions, hydrogen bonding, ionomeric coupling, a dispersed meltable thermoplastic phase and molecular diffusion.

In *extrinsic* self-healing, healing agents may be vascular or are in the form of capsules depending upon the type of storage container in polymer matrix. Without any external intervention healing agents are released by triggering mechanism. In contrast to the vascular network based self-healing coatings where the healants are usually stored in a network of hollow plastic/glass tubes, healing agents are confined in discrete spherical containers in microcapsules based self-healing coatings.

Various strategies have been developed in order to incorporate the self-healing moiety (functionality) into different polymer coatings.The most promising approach, capsule based self healing consist of healing agents, compartmentalized reactive

substances, solvents, corrosion inhibitors inside the containers. These capsules have varying size not exceeding 100 μm healants are enclosed in polymer matrix to protect them from undesireable reactions. Healants can be solid, liquid or gaseous material stored in polymer or ceramic matrix that upon crack is accelerated by capillary action to the failure site inducing polymerization hence, healing the damage. Reaction conditions control the morphology and service life of capsules generally containing oil as healing agent and polymer as shell material. **Fig.1.6** shows the self-healing mechanism showing the appearance of crack in coating, the release of healing agent from microcapsules and consequently healing mechanism by catalytic polymerization.

1.9.3.2 In situ polymerization using microemulsions

To synthesize core shell material the techniques used include core templating technique, microemulsion polymerization, interfacial polymerization, microemulsion polymerization, solvent evaporation/solvent extraction, sol–gel reaction, hollow mesoporous microcapsule infiltrated by healing agent, and porous carriers. Potentially controllable, flexible, scalable, and most effective technique used is **in situ polymerization using microemulsions**[28]**.** Polymerization regenerates the uniformity of coating, by the release of healing agent (reactive material) from core shell system. Properties that make microencapsulation a potential method for developing self-healing coatings are versatility, simplicity, scalability, low cost and various microcapsule sizes and shell thickness can be achieved and is controllable. In this method emulsion of organic polar compounds was produced in the presence of surfactants, reaction is initiated by vigorous stirring or sonication while the non-polar portion act as dispersed phase forming the core of microcapsule. Polar compounds are polymerized on the surface of core forming shell to fortify inner material this core-shell material can further be coated with various layers.

The microencapsulated coatings have already been employed on various metals like cast iron, ductile iron, brass, and copper surfaces. Recent developments in hybrid self helaing coatings are mainly based on micro encapsulation method. Uniform distribution poses various problems in it’s implementation and are addressed by making use of nano sized containers instead of microcapsules. These nano sized containers can be made more robust by controlling shell thickness and effective when corrosion inhibitors are used as core material.

1.9.3.3 Microcapsules

Fabrication of self-healing coatings require careful control of all these constituents including core and shell material as well as polymer matrices. Shell material must be stiff, prevent leakage of healants and must have good adhesion to the metal. On the other hand certain properties of core material must be optimized which includes viscosity, pH, volatility, reactivity, flowability and rapid consolidation. The chemical or physio-chemical encapsulation process involves generation of droplets of core material followed by deposition of shell. One of the two interfacial polymerization types , in situ polymerization is simple, convenient, easy to use, suitable, free flow of healants by capillary forces and has low requirements, was first employed by White *et al* to polyurea formaldehyde (PUF)[30] based autonomic self-healing coatings containing dicyclopentadiene (DCPD) core. In interfacial polycondensation one of the monomer is water soluble and other is oil soluble, that condenses on oil phase of interface. The extent of transfer of water soluble monomer to oil phase is controlled by pH, surfactant, temperature and nature of organic phase hence, healing time depends on reaction parameters.

1.9.3.4 Core material

Chemical reaction occurring at cracked site is responsible for healing therefore, careful selection of core material is important along with the matrix. It can be polymerizable agent or inhibitor. Healing agents are actually fluids that inhibit the propagation of crack by activating the damaged site thus, preventing dissolution of metal. The initiation of healing process is done by initiators in autonomic healing, and can be activated by physical stimuli (e.g. UV light, moisture or elevated temperatures) because they have exterminated chain ends capable of polymerizing multiple times. Process can be made more efficient by careful material transport, polymerization and catalyst dissolution. Kinetics of self-healing is still not well known and is important when quick healing is desirable especially when substrate is in contact with water. Photo activation has gained attraction because of it`s quick response. Two important parameters are time and healing efficiency where the former depends on substrate, healing kinetics and mechanism and the later is controlled by nature of shell material, capsule size, morphology, fluidity, adhesion strength and processing conditions. The diameter of microcapsules can be controlled by varying the agitation rate from 200 rpm to 2000 rpm. Common examples are DCPD, epoxy resin and 1H,1H`,

2H,2H`perfluorooctyltriethoxysilane (POTS), in PUF microcapsules[29]. Catalyst monomer ratio also affects healing process so catalyst free alternatives like liquid isocyanates (react with moisture), linseed oil, tung oil and other fatty acids have also been introduced.

1.9.3.5 Shell material

Porous, hollow or layered polymeric or ceramic structures that are rigid enough for incorporation into coating matrix and brittle to rupture upon cracking to release healants. Ideal diameter is in the range of 50-100 μm ensuring facile release of healing agent. The thickness of shell is also important very thin shell may undergo premature rupture resulting in loss of healing agent, therefore it must be thick enough to survive processing and coating manufacture conditions. Both thermal and solvent stability of capsule depends on the nature and thickness of shell material. For example polyurea-formaldehyde is capable of enduring shear forces during agitation, high processing temperature and reaction conditions. Anionic polymers and copolymers can be employed as surfactants to protect the coagulation of the core material, however higher concentrations may result in formation of smaller capsules.

1.9.3.6 Polymer matrices

They identify, activate and orientate the healing mechanism, adhere intrinsic and extrinsic elements and have the ability to transport healing agents to the damaged site. The size and morphology of penetrating microcapsules affect various properties of the polymer matrix such as stability, flexibility, mechanical strength and adhesion to the substrate. Therefore, to ensure the smooth embedment of microcapsules into the matrix the parameters that must be taken into account are wettability, thickness of capsules, adhesion to substrate without affecting its properties and compatibility of shell material and polymer binder.

The cost of marine corrosion is approximately 60 million dollars, although corrosion scientists have worked for decades to bring advancements in this field reducing corrosion damage. The infrastructure employing various metals from iron to brass is under corrosion attack. Integration of several capabilities in one material such as self-cleaning, hydrophobicity, self-healing in single material is the current goal of researchers and main constraints in transferring this version of technology directly into marine water are legislation and regulation on materials[30].

1.10 Coating methods

Various coating methods have been employed to protect metal surface against corrosion. Dip coating is one of the facile method of applying coatings on metal substrate. It involves following simple steps

1. *Immersion*: Substrate is immersed in coating solution for a certain time at constant speed.
2. *Deposition*: When substrate has remained inside solution for few minutes or seconds a thin film is deposited on the surface of substrate and thickness of film depends on the withdrawing speed.
3. *Drainage*: drainage of excess liquid
4. *Evaporation*: Solvent evaporates from the thin layer giving it a smooth appearance.

1.10.1 Curing and Annealing

Curing and annealing of coatings is also important to improve their mechanical strength and adhesion to the substrate.

1.11 Substrate selection

The metal alloys selected for corrosion studies in present study are aluminum alloys (AA2219-T6) and stainless steel SS-304. Stainless steel SS-304 is a high strength alloy with good corrosion resistance and wide applications. AA2219-T6 is highly stable, high strength alloy with high service temperatures and used in space shuttles along with cryogenic applications. The properties of alloys make them the suitable candidates for applications in the field of corrosion. SS-304 has already been employed in marine industry whereas AA2219-T6 is less extensively explored.

1.12 Plan of work

Fabrication and assessment of anti-corrosive moieties were planned in our present work. In first part of our work the corrosion resistant ability of some carbohydrate polymers were utilized undergoing synthesis of eco-friendly corrosion inhibitors via microwave assisted grafting with various monomers and nine different combinations of microwave grafted copolymers were realized using water as solvent and cerium ammonium sulfate (CAS) as initiator **SECTION A** (Figure 1.7-1.15).Three different types of anti-corrosive coatings organic acid (para-toluene sulphonic acid, camphor sulfonic acid, sulfamic acid and 5-sulfosalicylic acid) doped

conducting polymer (PANi, PPy) coatings **SECTION B** (Figure 1.16-1.23), adduct modified clay (montmorillonite, bentonite and amberlite) based composite coatings **SECTION C** (Figure 1.24-1.29) and poly-thiourea formaldehyde based self-healing coatings **SECTION D** (Figure 1.30) using different polymerization techniques. Structure elucidation were planned to be performed applying different analytical techniques like spectroscopic studies. For exploring their properties with respect to applications thermal analysis, morphological studies and electrochemical studies were planned.

SECTION A

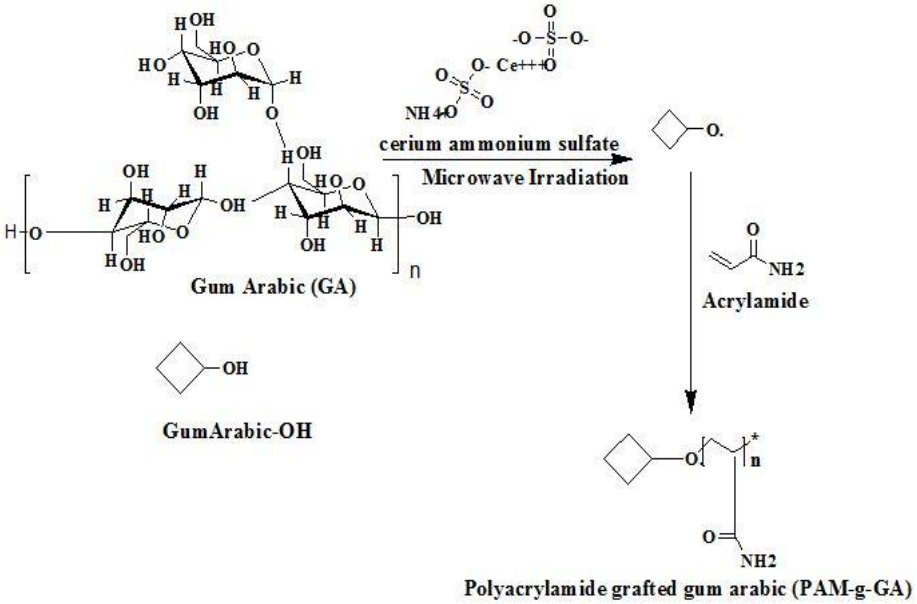

Fig.1.7 Synthesis of polyacrylamide grafted gum arabic (PAM-g-GA)

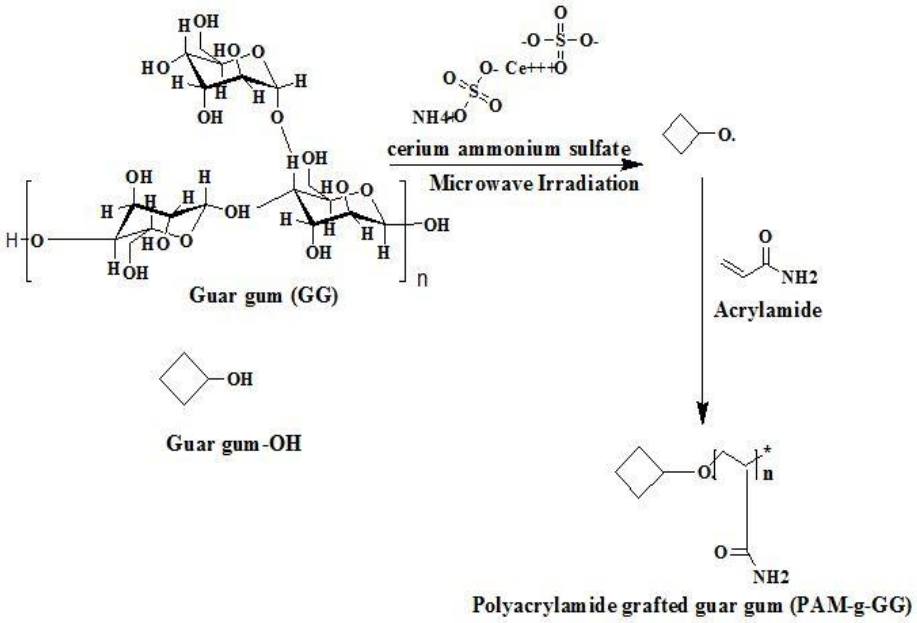

Fig.1.8 Synthesis of polyacrylamide grafted guar gum (PAM-g-GG)

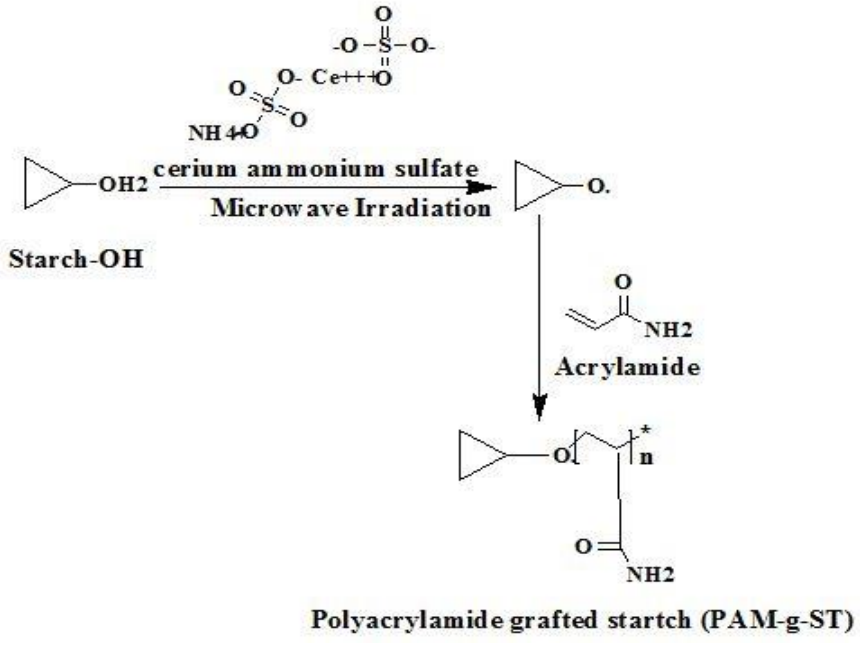

Fig.1.7 Synthesis of polyacrylamide grafted starch (PAM-g-ST)

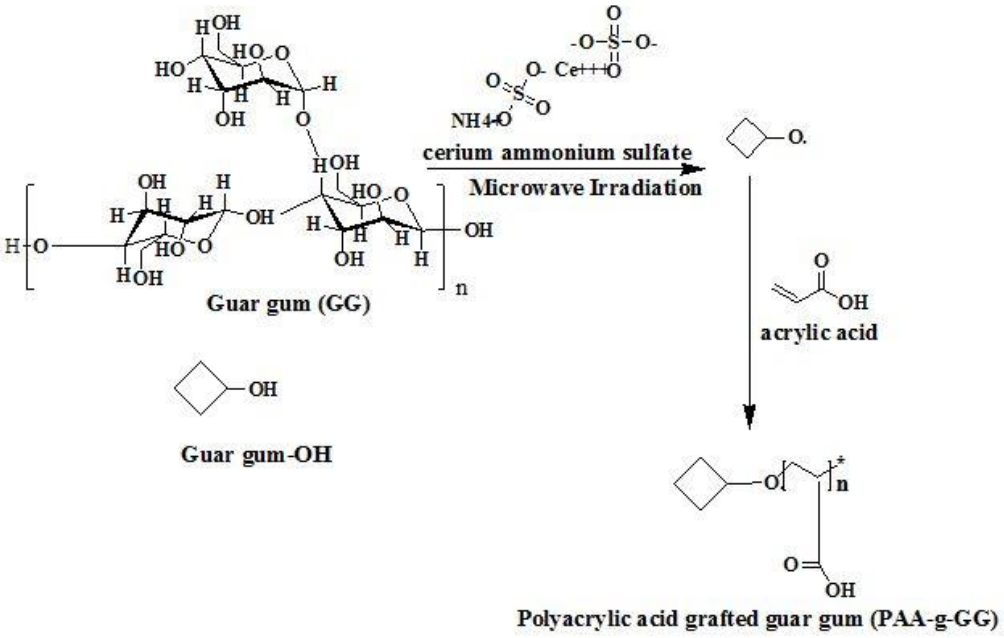

Fig.1.10 Synthesis of polyacrylic acid grafted gum arabic (PAA-g-GA)

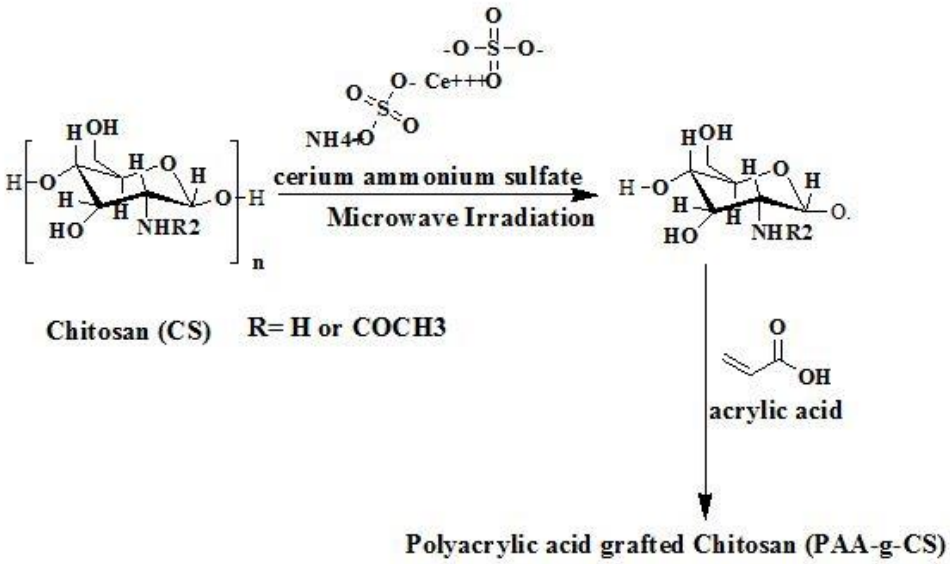

Fig.1.11 Synthesis of polyacrylic acid grafted chitosan (PAA-g-CS)

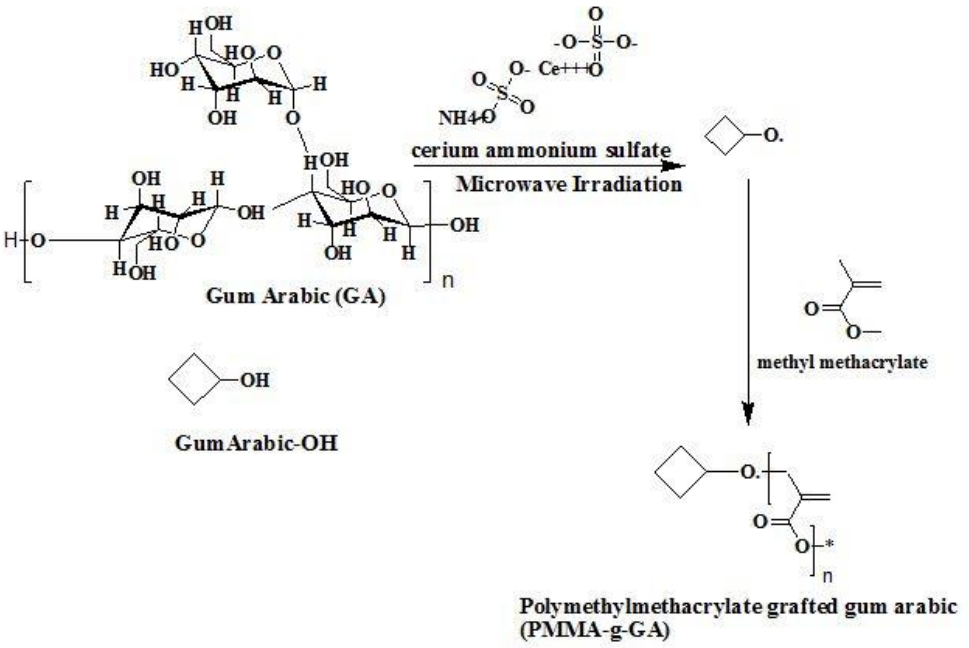

Fig.1.12 Synthesis of polymethylmethacrylate grafted gum arabic (PMMA-g-GA)

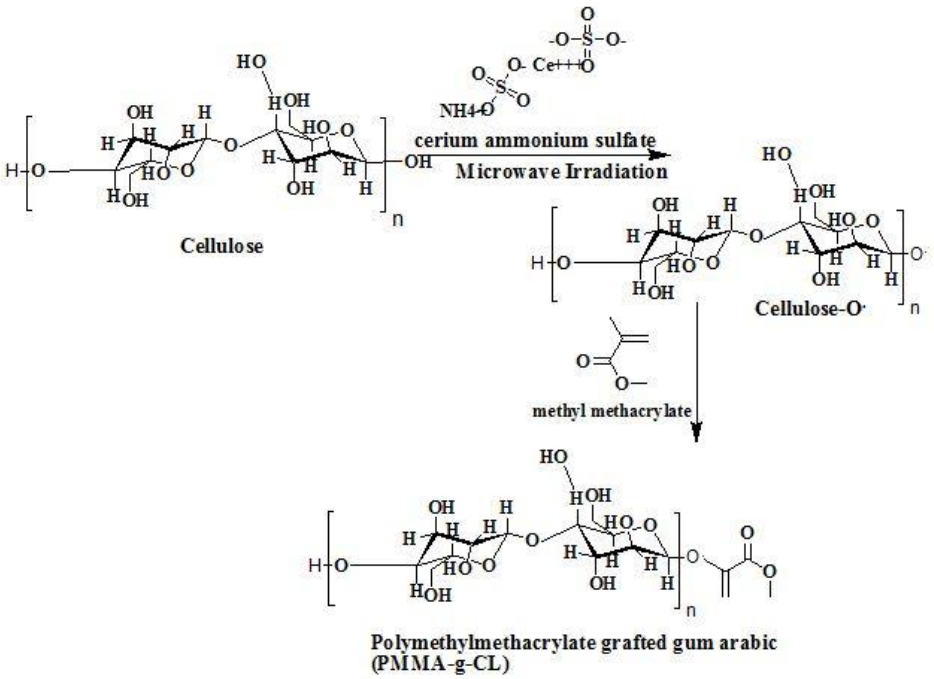

Fig.1.13 Synthesis of polymethylmethacrylate grafted cellulose (PMMA-g-CL)

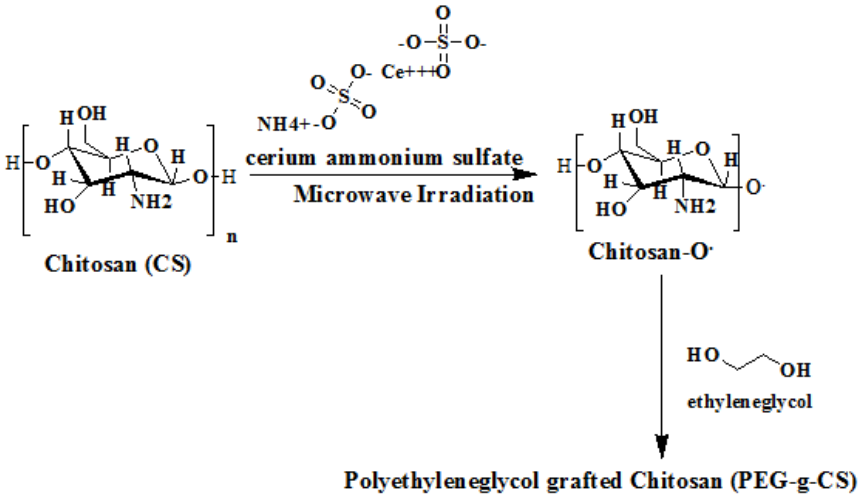

Fig.1.14 Synthesis of polyethylene glycol grafted chitosan (PEG-g-CS)

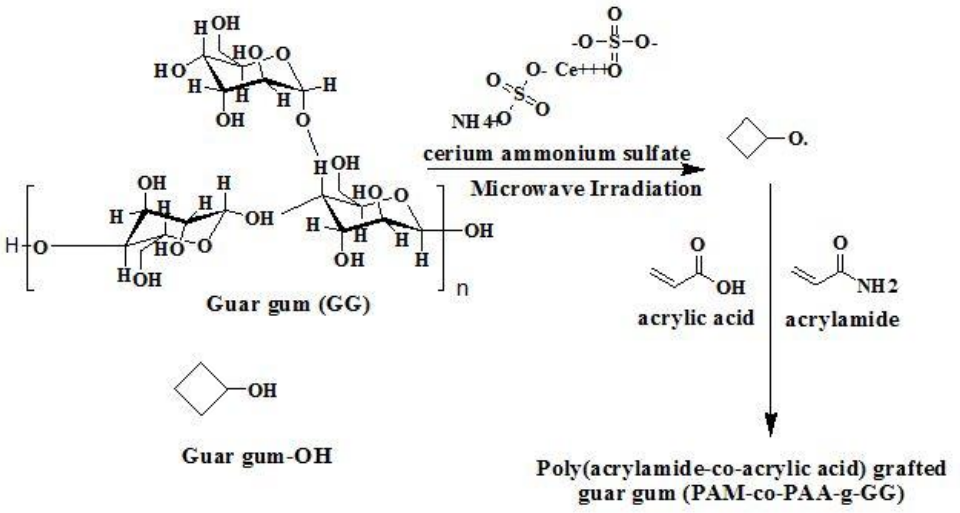

Fig.1.15 Synthesis of polyacrylamide-co-acrylic acid grafted gum arabic (PAM-g-GG)

SECTION B

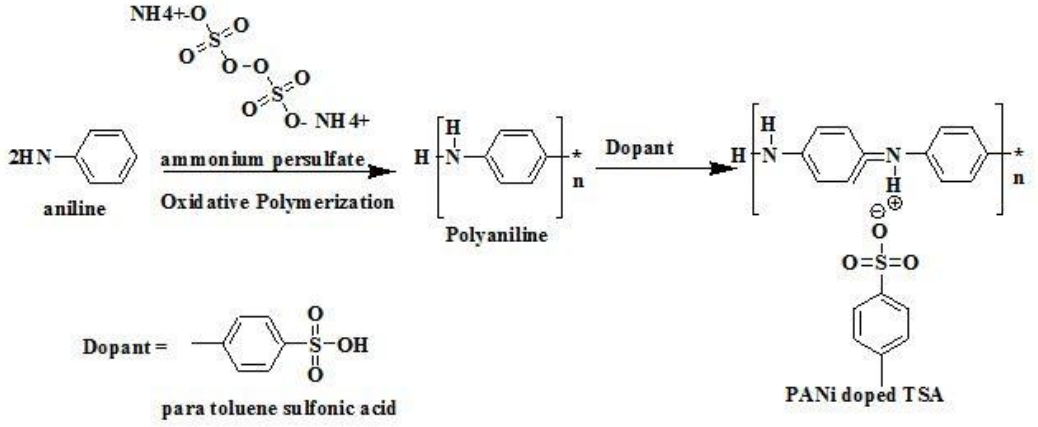

Fig.1.16 Synthesis of polyaniline doped para toluene sulphonic acid

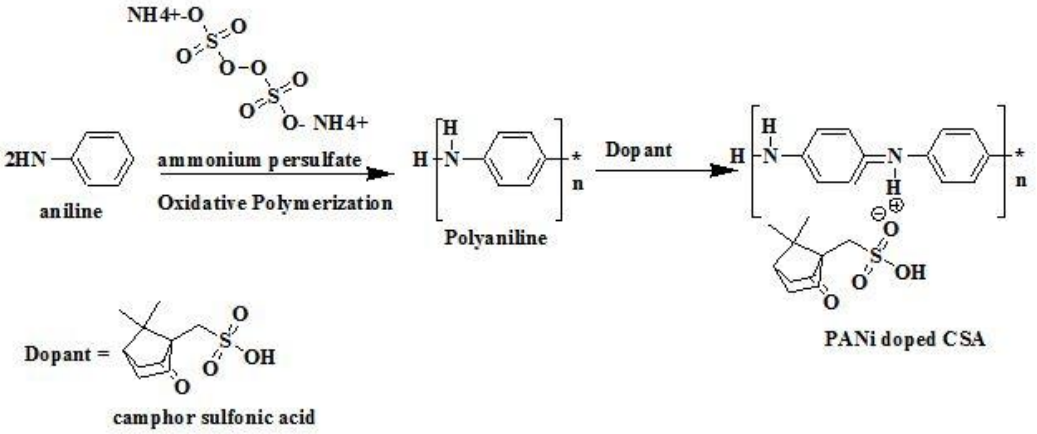

Fig.1.17 Synthesis of polyaniline doped camphor sulphonic acid

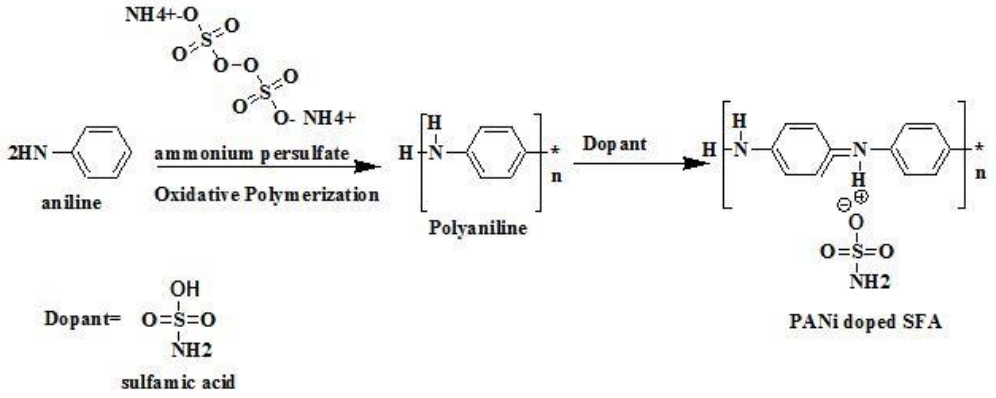

Fig.1.18 Synthesis of polyaniline doped sulfamic acid

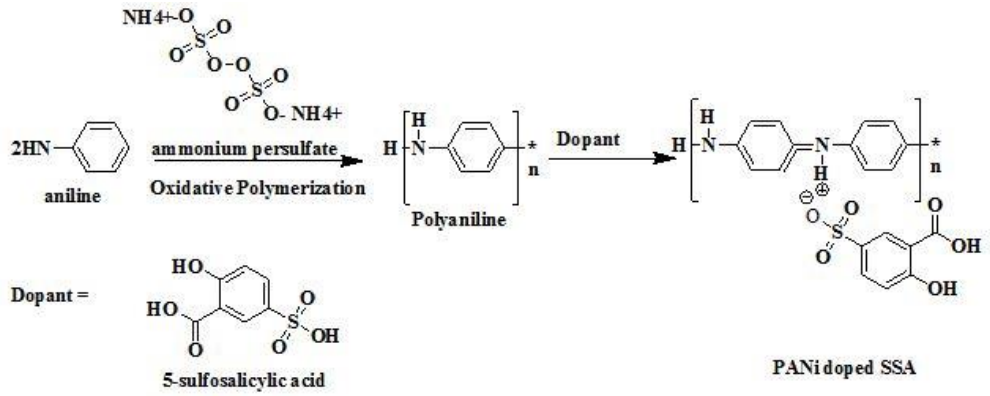

Fig.1.19 Synthesis of polyaniline doped 5-sulfosalicylic acid

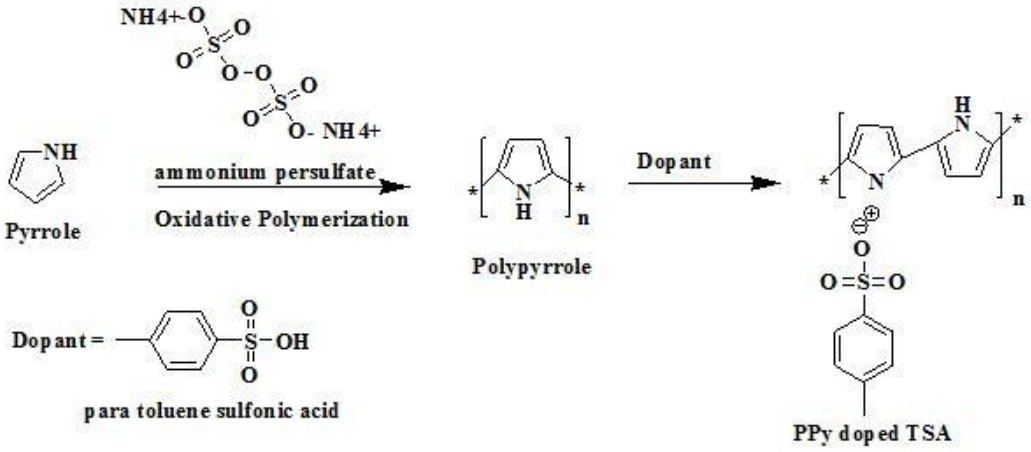

Fig.1.20 Synthesis of polypyrrole doped para toluene sulphonic acid

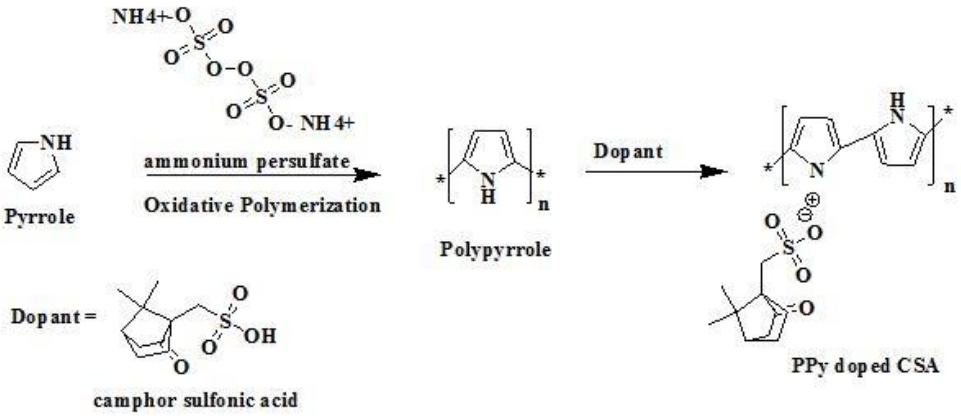

Fig.1.21 Synthesis of polypyrrole doped camphor sulphonic acid

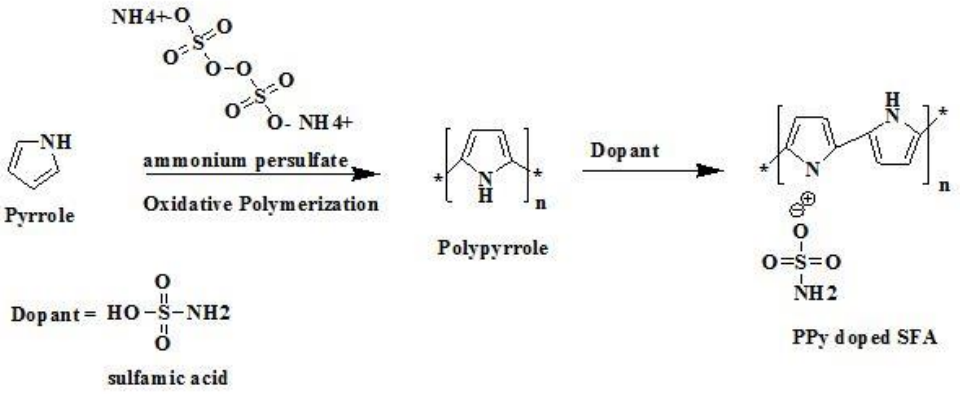

Fig.1.22 Synthesis of polypyrrole doped sulfamic acid

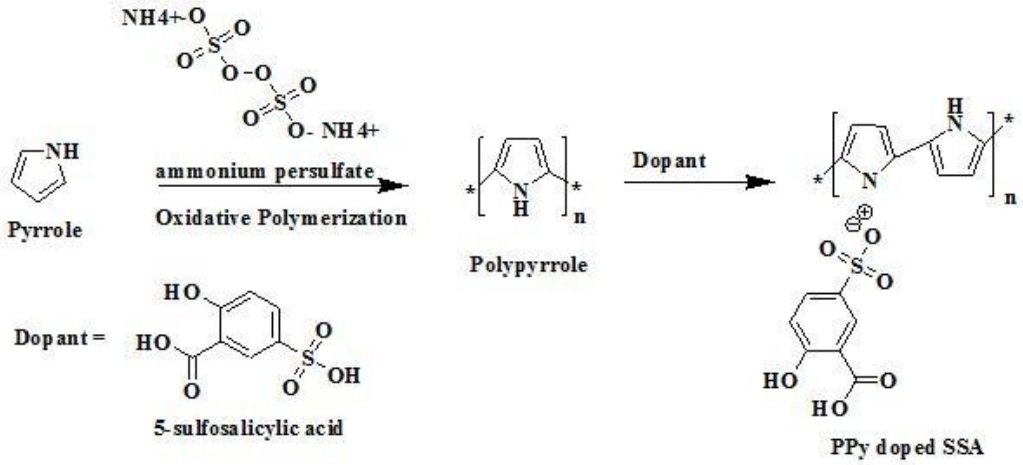

Fig.1.23 Synthesis of polypyrrole doped 5 sulfosalicylic acid

SECTION C

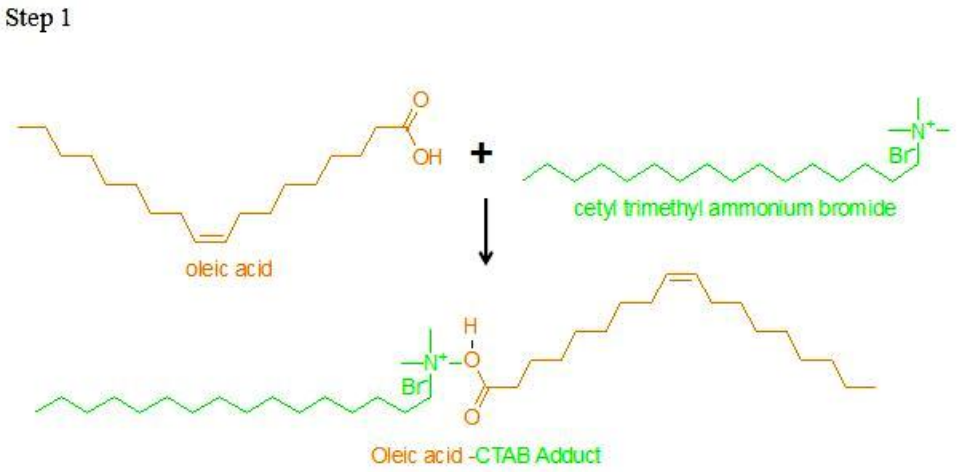

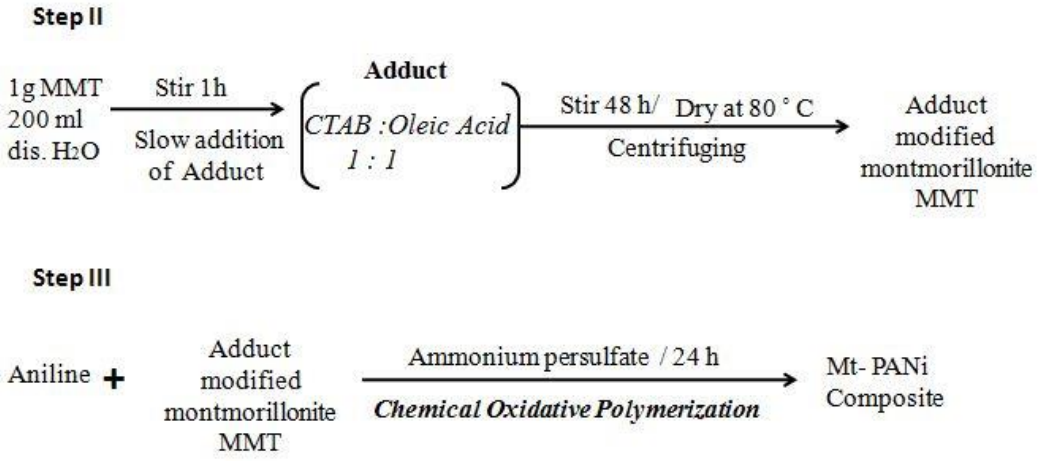

Fig.1.24 Synthesis of montmorillonite based polyaniline composite

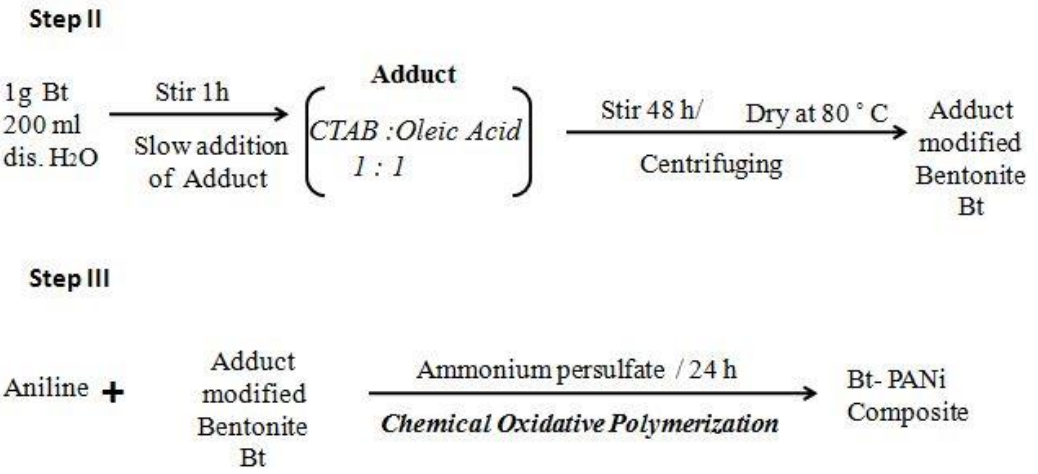

Fig.1.25 Synthesis of bentonite based polyaniline composite

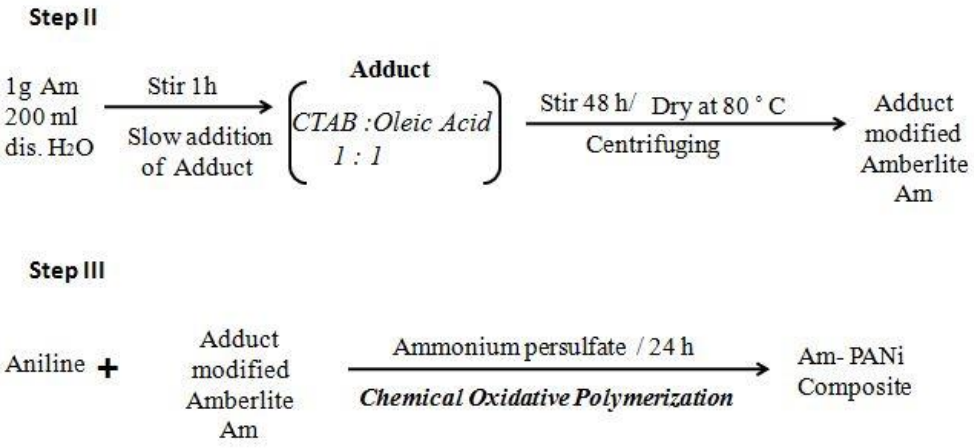

Fig.1.26 Synthesis of amberlite based polyaniline composite

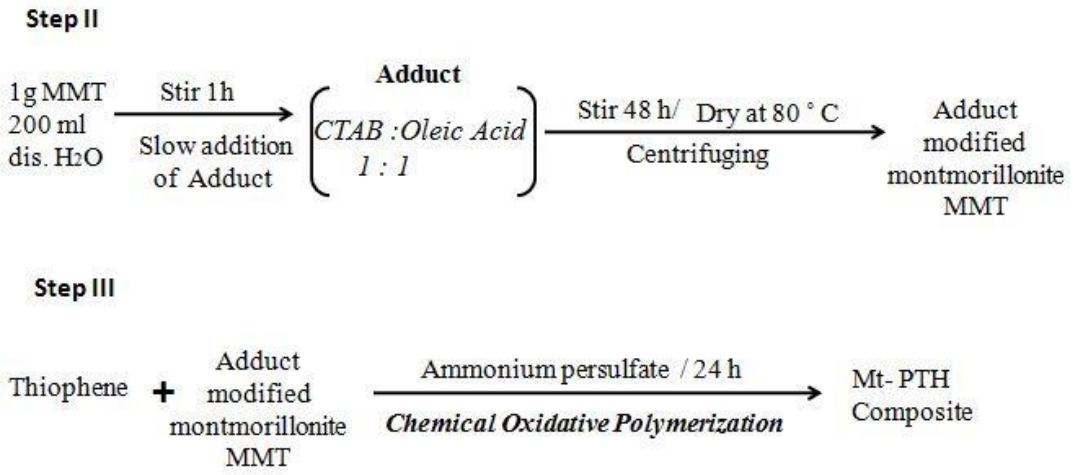

Fig.1.27 Synthesis of montmorillonite based polythiophene composite

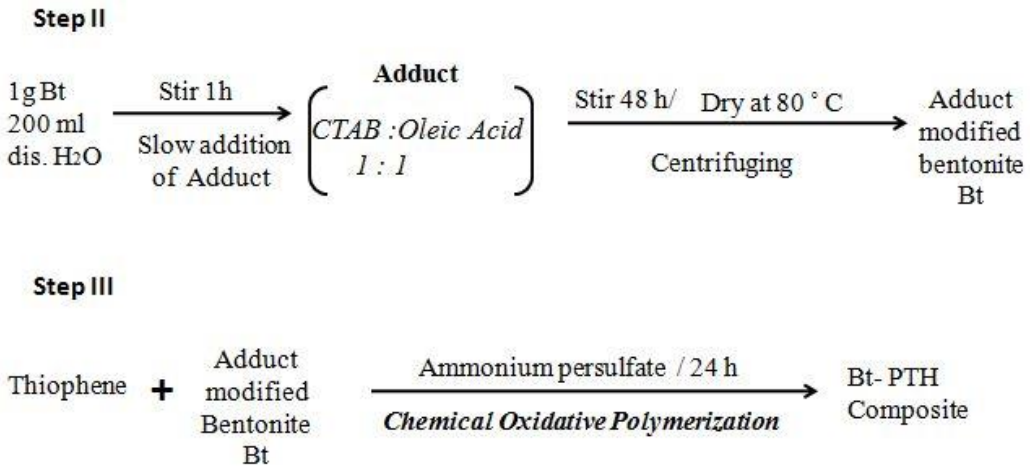

Fig.1.28 Synthesis of bentonite based polythiophene composite

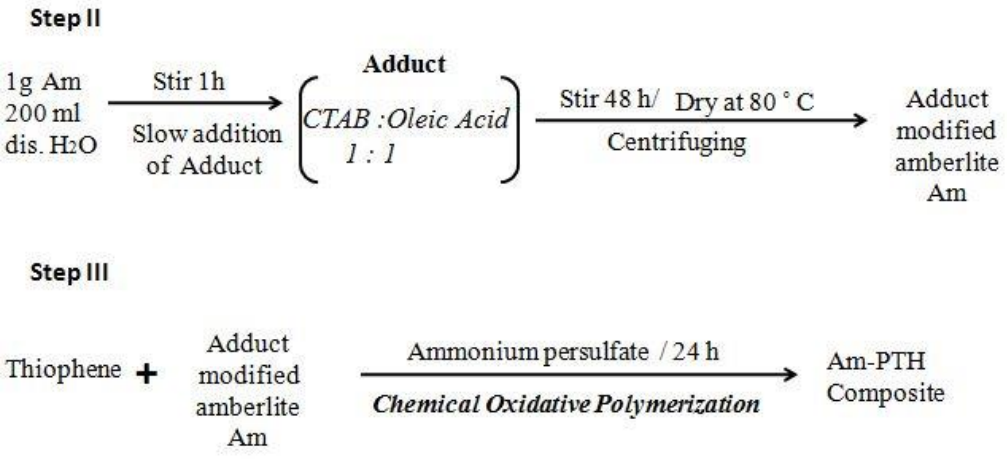

Fig.1.29 Synthesis of amberlite based polythiophene composite

SECTION D

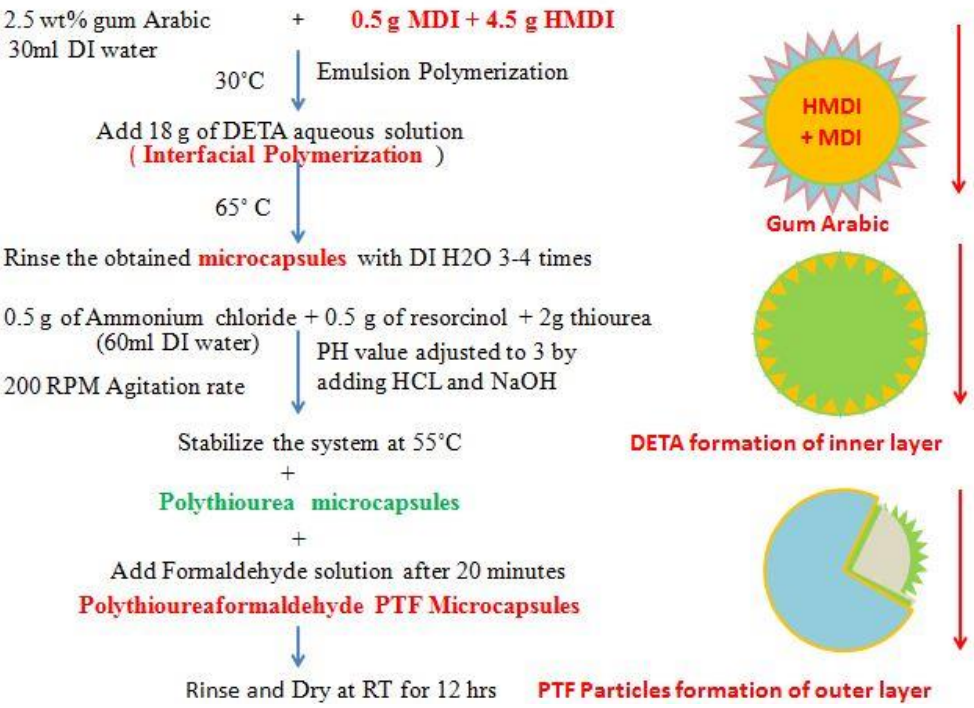

Fig.1.30 Synthesis of multilayered polythiourea formaldehyde microcapsules

2.1 Chemicals & Reagents

The chemicals used are of highest purity. Aniline, pyrrole, thiophene, hexamethylenediisocyanate (HMDI), 4,4-diphenylmethane diisocyanate (MDI), diethylenetriamine (DETA), ammonium chloride, para-toluenesulfonic acid (p-TSA),sulfamic acid (SFA), 5-sulfosalicylic acid (SSA), acrylamide (AM), potassium bromide, camphor sulphonic acid are procured from Merck, Germany. Chemicals purchased from Sigma Aldrich include bisphenolA, ethylene glycol, acrylic acid. Salts such as sodium hydroxide, sodium chloride, magnesium chloride, sodium sulfate, calcium chloride, potassium chloride, sodium bicarbonate, boric acid, strontium chloride, sodium flouride are purchased from Riedel-De-Haen. Methyl methacrylate (MMA), oleic acid (OA), cellulose (CL), chitosan (CS), gum arabic GA, starch (ST), clay montmorillonite (MMT), bentonite (Bt) and amberlite (Am) were obtained from Daejung, Korea. Guar gum from Lab chemicals, Germany, cetyltriethylammoniumchloride (CTAB) from ApplichemBiochemicals, ammonium persulfate (APS), cerium ammonium sulfate (CAS) from Panreacquimica (PRS). Other chemicals that were used include polyamide hardener and clay filler.

2.1.1 Solvents

Methanol, chloroform, xylene and acetone were obtained from Merck Germany, ethanol was procured from Riedel-de Haen, Germany, m-cresol from Fluka, Switzerland, Hydrochloric acid solution (HCl, 0.1 M) was purchased from Sigma Aldrich and doubly distilled water was used for carrying out the synthesis.

2.1.2 Purification of the chemicals and reagents used

The chemicals used were purified by distillation and in order to remove moisture from solvents dehydrating agents were used following standard procedures.

Toluene, b.p. 110.6˚C, was pre-dried over CaH_2 for about 12h and by using benzophenone as indicator was then dried over sodium wires.

Methanol, b.p. 64.5˚C, was also pre-dried over CaH_2 followed by stirring of 12h and then distilled with magnesium turning using iodine as indicator.

Ethanol, b.p. 78˚C was dried using CaH_2 with stirring for 12h followed by distillation over magnesium turnings using phenolphthalein as indicator.

Chloroform, having b.p of 61.2˚C, was pre-dried over $CaCl_2$ and refluxed over phosphorus pentoxide.

Aniline, b.p 184.1˚C was dried over CaH_2 with stirring for 10h followed by distillation under reduced pressure.

Pyrrole, b.p 129˚C was used after distillation under reduced pressure to get colourless liquid, and is considered pure as it boils at constant temperature.

Thiophene, b.p 84˚C was dried simply over solid KOH followed by distillation under reduced pressure.

2.2 Electrolyte preparation

The electrolyte used for electrochemical studies in the present study was artificial seawater. It was prepared according to **ASTM** D1141-52 standard methods by using exact concentrations of various salts such as chlorides, sulfates, carbonates and bicarbonates. About 41.953g of salts were dissolved in distilled water to prepare 1L seawater and pH of the solution was adjusted to 8.3 by adding few drops of 0.1M NaCl and HCl aqueous solutions.**Table 2** shows the typical composition of marine water containing various salts and their concentration in g/L

Table 2 Typical composition of marine water containing various salts and their concentration in g/L

Salts	Concentration (g/L)
Sodium Chloride	24.530
Sodium sulfate	4.0900
Magnesium Chloride	11.100
Calcium Chloride	1.1600
Potassium Chloride	0.6900
Sodium bicarbonate	0.2000
Potassium Bromide	0.9900
Boric Acid	0.2800
Strontium Chloride	0.0030
Sodium Fluoride	0.0002

2.3 Pretreatment of substrate

High strength aluminum alloy AA2219-T6 and high strength stainless steel SS-304 alloys are used as coating substrates. These alloys are the most widely used structural alloys for marine applications. Substrates were abraded with 600, 800 and 1200 grit emery paper. The coupons were then conditioned by immersion in 5% NaOH of pH~10 for two minutes in order to activate -OH group for proper adhesion, followed by freshly distilled water washing, acetone rinsing to dry the surface and finally washing them with freshly distilled water again[26].

2.3.1 Composition of coating

Take equivalent amount of Epoxy resin bisphenol A and polyamide hardener. And mix them preferably with wooden rod along with required amount of clay filler .The solvent employed for coating formulation is 15 mL of xylene

2.4 Analytical techniques and instrumentation

2.4.1 FT-IR spectroscopic studies

Fourier transform infrared study was performed on the Perkin Elmer Spectrum One (Ver. B) FTIR spectrometer.The analysis was accomplished at room temperature.

2.4.2 XRD analysis

XRD spectra of the powdered composites were taken by Phillip 3040/60 X pert PRO Diffractometer equipped with Cu-Kα radiation source. The analysis was accomplished at room temperature in range of 0 to 40˚C.

2.4.3 Thermal analysis

Thermal behavior of powdered composites was recorded employing TGA and DSC studies.

2.4.3.1 Thermogravimetric analysis

Thermogravimetric analysis was executed employing Mettler Toledo Perkin Model Q 500, at the heating rate of 10˚C/min in argon atmosphere.

2.4.3.2 DSC measurements

To evaluate weight change with respect to temperature DSC curves were recorded at heating rate of 20ºC/min under nitrogen atmosphere by using Mettler Toledo Perkin Model DSC-823.

2.4.4 Scanning electron microscopy

The surface morphology of material coated substrates was analysed using scanning electron microscope.

2.4.5 Electrochemical measurements

Potentiodynamic polarization and electrochemical impedance spectroscopy

The electrochemical studies were carried out by potentiodynamic polarization and electrochemical impedance spectroscopy (EIS) using Gamry instrument reference 3000 potentiostat /galvanostat ZRA. A three electrode cell incorporating a saturated calomel reference electrode, graphite counter electrode and AA2219-T6 and SS-304 with an exposed area of $1cm^2$ were used as working electrodes. In order to achieve potential and environmental stabilization all of the test specimens were immersed in test solution 1 day prior to the electrochemical test. Spectra were acquired in the frequency range from 10^6 to 10^{-2} with an AC amplitude of 10 mV. Data were fit using gamry software.

2.5 Synthetic methodology

SECTION A Microwave assisted synthesis of grafted polysaccharides

Carbohydrate polymers were treated with various monomers to synthesized nine graft copolymers via microwave irradiation and their general scheme of synthesis is shown in **Fig.2.1**

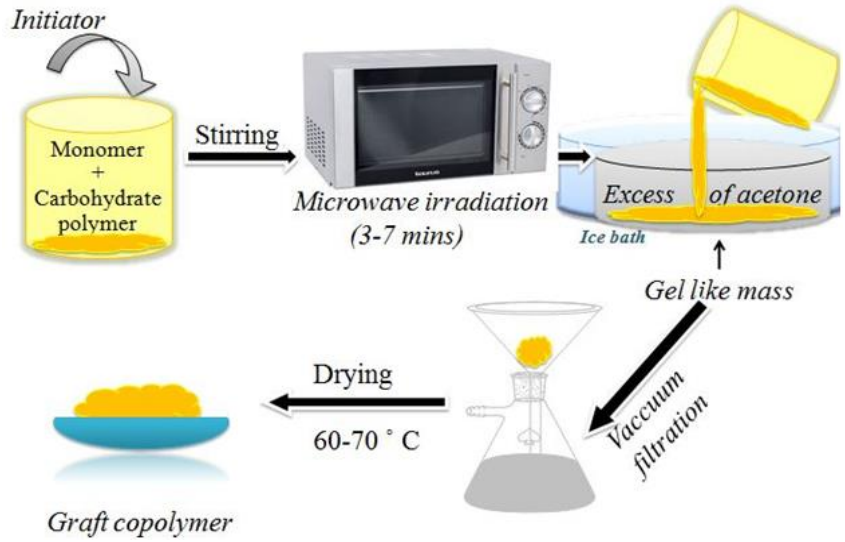

Fig.2.1 General scheme for the synthesis of microwave assisted polysaccharide grafting

2.5a.1 Microwave initiated synthesis of grafted polysaccharides

Synthesis of grafted polysaccharides is done by previously reported method.1g of carbohydrate polymer (guar gum/gum arabic/starch/cellulose/chitosan) is dissolved in 40 mL of distilled water in 1000 mL borosil beaker and stirred until a homogenous solution is formed. Now add 1.5-3.5g or 1:1 of monomer (acrylamide/ methyl methacrylate/ethylene glycol /acrylic acid) in 10ml of distilled water. Mix both the solutions and allow constant stirring for 15 mins, followed by addition of required amount of cerium ammonium sulfate (CAS). Prior to the addition of initiator, few drops of concentrated HCl were added. The solution so obtained is irradiated by a domestic microwave oven (850 Watt of power) for 3-7 mins. The gel like mass is then cooled by placing the reaction vessel in cold water or ice, and then poured into excess of acetone with constant stirring. The precipitated grafted copolymer is filtered and washed with acetone and alcohol water mixture.

2.5a.2 Drying and weighing of the grafted copolymers

The residue after drying in oven for 2h at 70-80˚C, is kept in a vacuum desiccator to obtain a constant weight. It is proposed that some of the free -OH groups of mannopyranose backbone convert into O˙ radicals by the action of the free radical initiator and the microwave irradiation, which in turn, reacts with the AM/MMA/EG/AA monomer resulting into grafted polysaccharide.

2.5a.3 Calculation of percentage grafting of grafted copolymers

The percentage grafting (%G, Eq.1) as obtained for different combinations of grafted polysaccharides, are summarized in **Table 3**

$$\%G = \frac{\text{Mass of the grafted product - mass of polysaccharide taken}}{\text{Mass of polysaccharide taken}} \times 100 \quad \text{…….(Eq.1)}$$

Table 3 Synthetic details of microwave-assisted grafting of corrosion inhibitors

System	Weight of inhibitor (g)	Monomer/ monomer ratio (g)	Weight of CAS (g)	Final Weight of grafted copolymer (g)	Times of irradiation (min)	% G
PAM-g-GA	1	1.5	0.01	1.49	3	85
PAM-g-GG	1	1.5	0.01	1.37	3	82
PAM-g-ST	1	1.5	0.01	1.34	3	64
PAA-g-GG	1	1.5	0.01	1.23	4	88
PAA-g-CS	1	1.5	0.01	1.67	5.5	85
PMMA-g-GA	1	3.5	0.01	1.01	6	25
PMMA-g-CL	1	3.5	0.01	1.53	7	79
PEG-g-CS	1	1.5	0.01	1.42	6.5	89
PAM-co-PAA-g-GG	1	1:1	0.01	1.41	4	93

SECTION B Sulphonate doped conducting polymer coatings

2.5b.1 Synthesis of Polymer

Synthesis of PANi

1 mL of freshly distilled aniline is added in 100 mL of 0.1M aqueous HCl solution stirred for 15 mins add 3.5g of ammonium persulfate initiator dropwise with constant stirring and temperature is maintained at 5˚C throughout. shiny orange solution turns dark green on complete polymerization of aniline. Precipitates are filtered, washed with distilled water 2-3 times and finally dried at 60˚C for 24h. Dark green precipitates indicate the synthesis of PANi.

Synthesis of Polypyrrole

1 mL of pyrrole is dissolved in 100 ml distilled water. After stirring for 30 minutes oxidant (3.5 g of ammonium persulfate) in 100 ml distilled water at RT is added dropwise via dropping funnel. Mixture is stirred for 24 hrs. Precipitates are filtered, washed with distilled water 2-3 times and then dried at 25˚C. Black Precipitates of polypyrrole are formed.

2.5b.2 Doping of Polymer

General synthesis of doped Polymer

PANi/PPy was synthesized by chemical oxidative polymerization of 0.08 M solution of aniline/pyrrole in aqueous 0.02 M HCl using 0.04 M ammonium persulfate (APS). The monomer solution was initially stirred for 6h at room temperature and then maintained at 5˚C. Drops of APS were slowly added to the solution to precipitate the polymer. A dark green and black color ensures the complete polymerisation of aniline and pyrrole respectively. The solution was then filtered and washed with distilled water; then de-doped in NH_4OH solution, filtered and dried again in a vacuum oven. The dried material was re-doped via exposure to a 0.02 M dopant solution. The solution was stirred for 4h at RT, then filtered and dried in vacuum oven at 40-60˚C for 24h to yield doped polymer. **Fig.2.2** shows the general scheme for the synthesis of sulphonate doped conducting polymer coatings.

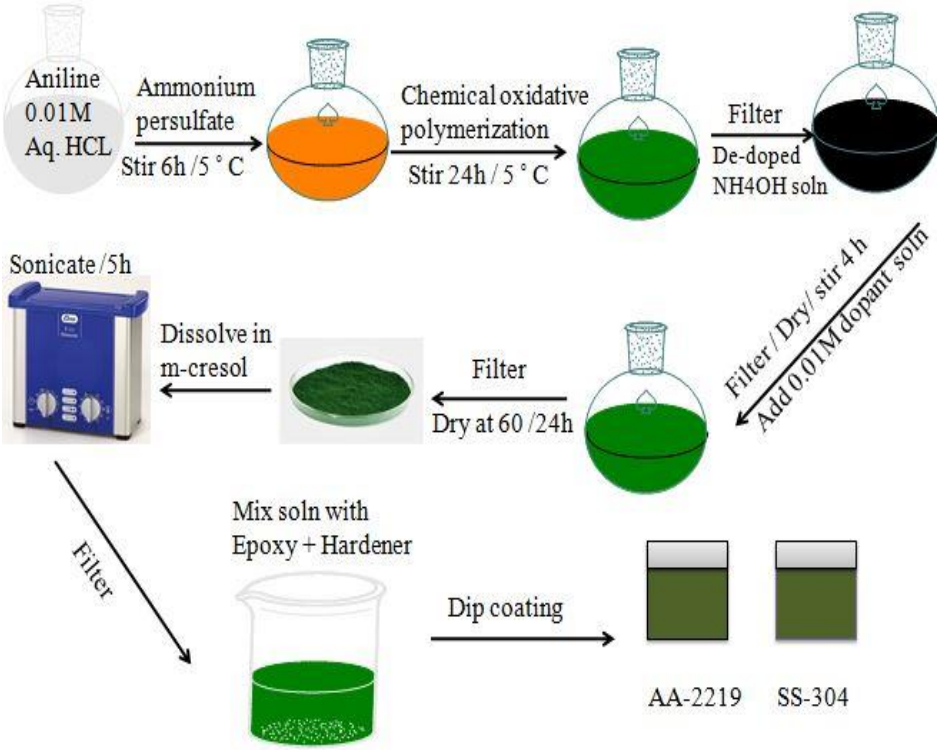

Fig.2.2 General scheme of synthesis of sulphonate doped conducting polymer coatings

2.5b.2.1 Synthesis of PANi doped Para toluene sulfonic acid

PANi doped para-toluene sulfonic acid was synthesized by chemical oxidative polymerization of aniline. After polymerization the solution was de-doped, filtered and dried in a vacuum oven. The dried material was re-doped via exposure to a 0.02M para-toluenesulfonic acid solution. The solution was stirred for 4h at RT, then filtered and dried in vacuum oven at 60˚C for 24h to yield p-TSA doped polyaniline. **Fig.2.3** showing the structure of PANi-TSA

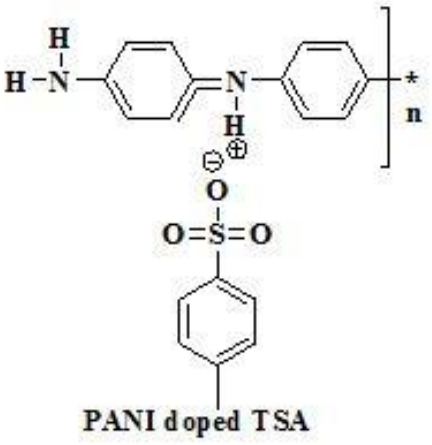

Fig.2.3 Structure of PANi-TSA

2.5b.2.2 Synthesis of PANi doped camphorsulfonic acid

PANi doped camphorsulfonic acid was synthesiszed by the same procedure as mentioned above re-doping in this case was done by using 0.02M camphor acid solution. The solution was stirred for 4h at RT, filtered and dried in vacuum oven at 60˚C for 24h to yield CSA doped polyaniline. **Fig.2.4** shows the structure of PANi-CSA

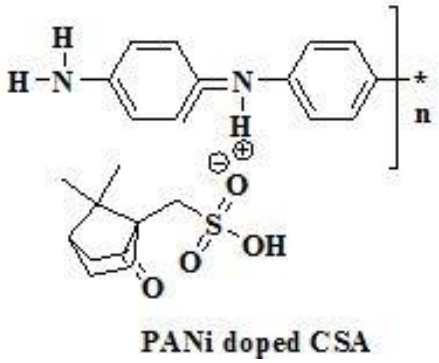

Fig.2.4 Structure of PANi-CSA

2.5b.2.3 Synthesis of PANi doped sulfamic acid

PANi doped sulfamic acid was synthesised by chemical oxidative method. PANi was first de-doped then re-doped via exposure to a 0.02M sulfamic acid solution. The solution was stirred for 4h at RT, filtered followed by drying at 60˚C for 24h to yield PANi-SFA. **Fig.2.5** shows the structure of PANi-SFA

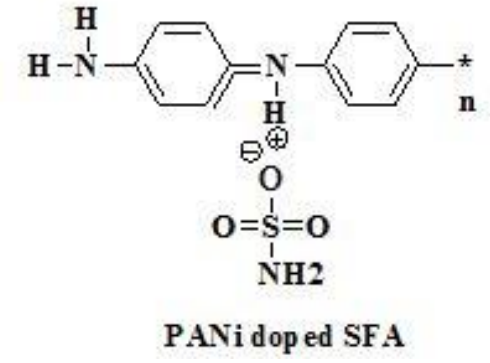

Fig.2.5 Structure of PANi-SFA

2.5b.2.4 Synthesis of PANi doped 5-sulfosalicylic acid

PANi doped 5-sulfosalicylic acid was synthesised by chemical oxidative polymerization of the monomer. Re-doping was done with 0.02M 5-sulfosalicylic acid solution. The solution was stirred for 4h at RT, then filtered and subsequently dried in vacuum oven at 60˚C for 24h to yield PANi-SSA. **Fig.2.6** shows the structure of PANi-SSA

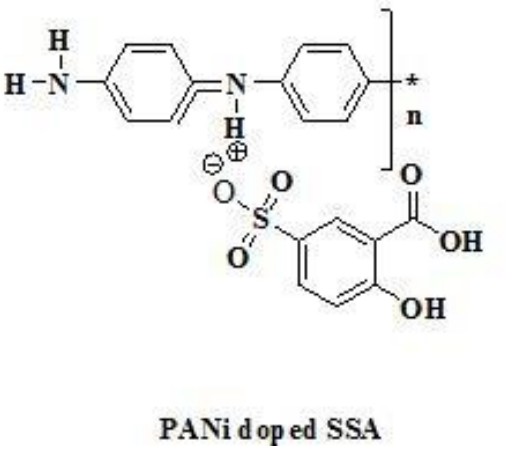

Fig.2.6 Structure of PANi-SSA

2.5b.2.5 Synthesis of polypyrrole doped para toluene sulfonic acid

Dried product of chemical oxidative polymerization of pyrrole, the black precipitates of PPy were stirred in 1:1 (Polypyrrole: TSA) dopant solution for 24h. The solution was then filtered and dried in vacuum oven at 25˚C for 24h to yield p-TSA doped polypyrrole. **Fig.2.7** showing the structure of PPy-TSA

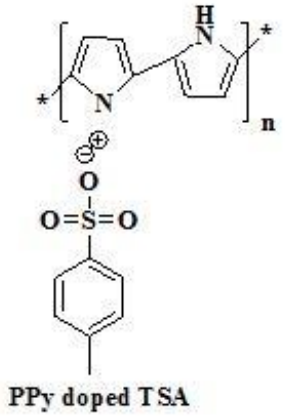

Fig.2.7 Structure of PPy-TSA

2.5b.2.6 Synthesis of Polypyrrole doped camphorsulfonic acid

Precipitates of polypyrrole obtained as a result of chemical oxidative polymerization of pyrrole were stirred in 1:1 (Polypyrrole: CSA) dopant solution. The dopant solution was then filtered and dried in vacuum oven at 25˚C for 24h to yield Ppy-CSA. **Fig.2.8** shows the structure of PPy-CSA

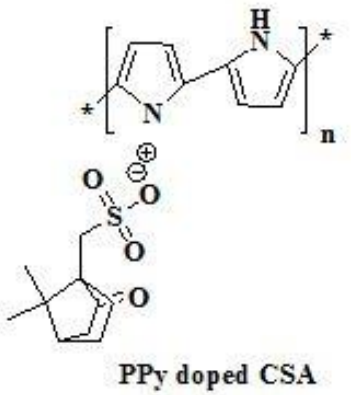

Fig.2.8 Structure of PPy-CSA

2.5b.2.7 Synthesis of Polypyrrole doped sulfamic acid

Stirring of polypyrrole:dopant solution 1:1 (Polypyrrole:SFA) containing dried precipitates of polypyrrole for 24h and then filtration of the dopant solution followed by drying in vacuum oven at RT for another 24h gives SFA doped polypyrrole. **Fig.2.9** shows the structure of PPy-SFA

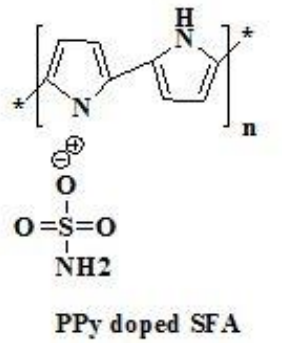

Fig.2.9 Structure of PPy-SFA

2.5b.2.8 Synthesis of Polypyrrole doped 5-sulfosalicylic acid

The dried precipitates of polypyrrole were stirred in 1:1 (Polypyrrole:SSA) dopant solution for 24h. The dopant solution was then filtered and dried in vacuum oven at 25˚C for 24h to yield the doped product Ppy-SSA. **Fig.2.10**shows the structure of PPy-SSA

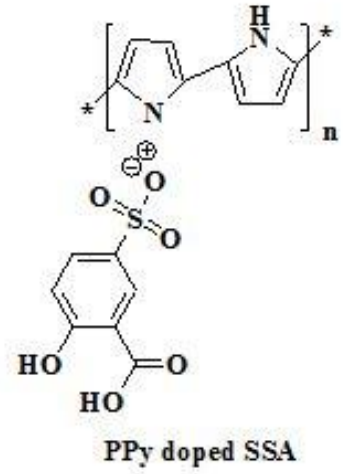

Fig.2.10 Structure of PPy-SSA

2.5b.3 Coating

2.5b.3.1 Composition

Polymer-Dopant/epoxy coatings were prepared by subjecting polymer-dopant particles in m-cresol to ultrasound for 5h. The resulting solution was vacuum filtered to eliminate solid residue. This solution was subsequently mixed with epoxy and polyamide as curing agent with suitable amount of clay filler. **Table 4a and 4b** shows the composition of the PANi and PPy doped coatings.

Table 4a Composition of PANi doped epoxy coatings

S.No	PANi Dopant (g)	Epoxy (g)	Hardener (g)	Solvent (ml)	Coating Designation
1	5.0	35	15	15	PANi-CSA
2	5.0	35	15	15	PANi-TSA
3	5.0	35	15	15	PANi-SFA
4	5.0	35	15	15	PANi-SSA

Table 4b Composition of PPy doped epoxy coatings

S.No	Ppy Dopant (g)	Epoxy (g)	Hardener (g)	Solvent (ml)	Coating Designation
1	5.0	35	15	15	PPy-CSA
2	5.0	35	15	15	PPy-TSA
3	5.0	35	15	15	PPy-SFA
4	5.0	35	15	15	PPy-SSA

2.5b.3.2 Method and curing

Dip coating method was employed making the use of pre-treated SS-304 panels. The coupons/ panels were dipped in the formulated system for 60s, all the panels were coated using the same method repeatedly after 30 secs for 3 mins.After coating the coated panels were cured at RT for 12h, followed by curing at 60˚C for 12h.

SECTION C Adduct modified clay based composite coatings

2.5c.1 Synthesis of adduct modified clays

2.5c.1.1 Synthesis of Adduct

Take equivalent ratio of oleic acid and cetyltriethylammonium bromide (CTAB) in suitable amount of distilled water stir the mixture until a homogenous solution is obtained. This results in the formation of adduct named as Oleic acid-CTAB.

2.5c.1.2 Synthesis of organomodified clays

Using a typical procedure for the preparation of adduct modified materials, 1g of clay/ion exchange resin (montmorillonite, bentonite and amberlite) was introduced into 200 mL of distilled water and was magnetically stirred for 1h at RT followed by the addition of the already prepared adduct (*CTAB: Oleic Acid::1:1*) until homogenous mixture is obtained which was further stirred uninterrupted for 48h at RT. The pH of clay dispersion was adjusted to about 3-4 by using 1.0M HCl solution. Finally, adduct modified clay was recovered by ultra-centrifuging and was dried overnight in a vacuum oven at 80°C.The adduct modified clays obtained were named accordingly. Adduct modified montmorillonite and was designated as (OC-AMt). The same procedure was used to prepare oleic acid-CTAB modified bentonite and oleic acid-CTAB modified amberlite respectively. The resultant modified clays were identified as OC-AMt, OC-ABt and OC-AAm respectively.

2.5c.2 Synthesis of adduct modified clay composites

Synthesis of adduct modified PANicomposites

Take 1 ml of aniline in a two neck round bottom flask. Add 2 wt% of adduct modified clay and sonicate this mixture for about 90 minutes. After stirring for an additional 2h at room temperature subsequently, a solution of 0.02M (4.064 g) of APS in 100 ml of distilled water was introduced into the emulsion solution and is stirred for 24h. Meanwhile maintain the temperature of 0-5˚C throughout polymerization. PANi/clay dispersion thus obtained, was filtered, washed with distilled water twice and then placed in vacuum oven for drying of the precipitates at 60˚C for about 24h. **Fig.2.3** depicts the general scheme for the synthesis of adduct modified clay based composite coatings.

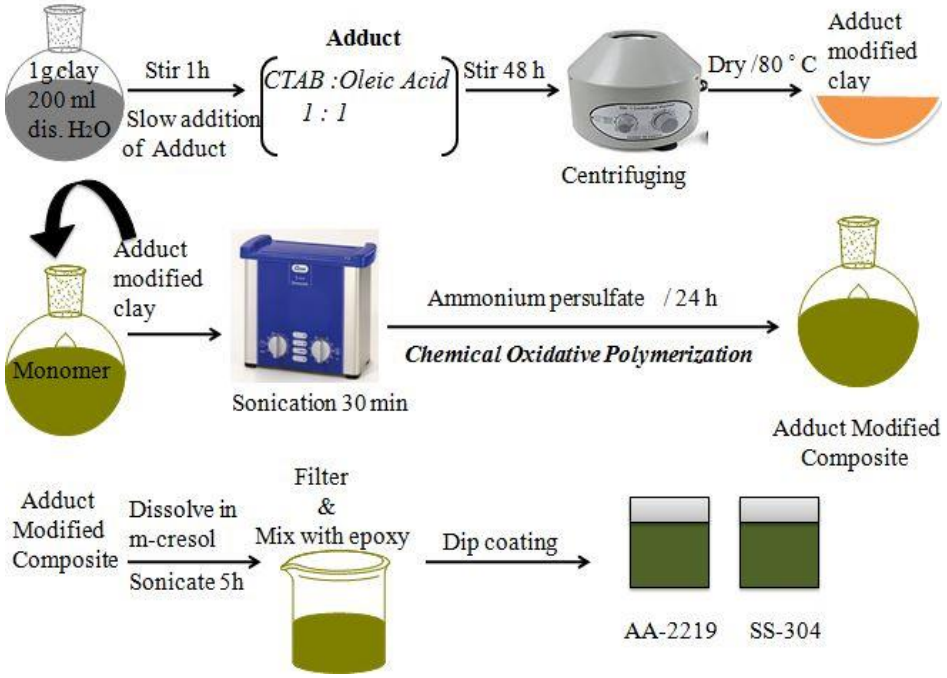

Fig.2.11 General scheme for the synthesis of adduct modified clay composite coatings

2.5c.2.1 Synthesis of montmorillonite based PANi composite

Using the same general procedure 2 wt% of the adduct modified montmorillonite was added into the reaction mixture, sonicated for about 90 mins followed by stirring for an additional 2h at RT. Oxidant was introduced to the emulsion and was stirred for 24h maintaining the temperature of 0-5 ˚C throughout. Dispersion thus obtained, was filtered, washed and then placed in oven for drying of the precipitates at 60˚C for about 24h. Montmorillonite based PANi composite was obtained.

2.5c.2.2 Synthesis of bentonite based PANi composite

During chemical oxidative polymerization of PANi 2 wt% of adduct modified bentonite (OC-ABt) was added, sonicated and mixture was stirred until complete polymerization. Dispersion obtained was filtered, washed with distilled water followed by drying at 60˚C for about 24h. Bt-PANi composite was obtained.

2.5c.2.3 Synthesis of amberlite based PANi composite

To synthesize Am-PANi composite the modified clay used was replaced with 2 wt% of adduct modified amberlite (OC-AAm). Polymerization was done using the

same general procedure including sonication and stirring followed by drying and washing to yield amberlite based PANi composite.

Synthesis of adduct modified PTH composites

Take 2 mL of thiophene in 70 mL of Chloroform in a two neck round bottom flask equipped with reflux condenser. Add 2 wt% of adduct modified clay and sonicatethis mixture for about 90 mins. After stirring for an additional 2h at RT, a solution of 9g of $FeCl_3$ in 150 mL of $CHCl_3$ was introduced into the solution which was then refluxed at 55˚C for 24h. Brown precipitates of polythiophene/clay dispersion thus obtained, were filtered, washed with methanol, 0.01M HCl solution, acetone and again with boiling methanol. The precipitates obtained were then dried at RT for about 24h.

2.5c.2.4 Synthesis of montmorillonite based PTH composite

Employing the same general procedure for the synthesis of adduct modified polythiophene composites, the modified clay used was 2 wt% of the adduct modified montmorillonite (OC-AMt), mixture was sonicated stirred at RT, followed by addition of a solution of 9g of $FeCl_3$ in $CHCl_3$. After reflux at 55˚C for 24h, brown precipitates of polythiophene/montmorillonite dispersion were obtained which were then filtered, washed with methanol, HCl solution, acetone and boiling methanol. The precipitates were then dried at RT for 24h.

2.4c.2.5 Synthesis of bentonite based PTH composite

In this case the modified clay used was bentonite 2 wt % of which was used to obtain brown precipitates of polythiophene/bentonite dispersion. The dispersion obtained was sonicated, stirred, filtered and washed with previously mentioned solvents in the general procedure. Bt-PTH composite was dried at RT for 1 day.

2.4c.2.6 Synthesis of amberlite based PTH composite

Amberlite, an ion exchange resin based polythiophene composite was synthesized using exactly the same procedure used for the synthesis of adduct modified polythiophene composite. In 2 mL of thiophene 2wt % of adduct modified amberlite (OC-AAm) was added, sonicated for 90 mins. After stirring for 2h, $FeCl_3$ solution was introduced, solution was then refluxed at 55˚C for 24h polythiophene/amberlite dispersion was obtained. Am-PTH dispersion was filtered, washed and dried at RT for 24h.

2.5c.3 Coating

2.5c.3.1 Composition

Adduct modified clay composite coatings were prepared by introducing the composite material into xylene for sonication. After 6h sonication, the obtained solution was filtered to eliminate residue and solution was mixed with appropriate amount of epoxy, hardener and filler. **Table 5** shows the composition of PANi and PTH based composite coatings.

Table 5 Composition of PANi and PTH clay based composite coatings

S.No	Composite (wt %)	Epoxy (g)	Hardener (g)	Solvent (ml)	Coating Designation
1	10	35	15	15	Mt-PANi
2	10	35	15	15	Bt-PANi
3	10	35	15	15	Am-PANi
4	10	35	15	15	Mt-PTH
5	10	35	15	15	Bt-PTH
6	10	35	15	15	Am-PTH

2.5c.3.2 Method and curing

Dip coating method was used, pre-treated SS304 panels were dipped in the formulated coating system for 60s, all the panels were coated using the same method repeatedly after 30s for 3 mins to ensure uniform coating thickness.After coating the coated panels were cured at RT for 12h, followed by another curing at 60 ˚C for 12h.

SECTION 4 Poly-thioureaformaldehyde based smart functional self healing coatings

2.5d.1 Synthesis of Polythiourea formaldehyde PTF microcapsules

2.5d.1.1 Synthesis of double-shelled microcapsules

The HMDI (hexamethylenediisocyanate) encapsulating microcapsules were synthesized by the coalesce of interfacial and in situ polymerization. Polythiourea microcapsules were initially prepared by employing interfacial polymerization followed by a further coat with a layer of poly-thiourea formaldehyde (PTF) shell via in situ polymerization.

2.5d.1.2 Synthesis of HMDI containing microcapsules

The microcapsules containing HMDI as core material were prepared via interfacial polymerization in an oil-in-water emulsion system. Firstly, the aqueous phase, 2.5 wt% of gum Arabic was added to 30 mL of deionized water (DI) in a 250 mL beaker placed in a temperature controlled water bath, which was then positioned on a programmable hotplate and the solution was heated up to 30˚C. Later, the homogeneous oil phase containing 0.5g of Suprasec 2644 and 4.5g of HMDI was emulsified in the surfactant aqueous solution under certain agitation rate. After the system was stabilized for 45 mins at 30˚C, 18.0g of DETA (diethylenetriamine) aqueous solution (30 wt%) was added to initiate the interfacial polymerization. Meantime, the system temperature was raised to 65˚C. After reaction for 30 min at the designated temperature, the obtained suspension of microcapsule slurry was rinsed with DI water for 3-4 times followed by further coat of PTF shell, as described hereafter.

2.5d.1.3 Formation of PTF shell on HMDI filled microcapsules

2g thiourea, 0.5g ammonium chloride and 0.5g resorcinol were initially dissolved in 60 mL DI water in a 250 mL beaker under agitation rate of 200 RPM. Afterwards, the pH value of the solution was adjusted to approximate 3.5 using NaOH and HCl solutions. After stabilization at 55˚C, the system was introduced the formerly synthesized microcapsules and 4.5 mL of formaldehyde solution (37 wt%). After reaction for 20 mins, the microcapsules suspension was rinsed and washed with DI water for 3 times before air dried for 12h**. Fig.2.4** shows the general scheme for the synthesis of poly thiourea formaldehyde based smart functional self-healing coatings.

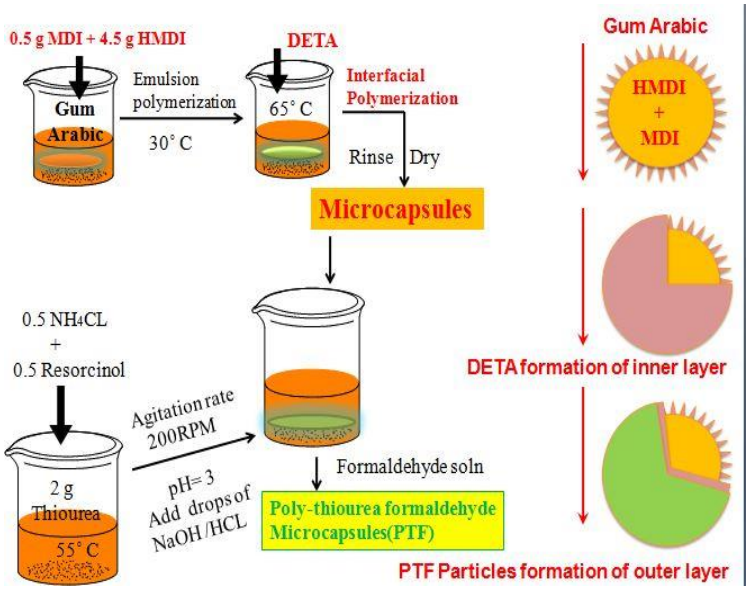

Fig.2.12 General scheme for the synthesis of poly-thiourea formaldehyde based smart functional self-healing coatings

2.5d.2 Coating

2.5d.2.1 Composition

Self-healing poly-thiourea formaldehyde coatings were prepared by dispersing 10 wt% of the PTF microcapsules in 15 mL of xylene via sonication for 5h. The resulting solution was subsequently mixed with appropriate amount of epoxy, hardener and filler.

2.5d.2.2 Method and curing

Dip coating method was employed making the use of pre-treated aluminum alloy AA2219-T6 and SS-304 panels. The coupons/ panels were dipped in the formulated solution for 60s, all the panels were coated using the same method repeatedly after 30s for 2-3 mins.After coating the coated panels were cured at RT for 12h, followed by curing at 60 ˚C for another 12h.

3.1 Structure Elucidation and Properties

SECTION A

3a.1 FT-IR studies of the synthesized corrosion inhibitors

A comprehensive study on FT-IR spectra of polysaccharides and their grafted products has revealed some valuable informations concerning their modes of vibration. Comparative study of FT-IR spectra of polysaccharides and their final products after treatment with various monomers hints the successful grafting by microwave irradiation. Comparative FT-IR spectra of the representative corrosion inhibitor is shown in **Fig.3.1.**

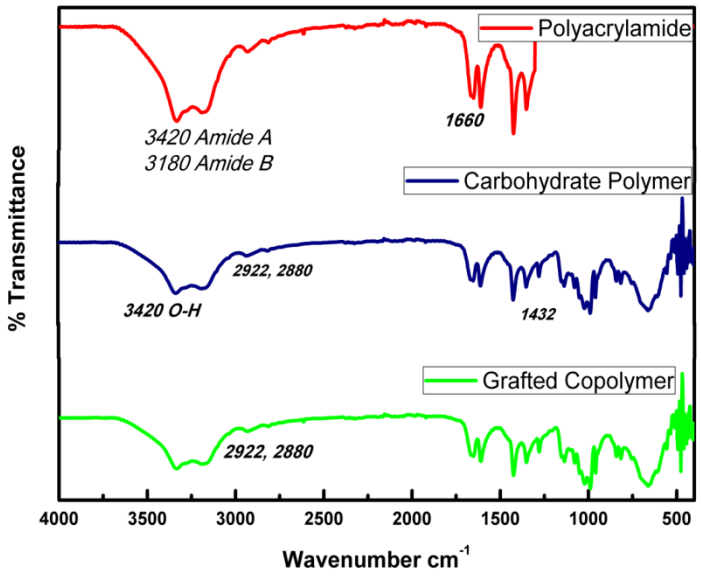

Fig.3.1 Comparative IR spectra of the representative corrosion inhibitor (PAM-g-GA)

3a1.1 FT-IR studies of PAM-g-GA, PAM-g-GG and PAM-g-ST

The characteristic peaks shown in **Table 6** elucidate the structures of gum arabic, guar gum, starch as well as their microwave irradiated products with polyacrylamide. From IR vibration modes of gum arabic a broad band around 3426 cm^{-1} was observed indicative of the O-H stretching vibrations, a smaller band at 2923 cm^{-1} was accredited to C-H stretching mode of vibrations. The peaks at 1149, 1076 and 845 cm^{-1} were attributable to the stretching vibrations of C–O–C. Similarly in

guar gum a broad peak around 3420 cm^{-1} was observed indicating the O-H stretch, a smaller band at 2925 cm^{-1} was ascribed to C-H stretching ambiance and the peaks at 1155, 1075 and 868 cm^{-1} were due to C–O–C stretch. In IR spectrum of starch a wide O-H band appeared at 3298 cm^{-1}, smaller C-H stretch appeared at 2922 cm^{-1} whereas, C-O-C stretching mode of vibrations appeared at 1156 and 1018 cm^{-1}.

Table 6 IR data of a) PAM-g-GA b) PAM-g-GG and c) PAM-g-ST

Functional Group	**Characteristic absorption (cm^{-1})**						
	PAM	**GA**	**GG**	**ST**	**PAM-g-GA**	**PAM-g-GG**	**PAM-g-ST**
O-H stretch	-	3427	3422	3298	3489	-	-
Amide A	3420	-	-	-	3333	3420	3492
Amide B	3183	-	-	-	3192	3179	-
C-H stretch	-	2922	2924	2922	2893	2926	2828
Amide I C=O stretch	1660	-	-	-	1676	1656	1678
Amide II N-H bending	1600	-	-	-	1595	1595	1585
CH_2 scissoring	1443	1439	1429	1438	1425	1439	1440
C-N stretch	1403	-	-	-	1352	1423	1395
O-H in plane bending	-	1380	1377	1379	1388	1380	1380

In the first grafted product PAM-g-GA, O-H of GA overlaps with N-H of amide group of polyacrylamide leading to broadening of peak that came into sight at 3489 cm^{-1}. A small band at 2893 cm^{-1} was alloted to the C-H stretching mode of vibrations. The peaks at 995 and 952 cm^{-1} were attributed to C-O-C stretching. The jagged peaks at 1676 and 1595cm^{-1} of grafted GA were due to N-H and C-O stretch resp. The peak at 1425 cm^{-1} was assigned to CH_2 scissoring. Added there is an additional peak present in microwave irradiated product i.e. 1352 cm^{-1}, which was consigned to the C-N stretching. Hence, the occurrence of these supplementary peaks in case of grafted copolymer compared to that of GA verifys the affluent grafting of PAM chains onto the moral fiber of GA. Similarly, in case of grafted products of both guar gum and starch, O-H stretching peak of hydroxyl group and N-H stretching band of amide group of PAM overlie each other, leading to broadening of band appearing

at 3420 and 3498 cm^{-1} resp. A small peak at 2926 and 2828cm^{-1} corresponds to the C–H stretching vibration of GG and ST resp. The bands at 1151, 1075 and 842 cm^{-1} were attributed to C-O-C stretching vibrations of grafted GG while C-O-C peaks appeared at 1084 and 1010 cm^{-1} in PAM-g-ST.

The sharp peaks at from 1550-1680 $cm^{-1}$of grafted products of GG and ST are due to C-O and N–H stretching respectively. Further, there is an extra peak present in the grafted product i.e. 1380 cm^{-1}, alloted to the C-N stretching mode. Hence, the occurrence of the supplementary bands in case of grafted copolymers demonstrates the grafting of PAM chains on respective polysaccharides.

3a.1.2 FT-IR studies of PAA-g-GG and PAA-g-CS

The characteristic bands of guar gum are shown in **Table 6**. The microstructural evidence of grafting of guar gum on polyacrylic acid was obtained from the appearance of intense peak at 1705 cm^{-1} ascribed to symmetric and anti-symmetric stretching of pendant acid unit of GG. ß-carbon of pyranose ring of GG reacts with acid radical and due to proton elimination the carbon of the ring was converted into an aldehyde but it is intricate to trace due to strong overlapping. C-O stretch appears at 1170cm^{-1}, ethereal C-O-C peak around 1134 cm^{-1} in case of grafted copolymer (PAA-g-GG). Peaks for CH-O-CH bond that appear at 847 and 1016 cm^{-1} for GG are now shifted towards lower frequencies i.e, at 812 and 1030 cm^{-1}resp. Polymerization of alkyl acid units lead to an emergence of a prominent C-H stretch at 2983 cm^{-1}.

Grafting of polyacrylic acid onto chitosan is indicated by their modes of vibration. Characteristic O-H band of CS appear at 3445 cm^{-1}, C-H at 2877cm^{-1}, N-H at 1598 cm^{-1}, C-N at 1327 cm^{-1}, C-O stretch at 1094 cm^{-1}, bridge O stretch at 1154 cm^{-1}. In addition to the typical peaks of chitosan (CS), a new peak at 1718 cm^{-1} appears due to carboxyl absorption from grafted PAA along with the characteristic peaks of polyacrylic acid at 809 and 620cm^{-1}.Hence, FT-IR spectrum confirms successful grafting.

3a.1.3 FT-IR studies of PMMA-g-GA and PMMA-g-CL

The characteristic absorption peaks of gum arabic are summarized in **Table 6**. In addition to the characteristic peaks of gum arabic like O-H stretch, C-H stretch and bands at 1149, 1076 and 845cm^{-1} allocated to C-O-C stretching vibrations, additional peaks appear in grafted product i.e, PMMA-g-GA. These peaks are due to grafting of

PMMA. C-O stretch appears at 1687 cm^{-1} along with a peak at 1029 cm^{-1} ascribed to coupling of C-O stretch with O-H in plane bending vibrations.

Characteristic band of PMMA appears at 1731 cm^{-1} due to C=O stretching vibration of ester. O-H stretch of cellulose appears at 3391 cm^{-1}, C-H stretch at 2922 cm^{-1}, C-C stretch at 1432 $cm^{-1}$and C-O stretch at 1156 cm^{-1}. When grafting of PMMA and CL was done strong additional peaks appear at 1436 and 1156 cm^{-1} along with peak for C-O stretch at 1730 cm^{-1}. The results indicate the successful grafting of cellulose with PMMA.

3a.1.4 FT-IR studies of PEG-g-CS

Comparative data of the synthesized inhibitor indictes the grafting of chitosan on polyethylene glycol. Characteristic band for PEG appears at 1110 cm^{-1} because of C-O stretch. C-H stretch appears at 2900 cm^{-1} and is more intense in case of grafted product. Overlapping of O-H stretch and N-H stretch results in the emergence of a characteristic band at 3381 cm^{-1} in chitosan. The characteristic bands of at 1608 and 1442 $cm^{-1}$are attributed to C-O stretch of acetylated amino groups of chitosan. They correspond to Amide I and Amide I, respectively and show a unique behavior, by remaining unaffected even after grafting. In chitosan primary amine bend appears at 1590 cm^{-1} which is then shifted to 1536 cm^{-1}due to conversion of primary amine into secondary amine.

3a.1.5 FT-IR studies of PAM-co-PAA-GG

The FT-IR spectrum of polyacrylamide-co-polyacrylic acid grafted guar gum was recorded. O-H stretch of acrylic acid appears at 2935 cm^{-1}, C-O stretch of Amide I at 1717 cm^{-1} while N-H in plane bending occurs at 1165 cm^{-1}. C-N stretching vibration of Amide III band appears at 1246 and 1167 cm^{-1} whereas OCN deformation of Amide IV band appears at 513 cm^{-1}. The characteristic bands of polyacrylamide and guar gum are shown in **Table 6.** The intensity of the characteristic peaks in grafted product is enhanced.

3a.2 Thermogravimetric properties of synthesized corrosion inhibitors

Thermal properties of all the synthesized corrosion inhibitors were analyzed and results have shown an increase in overall stability of all the grafted samples compared with the monomers and the carbohydrate polymers used. All nine inhibitors show degradation in the range of 450˚C to 700˚C, an increase in final decomposition

temperature indicates that grafting and cross linking has occurred leading to more compact structures of the grafted samples. TGA data of all the synthesized corrosion inhibitors have been explained below. Comparative thermogravimetric curve of one of the representative corrosion inhibitor is shown in **Fig.3.2**

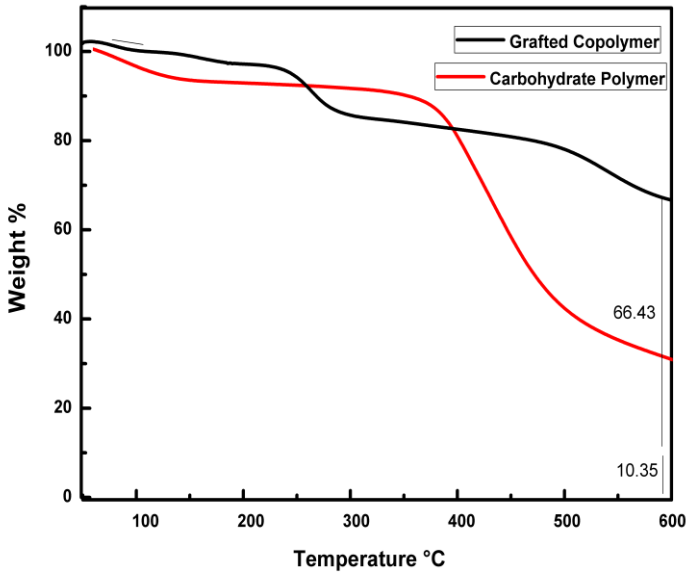

Fig.3.2 Comparative TGA curve of the representative corrosion inhibitor (PAM-g-GA)

3a.2.1 Thermogravimetric analysis of PAM-g-GA, PAM-g-GG and PAM-g-ST

Due to loss of moisture TGA of GA initially shows weight loss between 10˚C-120 ˚C and it completely degrades at 225˚C. In case of grafted sample PAM-g-GA, besides above zones of weight loss, a further zone between 480˚C to 550˚C was observed indicating that grafting has occurred and increase in temperature was due to the amide group.

TGA data of three step degradation of GG with initial weight loss between 30 ˚C and 120 ˚C was observed indicating loss of adsorbed water molecules. The second zone of weight loss of 230-335 ˚C was due to decomposition of polysaccharide backbone and finally decomposes in the range of 330-680 ˚C. Conversely grafted sample an extra weight loss zone at 560-700 ˚C due to loss of amide group was observed confirming grafting and indicating an increase in stability of grafted sample. Thermal stability of the grafted starch was much higher than pure polymer. Extra zones of decomposition were observed in case of PAM-g-ST at 375˚C and

690˚Crespectively. Starch on the other hand has three step decompositionat 31 ˚C, 200 ˚C and maximum weight loss occurred at 400 ˚C as a result of backbone degradation of the parent polymer.

3a.2.2 Thermogravimetric analysis of PAA-g-GG and PAA-g-CS

Thermal degradation of GG demonstrates the grafting effect as between 150˚C and 300 ˚C, compared to GG weight retention was lower in the grafted sample a steady and continuous decrease in weight retention since beginning of the experiment was observed. Beyond 300 ˚C, GG recorded drastic weight loss of nearly 55% at 320 ˚C leading to the complete degradation loss (0% retention) before 500 ˚C. Conversely, in the grafted product a steady weight loss up to 500 ˚C retaining 30% of its original weight.

At first about 10 % weight loss was observed for chitosan between 10˚C and 100 ˚C attributed to adsorbed species. Second weight loss begins at 209 ˚C up to 360 ˚C. Difference in degradation behavior of grafted sample was observed, three step decomposition begins after 180 ˚C up to 340 ˚C with less weight loss compared with chitosan, another weight loss between 340˚C to 420 ˚C before it finally decomposes around 500 ˚C indicating an increase in thermal stability.

3a.2.3 Thermogravimetric analysis of PMMA-g-GA and PMMA-g-CL

Gum arabic degrades at 225˚C while PMMA at 403 ˚C grafting has resulted in an appreciable increase in decomposition temperature of the grafted product (PMMA-g-GA). In grafted product degradation starts around 200 ˚C and second decomposition occurs at 403 ˚C while complete weight loss was observed at 483 ˚C.

The TGA curve of cellulose consist of single decomposition stage at 332 ˚C and for PMMA it is at 404 ˚C whereas during grafting of cellulose with methyl methacrylate a change in behavior was observed having two stage decomposition at 335˚C and 405˚C respectively. Thermal stability of the grafted product was enhanced.

3a.2.4 Thermogravimetric analysis of PEG-g-CS

At first about 10 % weight loss was observed for chitosan around 100 ˚C because of adsorbed water molecules. Another weight loss begins at 209 ˚C up to 360 ˚C. PEG itself was enough stable starts degrading beyond 200 ˚C and burn to ashes after 750 ˚C. Graft product shows an enhanced stability due to cross linking of polysaccharide.

3a.2.5 Thermogravimetric analysis of PAM-co-PAA-GG

Thermogravimetric analysis of PAM-co-PAA-GG was done at heating rate of 10˚C/min. Initial decomposition was observed at 164 ˚C, whereas final decomposition occurred at 560 ˚C on the contrary guar gum starts decomposing at 206.9 ˚C whereas completely degrades at 521 ˚C due to the formation of imide group decomposition of grafted sample occurs at lower temperature. Guar gum undergoes two stage degradation. Firstly, in the range of 207–331 ˚C with 46% weight loss and then 331-522˚C with 30% weight loss. In grafted copolymer decompositions were observed at 164-436 ˚C with 57% weight loss and 436.9-560.9 ˚C with 26% weight loss. Hence, through grafting and crosslinking stability was enhanced final decomposition temperatures of GG and grafted polymer were 520˚C and 558˚C respectively.

3a.3 Electrochemical measurements of the synthesized corrosion inhibitors

Electrochemical measurements were done by using conventional three electrode system comprising of aluminum AA2219-T6 as working electrode with an exposed area of 1cm^2. Platinum was used as counter electrode and saturated calomel electrode as reference. Gamry reference 3000 potentiostat/ galvanostat was used to carry out the experiments. Volume of test solution (artifical seawater) used was 100 mL. Before performing electrochemical tests the aluminium (AA2219-T6) coupons were immersed in test solution for 30 minutes. Open circuit potential (OCP) was then run for at least 10 mins for confirmation of steady state. EIS was performed in the frenquency range of 10^6 to 10^{-2} Hz.

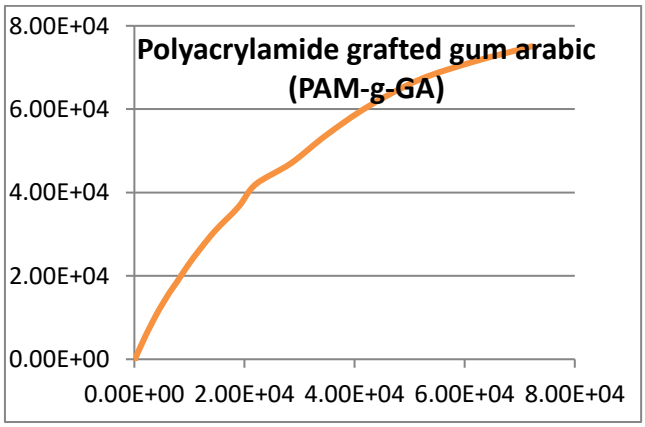

Fig.3.3a Nyquist plot of the representative corrosion inhibitor (PAM-g-GA)

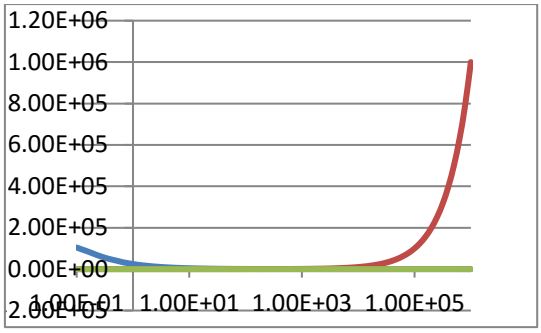

Fig.3.3b Bode plot of the representative corrosion inhibitor (PAM-g-GA)

Nyquist and bode plot of the representative corrosion inhibitor (polyacrylamide grafted gum arabic) are shown in **Fig.3.3a**. and **3.3b**. The resistance in charge transfer process is increased, on account of the formation of protective layer on the exposed surface of aluminum alloy used as working electrode. The inhibitor gets adsorbed on the surface of metal and inhibits the corrosion process. In nyquist plot, an increase in the diameter of the capacitative loop was observed on grafting. The tafel parameters were obtained using the same concentration of inhibitors, the tafel curves were fitted using Gamry software and results were mentioned in the **Table 7. Table 7** summarizes the values of tafel parameters which include I_{corr} and $-E_{corr}$ of the nine synthesized corrosion inhibitors. PAM-co-PAA-g-GG and PEG-g-CS have shown the best results in artificial seawater whereas PMMA-g-GA was comparatively less effective against corrosion.

Table 7 The Tafel parameters of the synthesized corrosion inhibitors

System	$-E_{corr}$ (mV/SCE)	I_{corr} (mA cm^{-2})
Sea water	427	0.68
PAM-g-GA	478	0.37
PAM-g-GG	489	0.39
PAM-g-ST	496	0.47
PAA-g-GG	501	0.27
PAA-g-CS	509	0.35
PMMA-g-GA	430	0.67
PMMA-g-CL	390	0.79
PEG-g-CS	623	0.25
PAM-co-PAA-g-GG	769	0.10

ECTION B

3b.1 FT-IR studies of the sulphonate doped conducting polymers

FT-IR spectra of sulphonate doped PANi and PPy was recorded and one of the characteristic peaks for PANi were observed at 1487 cm^{-1} and 1385 cm^{-1} attributing to C-N benzoid and quinoid rings, respectively. IR spectra of doped PANi and PPy has shown that their modes of vibrations were shifted slightly towards lower frequencies. This is because of doping of the polymer matrix with four afore discussed protonic acids. In all PANi doped polymers a prominent peak at 1024 $cm^{-1}$was oberved, due to $NH^{+}...SO_3^{-}$ interaction of PANi and sulphonate group of p-TSA, CSA, SFA and SSA. The absorption bands at 1300 cm^{-1} and 688 $cm^{-1}$are attributed to the symmetric and asymmetric vibration modes of sulphonic acid. The peak at 829 cm^{-1} was due to O-H out of plane bending. Hydrogen bonding between N-H and S=O peaks are consigned to 3280 cm^{-1}. Band at 3350 cm^{-1} was due to free N-H stretching vibration of aromatic amine. The peaks observed around 2900 cm^{-1} can be assigned to C-H stretch of the sulphonate dopant. Comparative FT-IR of one of the representative CP along with its doped counterpart is shown in **Fig.3.4.**

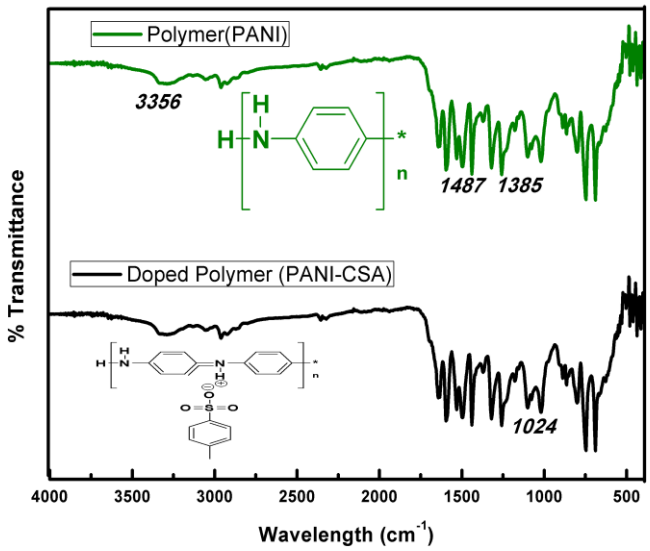

Fig.3.4 Comparative IR spectra of the representative sulphonate doped conducting polymer

In PANi-TSA the band observed at 1295 cm^{-1} was due to C-N stretch of sec aromatic amine, as doping was done with p-TSA π electrons are displaced. The major evidence of doping was the stretch observed at 1146 cm^{-1} attributed to $NH^{+}...SO_3^{-}$

linkage. In Ppy-TSA, sulfonic peak appeared at 1039 cm^{-1}. At 1709 cm^{-1} C=O stretch was found. C-N stretch at 1545 cm^{-1} in doped PPy instead of 1577 cm^{-1}, as observed in PPy.

In case of PANi-CSA stretch deformation of benzoid and quinoid appeared at 1576 and 1498 cm^{-1} respectively. C-N at 1302 cm^{-1}, C-H in plane bending at 1140 cm^{-1}, out of plane bending at 828 cm^{-1} and most important SO_3H linkage at 1040 cm^{-1} confirming PANi-CSA doping. In PPy-CSA the peak for C-H wagging was shifted from 793 and 928 cm^{-1} to 790 and 918 cm^{-1}, N-C stretch from 1200 cm^{-1} to 1185 cm^{-1}, in plane vibration from 1328 cm^{-1} to 1290 cm^{-1}, quinoid and bezoid peaks also showed slight shift towards lower frequencies and appeared at 1466 cm^{-1} and 1551 cm^{-1} and lastly, the peak at 1738 cm^{-1} for CSA.

In PANI-SFA characteristic PANi IR bands at 1575 and 1491 cm^{-1} ascribed benzoid and quinoid rings, C-N stretch of sec aromatic amine at 1303 cm^{-1}, aromatic out of plane stretch at 817 cm^{-1}were observed.C-H in plane bending occurred at 1011-1159cm^{-1} whereas the band in the range of 800-850 cm^{-1} determines the kind of substituted benzene. PPy-SFA the characteristic bands of pure PPy were shifted towards lower frequencies. The sulphonic peak appeared at 1038 cm^{-1} along with other characteristic peaks of PANi shifting slightly towards lower frequencies in PANi-SSA. PPy-SSA exhibits absorption bands at 1087 cm^{-1} due to S=O, at 1386 and 1636 cm^{-1} due to C=C stretch, broad band at 3444 cm^{-1} for O-H. The lowering of frequencies and appearance of band for $NH^{+}...SO_3^{-}$ linkage indicates that doping of pure PANi and PPy has occurred.

3b.2 Thermal analysis of the sulphonate doped conducting polymers

3b.2.1 Thermogravimetric analysis of the sulphonate doped conducting polymers

TGA analysis of doped PANi and PPy shows stepwise mass loss as shown in **Fig.3.5** The pure PANi, PPy have comparatively less thermal stability compared with their sulphonate doped counterparts. Their thermal stability ranges from 35 ˚C to 600 ˚C and sometimes beyond 600 ˚C. The primary mass loss, below 200 ˚C was assigned to gradual evaporation of moisture in both the doped polymers. The second loss was observed in the range of 350 ˚C which is attributed to the thermo-chemical breakdown of chemically active organic materials. In case of PANi/PPy-dopants breaking of $NH^{+}...SO_3^{-}$ linkage between PANi and sulphonate dopants. Third stage decomposition

was observed beyond around 600˚C and was due to the decomposition of the polymer backbone. The stability of polymers has increased upon doping with sulphonic acids.

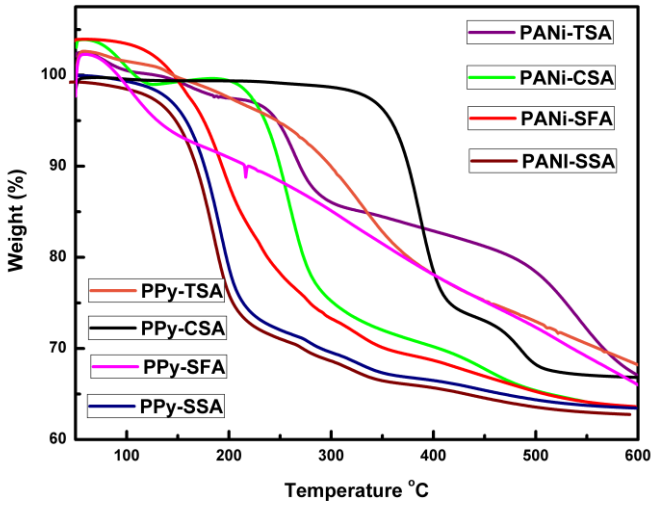

Fig.3.5 TGA curve of the sulphonate doped conducting polymers

3b.2.2 Differential scanning thermograms of the sulphonate doped conducting polymers

Thermal phase transition changes (i.e, the glass transition temperature T_g) of the eight synthesized doped conducting polymers were studied by recording their DSC thermograms. T_g were recorded and it was found in the range of 100-120 ˚C.

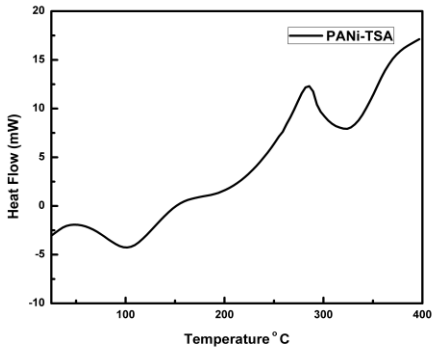

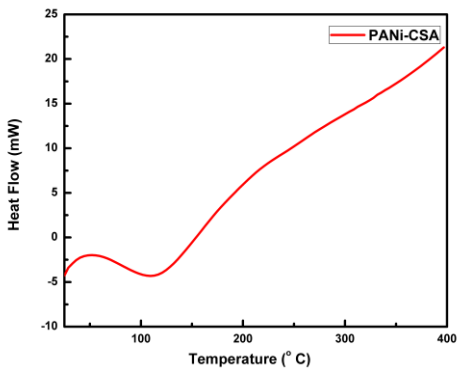

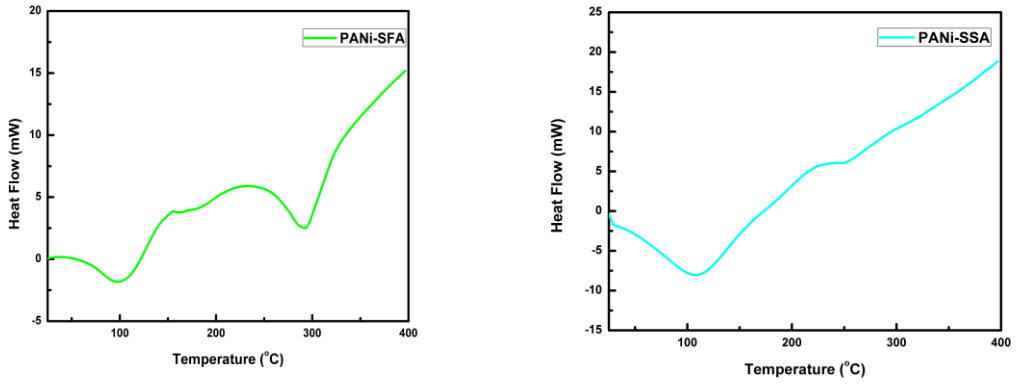

Fig.3.6a DSC thermograms of the sulphonate based conducting polymers (PANi)

Glass transition temperature (T_g) of the doped CPs were significantly higher than the undoped counterparts. DSC thermograms of all the eight synthesized doped conducting polymers were shown in **Fig.3.6a** and **3.6b.**

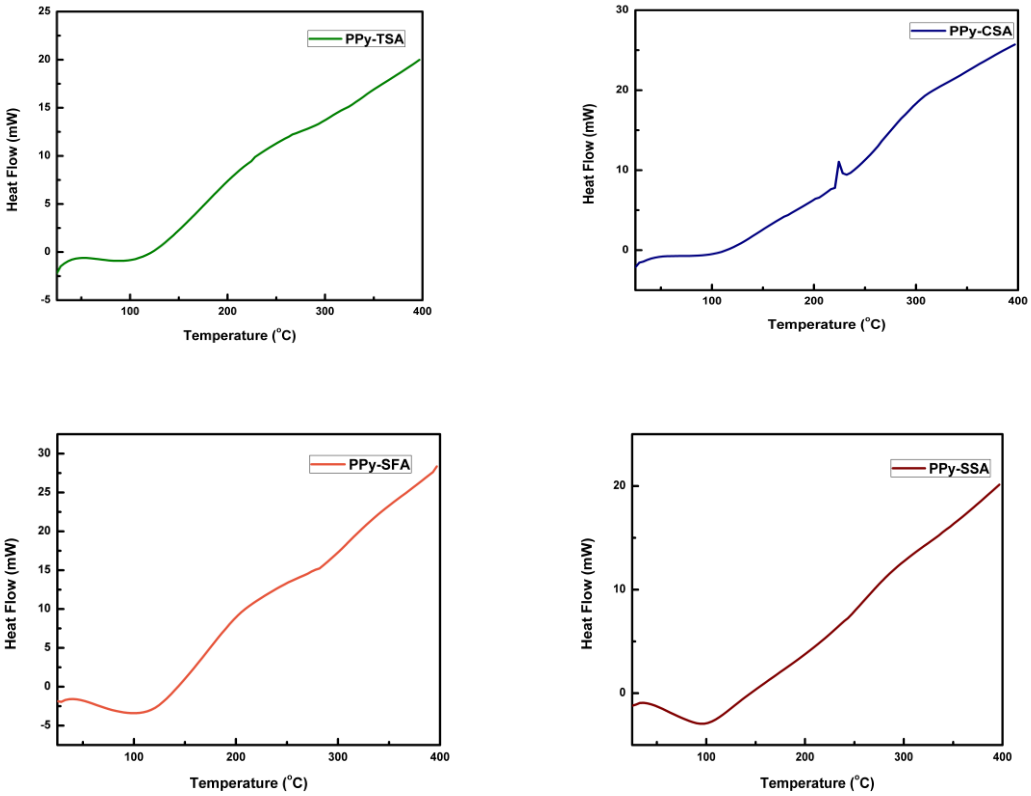

Fig.3.6b DSC thermograms of the sulphonate based conducting polymer (PPy)

3b.3 Scanning electron micrograph and elemental analysis data of the representative sulphonate doped conducting polymer coating

The surface morphology of PANi and PPy epoxy coatings were analysed using scanning electron micrograph. **Fig.3.7** shows the SEM image of one of the representative CP coating after electrochemical corrosion testing.

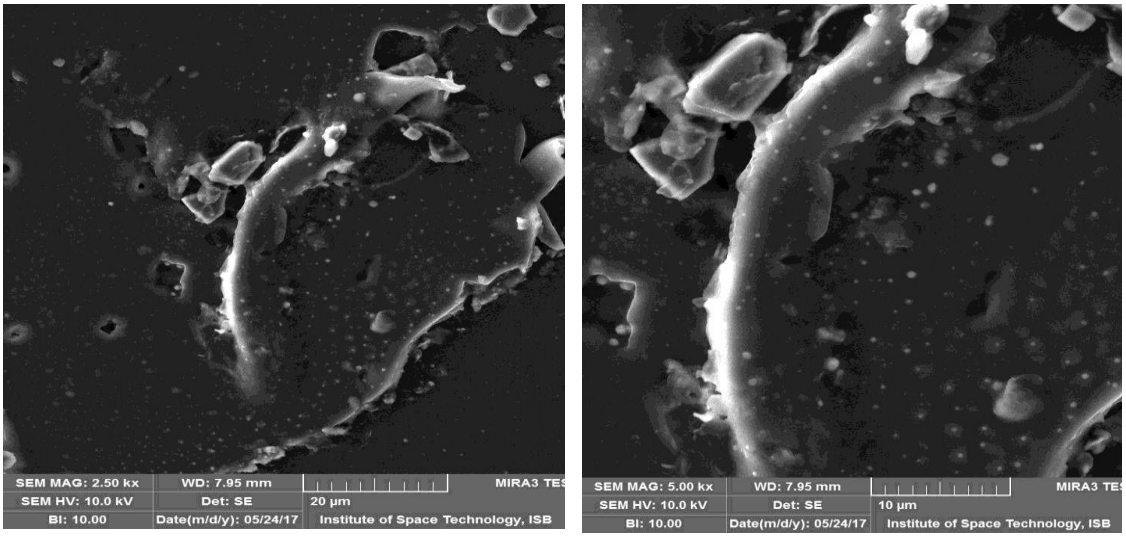

Fig.3.7 SEM image of the reprsentative sulphonate doped conducting polymer coating

The air gaps in epoxy coatings tends to disappear due to the addition of doping agents (sulphonate). Although particles are homogenously dispersed, agglomeration occurs when their concentration is increased.

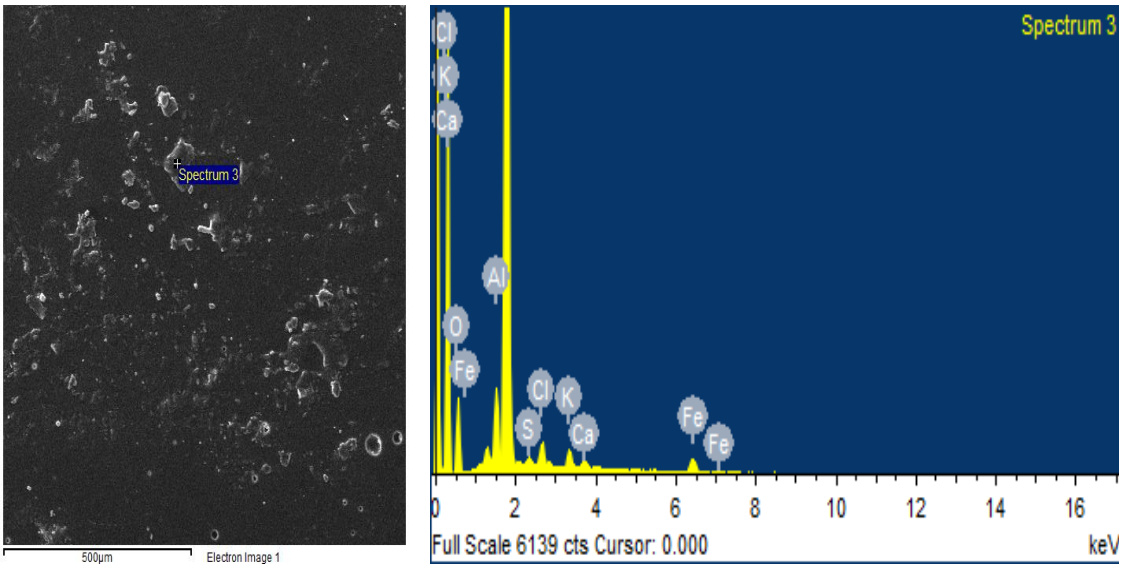

Fig.3.8 EDX spectrum of the representative sulphonate doped conducting polymer coating

SEM image also revealed the appearance of numerous small pits on the surface of coating due to the deposition of salts. EDX data is also in accordance with the SEM results, highest concentration of oxygen shows it's diffusion into the protective layer. Various salts get deposited on metal surface during electrochemical reactions, the EDX data of the representative coating was summarized in **Fig.3.8**.

Table 8 EDX data of the representative sulphonate doped conducting polymer coating

Element	Weight %	Atomic %
O	50.71	69.16
Al	19.80	16.01
S	1.59	1.08
Cl	6.78	4.17
K	5.49	3.06
Ca	2.55	1.39
Fe	13.08	5.11

3b.4 Electrochemical impedance and tafel measurements of the sulphonate doped conducting polymer coatings

Electrochemical measurements were performed using Gamry potentiostat/galvanostat in the frequency range of 10^6 to 10^{-2} Hz with an AC amplitude of 20 mV. The doped CP coated samples of SS-304 were used as working electrodes with exposed area of $1cm^2$ with SCE and graphite as reference and counter electrodes respectively. The nyquist plots of sulphonate doped PANi and PPy coatings were shown in **Fig.3.9** and EIS parameters obtained on fitting Reap2cpe (equivalent circuit model) using echem analyst were summarized in the appendix.

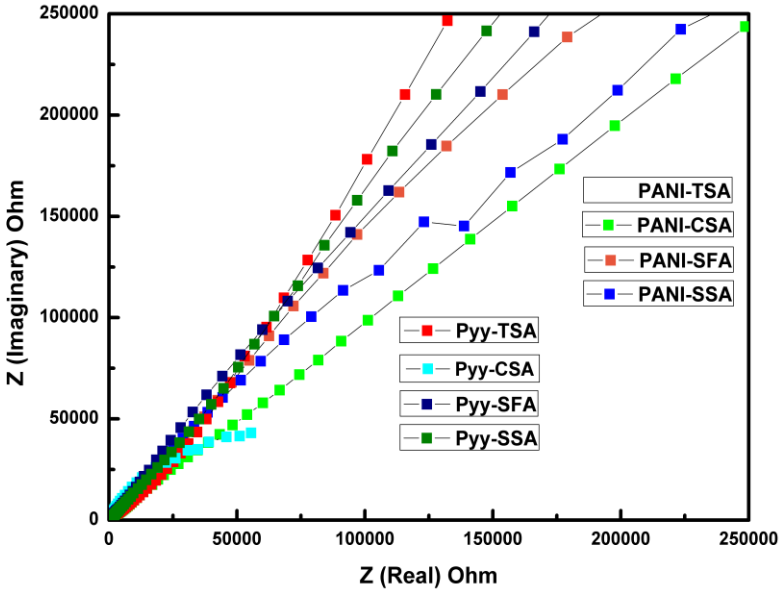

Fig.3.9 Nyquist plots of the sulphonate doped conducting polymer coatings

The tafel curves of the sulphonate doped PANi and PPy were shown in **Fig.3.10** while tafel parameters were summarized in **Table 9.** This table contains values of tafel parameters obtained after tafel fitting on curves. The values of corrosion rate were quite helpful in deciding which coating has given the best performance in corrosive media. PPy-SFA has shown the least value of corrosion rate depicting it`s superior behavior against corrosive media compared with the rest.

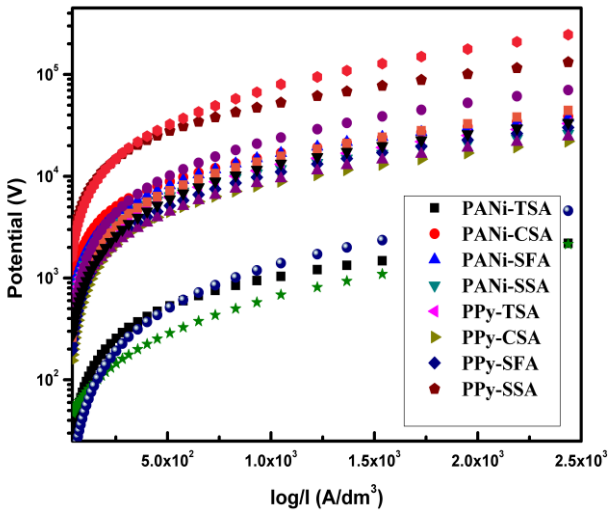

Fig.3.10 Tafel plots of the sulphonate doped conducting polymer coatings

Table 9 Tafel parameters of the sulphonate doped PANi and PPy coatings

System	Parameters		
	$-E_{corr}$ (mV)	**I_{corr} (µA)**	**Corrosion rate (mpy)**
PANi-TSA	51.70	2.240	2.877
PANi-CSA	148.0	0.0913	117.5e-3
PANi-SFA	79.60	0.167	215.1e-3
PANi-SSA	76.10	0.151	194.9e-3
PPy-TSA	104.0	0.00789	10.16e-3
PPy-CSA	83.10	1.170	1.509
PPy-SFA	117.0	0.175	225.3e-3
PPy-SSA	141.0	0.049	63.13e-3

SECTION C

3c.1 FT-IR studies of the modified clays

FT-IR studies of modified clays show the successful intercalation of adduct into the interlayer spaces of clays (Mt, Bt and Am). In IR spectra of clay montmorillonite and bentonite characteristic peaks were observed at 1028 cm^{-1} and 3445cm^{-1}attributed to Si-O-Si symmetric stretch of silicates and structural hydroxyls respectively. In case of their adduct moidified form OC-AMt and OC-ABt intense characteristic peaks at 2800 cm^{-1} and 2900cm^{-1} was observed due to CH_2 and CH_3 , respectively confirming the intercalation of alkyl group of CTAB in the interlayers of Mt and Bt. The changes in the spectra of clays after adduct modification confirms successful modification of clays with adduct. **Table 10** summarizes the IR data of adduct modified montmorillonite (OC-Amt) and **Fig.3.11** shows the IR spectra of the clay montmorillonite along with it's modified form. Similar behavior was observed for amberlite.

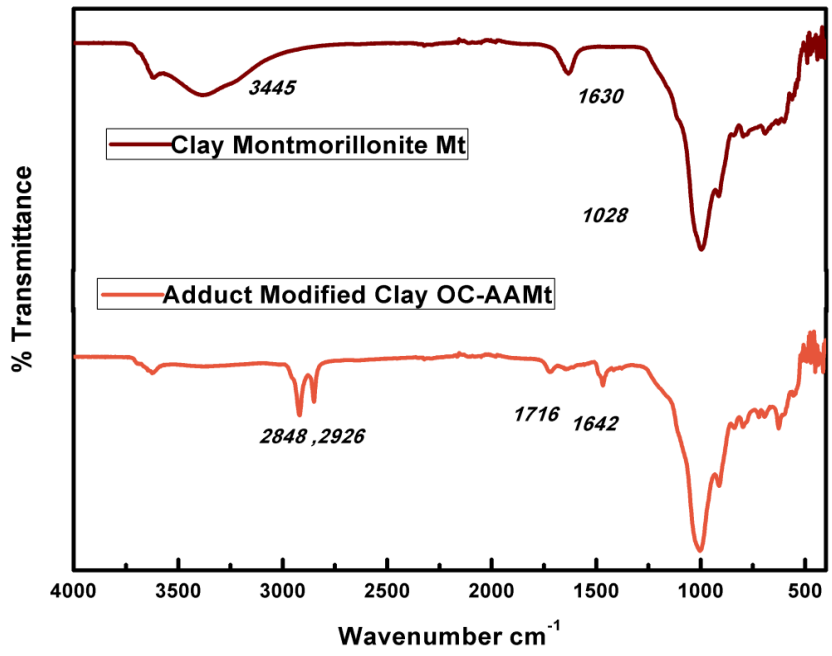

Fig.3.11 IR of the representative adduct modified clay

Table 10 IR data of the representative adduct modified clay

Functional Group	**Characteristic absorption (s) cm^{-1}**	
	Montmorillonite	Adduct modified montmorillonite
Si-O-Si silicates	1028	1028
O-H	**3445**	3445
CH_2 stretch	-	**2848**
CH_3 stretch	-	**2926**
C-C stretch	-	1642
CO stretch	-	1692

3c.2 XRD analysis of the adduct modified clay composites

The XRD results of adduct modified conducting polymer composites were shown in **Fig.3.12.** The analysis was done by comparing the XRD pattern of clay, it's adduct modified form and the polymer composite incorporating modified clays. The XRD of composites show that incorporation of modified clays have induced crystallinity in polymers due to intercalation.

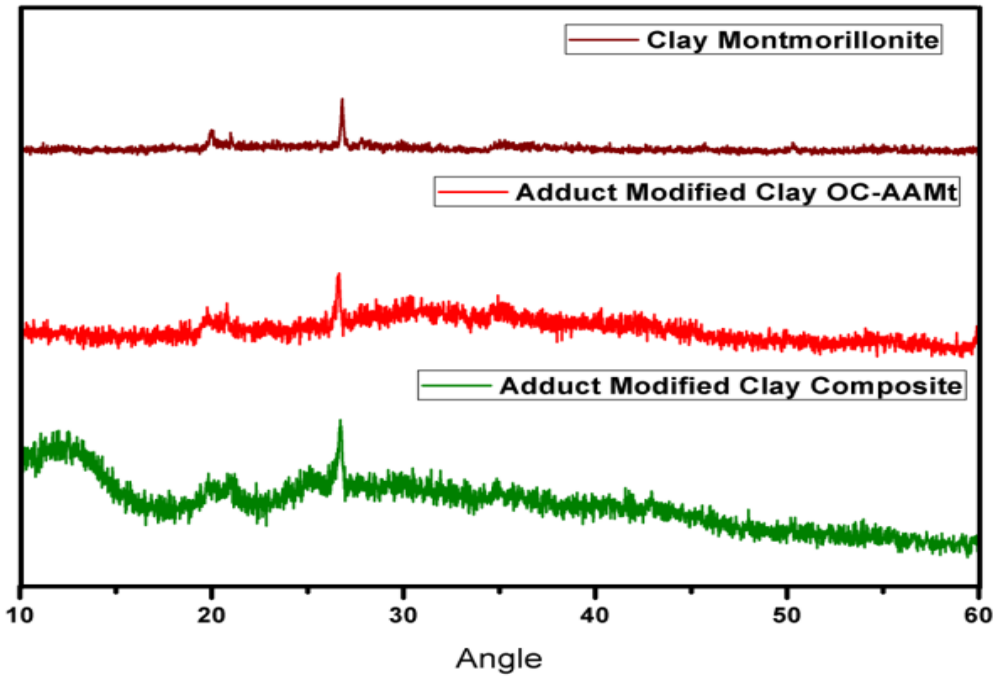

Fig.3.12 XRD plot of the representative adduct modified clay composite

Adduct modified PANi and PTH polymer composites were amorphous with small regions where crystallinity was induced due to incorporation of modified clays into the polymer matrices.

3c.3 Thermal analysis of adduct modified clay based composites

3c.3.1 Thermogravimetric analysis of the adduct modified clay based composites

The decomposition behavior of the six synthesized composites (Mt-PANi, Bt-PANi, Am-PANi, Mt-PTH, Bt-PTH and Am-PTH) was observed and their thermograms are shown in the **Fig.3.13** Decomposition has occurred in a step wise manner, in several stages ranging from 35˚C to 600 ˚C, which might corresponds to the degradation of intercalating agents followed by structural decomposition of PANi and PTH. Slightly higher decomposition temperatures of all the composites shows that intercalation of adduct modified moieties have increased the thermal stability of the synthesized composites.

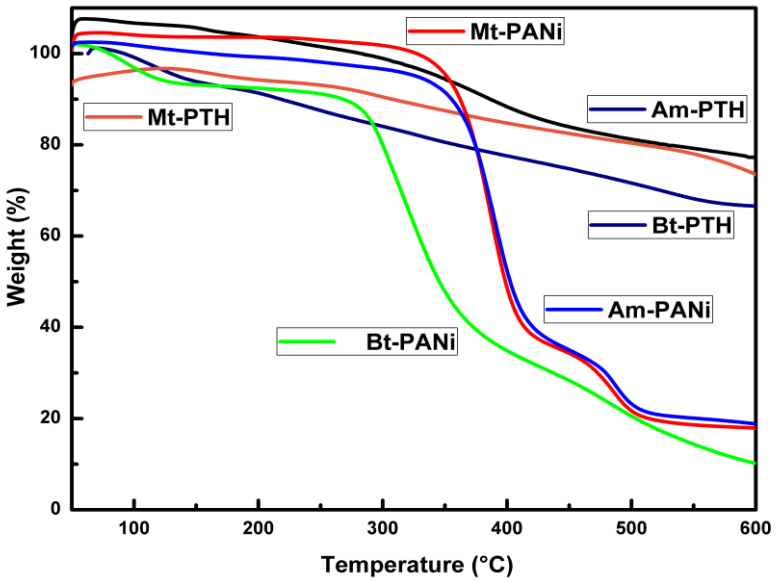

Fig.3.13 TGA curves of the adduct modified clay composites

3c.3.2 Differential scanning thermograms of the adduct modified clay composites

Thermal phase transition changes of adduct modified composites were studied by recording DSC at heating rate of 10 ˚C under nitrogen atmosphere. The T_g of all the synthesized composites were higher than their pristine polymers. Hence, it was concluded that the segmental motion of PANi and PTH matrices was retarded by the intercalating clays which results in increase in T_g of composites.

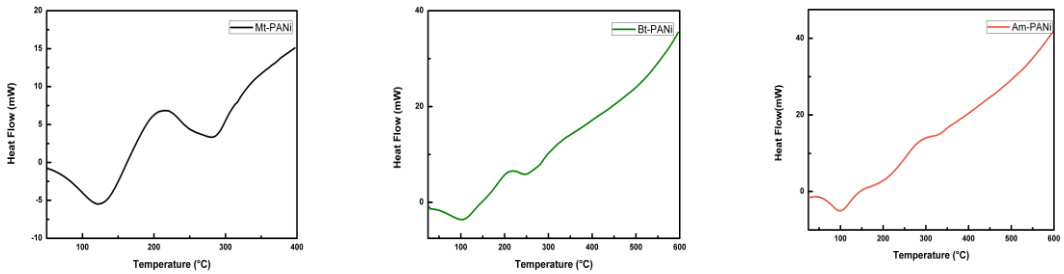

Fig.3.14a DSC thermograms of PANi based adduct modified clay composites

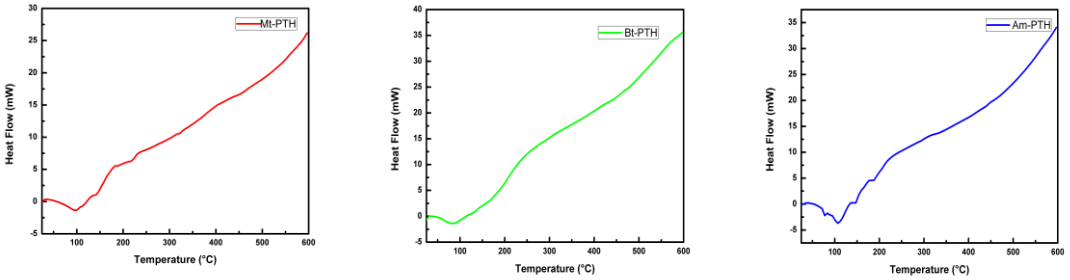

Fig.3.14b DSC thermograms of PTH based adduct modified clay composites

3c.4 Scanning electron micrograph and elemental analysis data of the adduct modified composite coatings

The particles size distribution and surface morphology and corrosion effects were explored through SEM-EDX. Representative SEM images of modified clay based composite coatings along with EDX data are shown in **Fig.3.15** and **3.16** respectively.

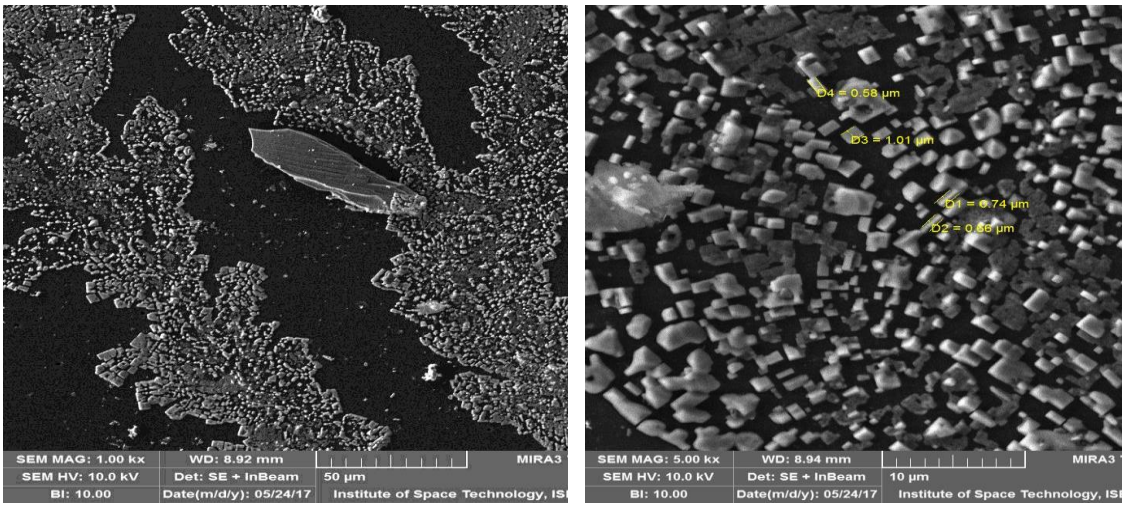

Fig.3.15 SEM image of the representative adduct modified clay composite

Corrosion signature was observed on SEM image of the composite coating. The EDX data is in complete agreement with the results of SEM indicated by the presence of chlorine and sodium.

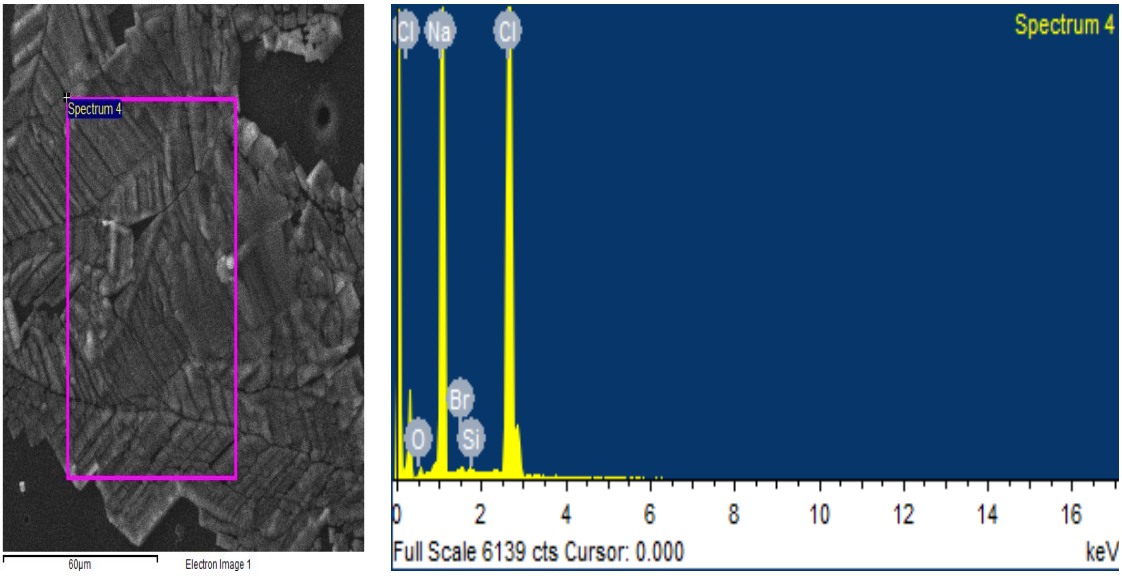

Fig.3.16 EDX of the representative adduct modified clay composite

The elemental composition of the representative adduct modified clay composite coating was presented in **Table 12.** The high concentration of sodium and chlorine suggests severe corrosion.

Table 11 EDX data of the representative adduct modified clay composite

Element	Weight %	Atomic %
O	4.83	8.44
Na	39.62	48.15
Si	0.23	0.22
Cl	54.42	42.88
Br	0.90	0.32

3c.5 Electrochemical impedance and tafel measurements of the synthesized clay composites

Electrochemical set up having conventional three electrode cell was used. The working electrode (SS-304) used, had an exposed area of $1cm^2$. The Nyquist plot of the six synthesized composites is shown in **Fig.3.17.** The property of enhanced corrosion protection was observed due to effective dispersion of the fillers in the polymer matrix.

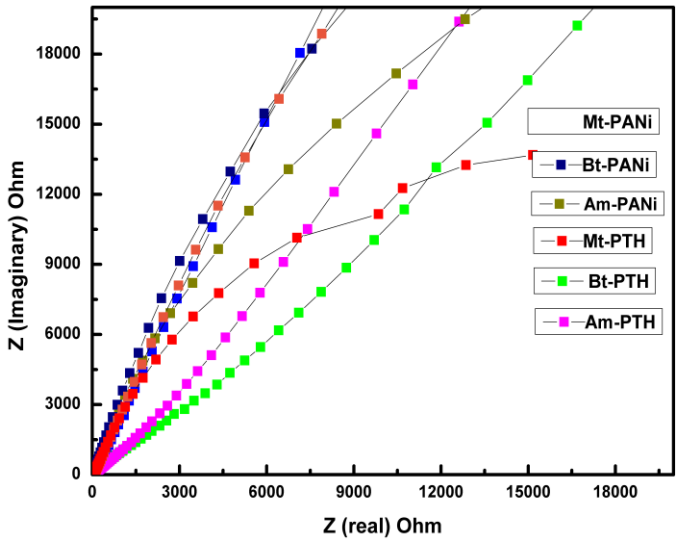

Fig.3.17 Nyquist plots of the adduct modified clay composites

The anticorrosion behavior of adduct modified clay composite coatings were also explored making use of tafel parameters that were fitted with echem analyst software. Tafel curves were shown in **Fig.3.18** along with tafel prameters such as - $E_{corr,}$ I_{corr} and corrosion rate in **Table 12** that suggest the better performance of Am-PTH weighed against the rest of the composites.

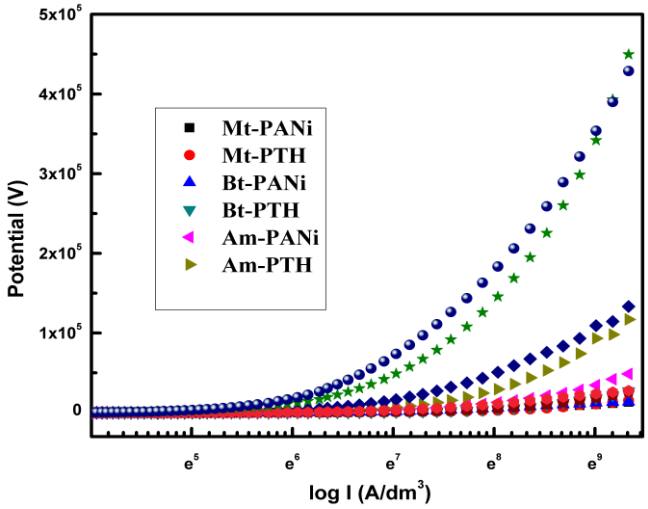

Fig.3.18 Tafel plots of the adduct modified clay composites

Table 12 Tafel parameters of the adduct modified clay composite coatings

System	Parameters		
	$-E_{corr}$ (mV)	**I_{corr} (µA)**	**Corrosion rate (mpy)**
Mt-PANi	137.0	5.030	6.471
Bt-PANi	119.0	3.720	4.787
Am-PANi	96.50	3.480	4.478
Mt-PTH	88.40	1.680	2.158
Bt-PTH	121.0	0.982	1.265
Am-PTH	54.30	0.236	303.4e-3

SECTION D

3d.1 FT-IR studies of self-healing poly-thiourea formaldehyde microcapsules

The FT-IR spectra of core material, HMDI, MDI, fresh and processed microcapsules is shown in Fig. The processed microcapsules were obtained by storing them in DETA solution and aqueous solution of pH=1 for 5 days. The spectrum of hexamethylene diisocyanate containing core material indicates the thriving encapsulationt. The phenyl group stretches at 1642 cm^{-1} and 1543 cm^{-1} were still in attendance but obscure because very small amount was encapsulated. In the FT-IR band of fresh PTF microcapsules, the characteristic peak at 2271 cm^{-1} indicates the successful incorporation. The NCO signal starts to disappear when the PTF microcapsules were treated with DETA solution. Again in case of PTF microcapsules that were immersed in highly acidic solution the NCO signal vanishes. The existence of NCO in PTF microcapsules is due dense outer layer (shell) of microcapsules and disappearance indicates the reactivity of NCO group.

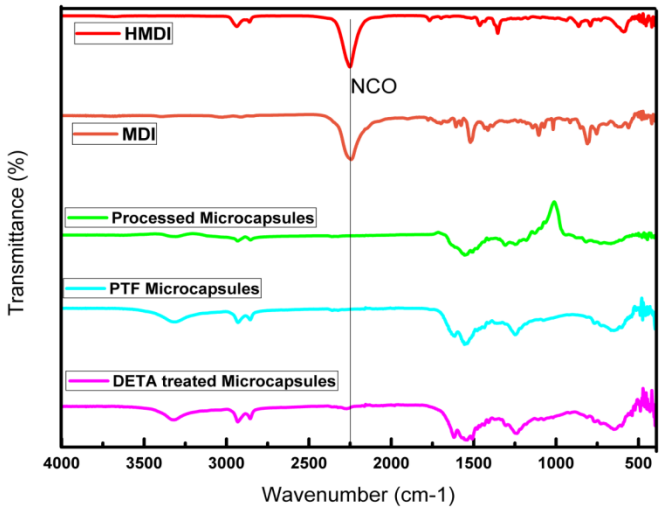

Fig.3.19 The IR spectra of the core material, fresh and processed PTF microcapsules

3d.2 Thermal analysis of self-healing polythiourea formaldehyde microcapsules

3d.2.1 Thermogravimetric analysis of self-healing polythiourea formaldehyde microcapsules

Thermal properties of PTF microcapsules at various stages were explored using thermogravimetric analysis. The weight loss curves of core material, shell material, fresh PTF microcapsules and processed PTF microcapsules as a function of temperature were recorded. Representative curves are shown in **Fig.3.20** PTF microcapsules started to lose mass before 100 °C, due to moisture and has experienced first major weight loss at 176 ˚C owing to isothermal route at 211°C followed by constant weight plateau. Second major weight loss occurs and it is completely decomposed around 600 ˚C with only small amount of residue left 41 wt%. Pure HMDI loses weight at 169 ˚C and after that starts evaporating only because of small shell thickness and larger surface area. Fresh PTF microcapsules are more thermally stable compared with their processed counterparts as indicated by high char yield. The curves of treated microcapsules were recorded after completely drying them at RT.

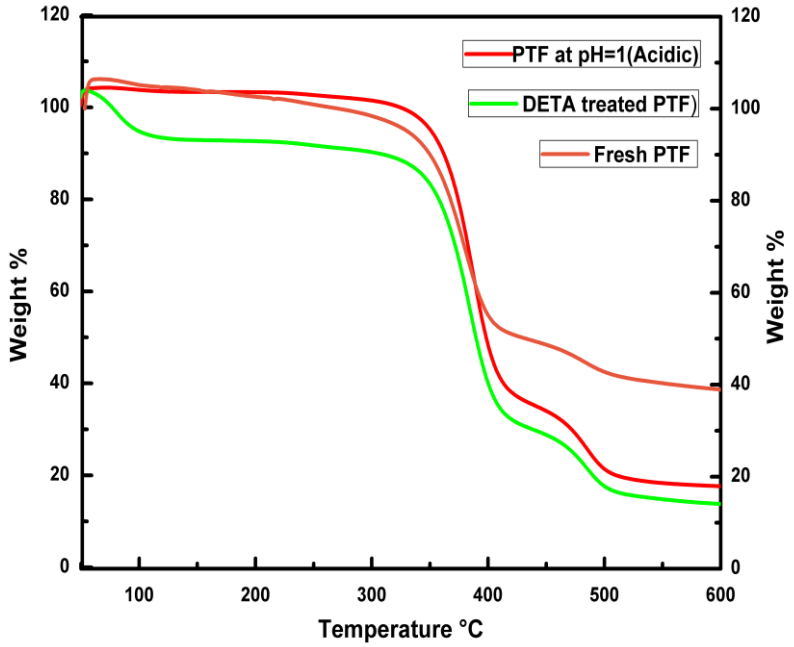

Fig.3.20 TGA curves of the fresh and processed PTF microcapsules

3d.2.2 Differential scanning thermogram of self-healing polythiourea formaldehyde microcapsules

This thermo-analytical technique was also used to check the effect of temperature on the properties of PTF microcapsules. Thermal transition of PTF microcapsules began at 31 ˚C and T_g was recorded at 106 ˚C. Melting temperature was 232 ˚C and degrades before 400 ˚C.

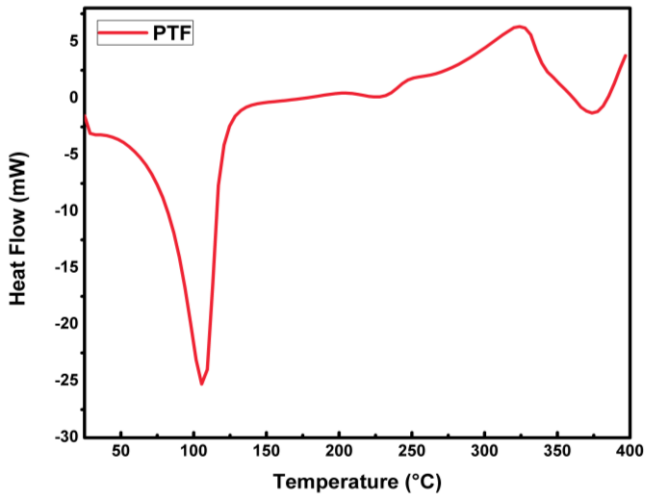

Fig.3.21 DSC thermogram of fresh PTF microcapsules

3d.3 Scanning electron micrograph of self-healing poly-thiourea formaldehyde microcapsules on SS-304 and AA2219-T6

The morphology of PTF microcapsules was observed using SEM and is shown in **Fig.3.22** Results show that these microcapsules have course outer layer, shape nearly irregular and related particle size distribution. Particle size greatly depends on the rate of agitation. SEM images were taken after electrochemical studies the deposition of salt and rupturing of microcapsules was observed. When the PTF microcapsule was cracked the core material oozes out of it to heal the coating. **Fig.3.22** and **Fig.3.23** shows the PTF microcapsules after corrosion testing on SS-304 and AA2219-T6 substrate with particle size at varied magnification.

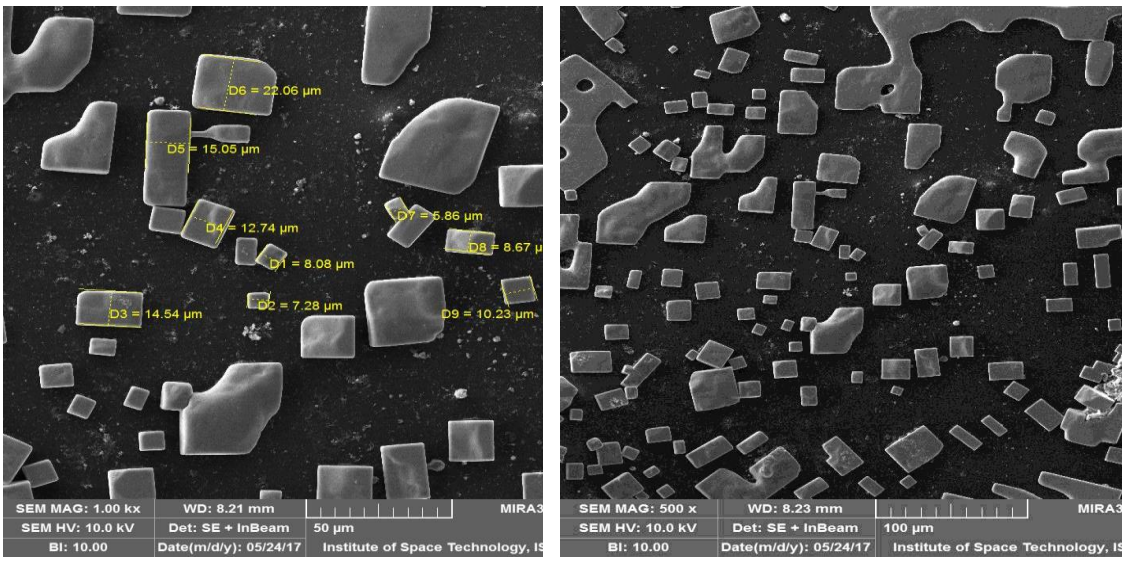

Fig.3.22 The SEM image of self healing PTF coating on AA2219-T6

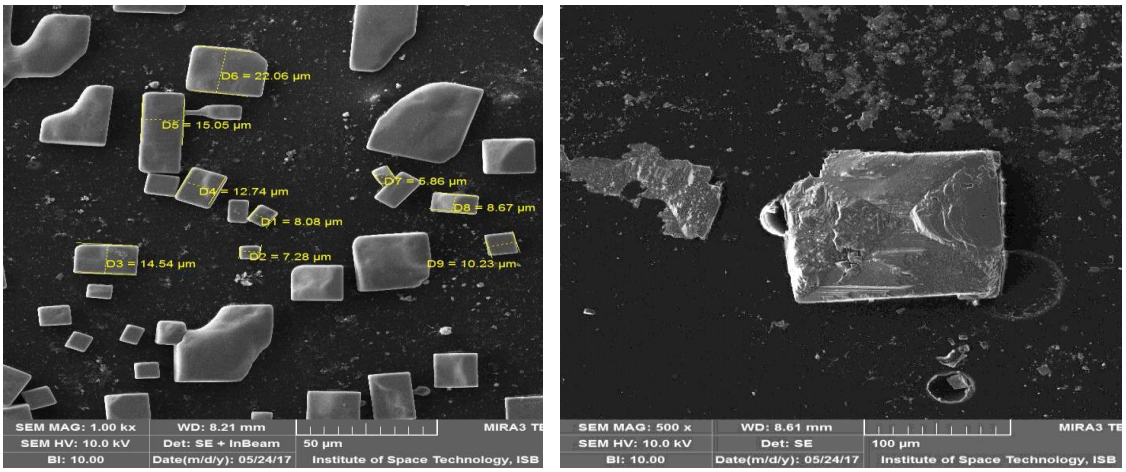

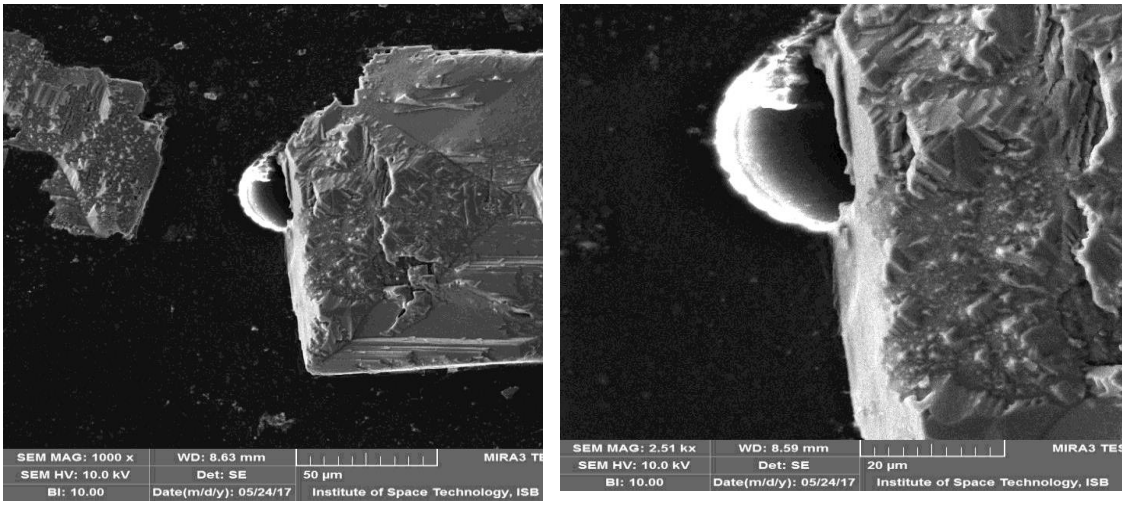

Fig.3.23 The SEM image of self healing PTF coating on SS-304

3d.4 Electrochemical impedance and tafel measurements of self-healing polythiourea formaldehyde microcapsules coatings on SS-304 and AA2219-T6

Self-healing PTF coatings were monitored by EIS and tafel measurements by means of Gamry Reference 3000 potentiostat/galvanostat in freshly prepared artificial sea water. The PTF coatings on SS-304 and AA2219-T6 were separately run for electrochemical analysis. The anticorrosion process of self-healing was characterized with EIS in the frequency range of 10^{6} to 10^{-1} with an AC amplitude of 20mV. The parameters obtained after fitting the EIS data on equivalent circuit (reap2cpe) through gamry software.

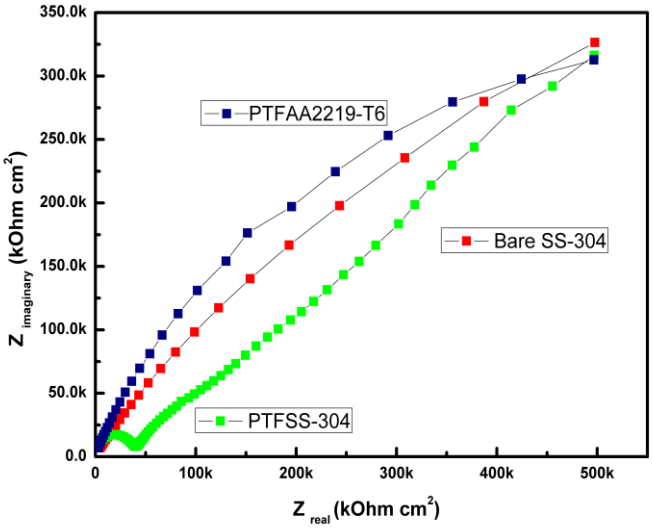

Fig.3.24 The Nyquist plots for bare SS-304, PTF coated SS-304 and AA2219-T6

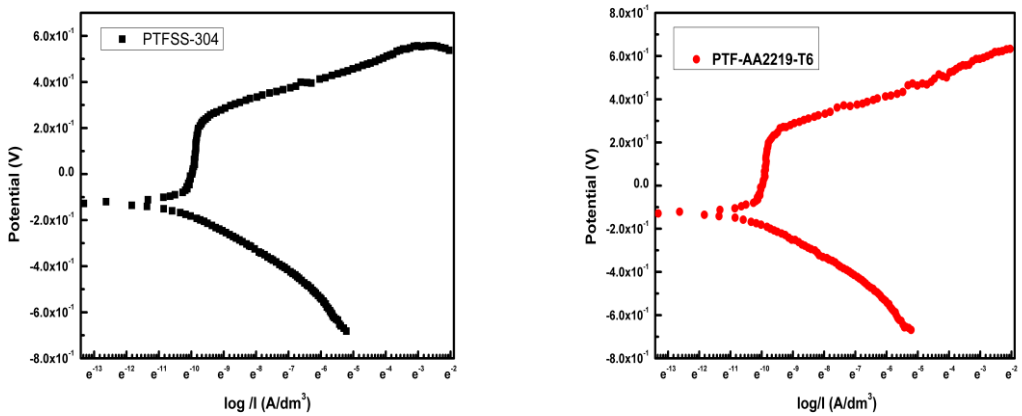

Fig.3.25 Tafel plot of poly-thiourea formaldehyde coating on SS-304 and AA2219

E_{corr} ,$I_{corr,}$ along with corrosion rate of bare, PTF coated SS-304 and AA-2219-T6 were obtained after tafel curve fitting.

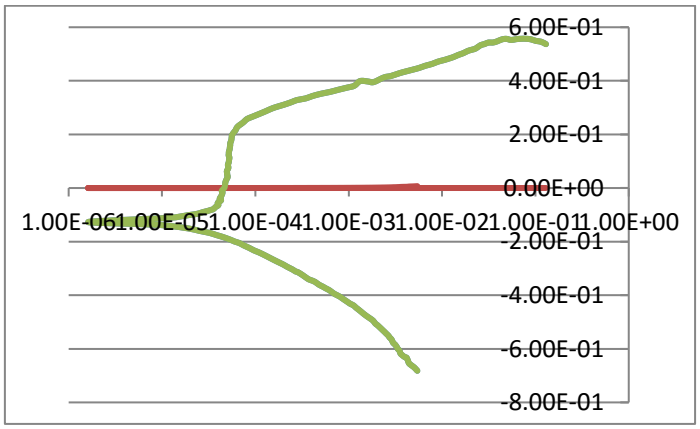

Fig.3.26 Tafel fitting of poly-thiourea formaldehyde coating on SS-304

Table 13 Tafel parameters of bare SS-304, PTF coated SS-304 and AA2219-T6

System	-E_{corr} (mV)	Corrosion Rate (mpy)
Bare SS-304	125.0	95.69
PTF-SS304	58.50	36.35e-3
PTF-AA2219-T6	504.0	2.420e-12

Tafel curves for PTF coating on both the substrates SS-304 and AA2219-T6 were presented in **Fig.3.25** with **Fig.3.26** showing tafel fitting, the results obtained

after tafel fitting were summed up in **Table 13.** The obtained data illustrates that PTF coating on AA2219-T6 shows superior resistance against corrosion.

The supplemenatary data including XRD of adduct modified clay based coatings, electrochemical impedance data of the synthesized material i.e, corrosion inhibitors and coatings along with their curve fitting was presented in appendix.

CONCLUSIONS

All nine graft polysaccarides were successfully synthesized via microwave assisted irradiation in company with three different types of anticorrosion coating; sulphonate based conducting polymer coatings, adduct modified clay based composite coatings and smart functional self healing coatings. The synthesized material was characterized analytically as well as electrochemically. Using FT-IR spectroscopic studies for functional group identification, XRD analysis done for phase identification. Thermal stability of the afore synthesized material was explored using thermogravimetric and differential scanning techniques. Surface morphology and particle size distribution was characterized using SEM and elemental composition was observed by EDX studies. Electrochemical studies include electrochemical impedance spectroscopy and tafel measurements.

Among corrosion inhibitors on AA2219-T6, PAM-co-PAA-g-GG and PEG-g-CS have shown the better resistance against corrosion in artificial seawater. Corrosion rate calculated from tafel curve fitting indicates that PPy-SFA, Am-PTH and PTF on SS-304 have exhibited better corrosion resistance in freshly prepared artificial sea water.

PPy-SFA < Am-PTH < PTF on SS-304

REFERENCES

1. Wroblowa, H. S. & Qaderi, S. B. Mechanism and kinetics of oxygen reduction on steel. *J. Electroanal. Chem. Interfacial Electrochem.* **279,** 231–242 (1990).

2. Almeida, M. E. M. Minimisation of steel atmospheric corrosion: Updated structure of intervention. *Prog. Org. coatings* **54,** 81–90 (2005).

3. Kingston, H. M. & Jassie, L. B. *Introduction to microwave sample preparation: theory and practice*. (American Chemical Society, 1988).

4. Jones, D. A. Corrosion in selected corrosive environments. *Princ. Prev. Corros. 2nd ed.(Upper Saddle River, NJ Prentice Hall, 1996)* 387–390 (1992).

5. Liu, L., Li, Y., Fang, Y. & Chen, L. Microwave-assisted graft copolymerization of ε-caprolactone onto chitosan via the phthaloyl protection method. *Carbohydr. Polym.* **60,** 351–356 (2005).

6. Deshpande, P. P., Jadhav, N. G., Gelling, V. J. & Sazou, D. Conducting polymers for corrosion protection: A review. *J. Coatings Technol. Res.* **11,** 473–494 (2014).

7. Robinson, J. *et al.* Electromagnetic simulations of microwave heating experiments using reaction vessels made out of silicon carbide. *Phys. Chem. Chem. Phys.* **12,** 10793–10800 (2010).

8. Singh, V., Kumar, P. & Sanghi, R. Use of microwave irradiation in the grafting modification of the polysaccharides–A review. *Prog. Polym. Sci.* **37,** 340–364 (2012).

9. Singh, V., Kumari, P. L., Tiwari, A. & Sharma, A. K. Alumina supported synthesis of Cassia marginata gum- g- poly (acrylonitrile) under microwave irradiation. *Polym. Adv. Technol.* **18,** 379–385 (2007).

10. Roy, P., Karfa, P., Adhikari, U. & Sukul, D. Corrosion inhibition of mild steel in acidic medium by polyacrylamide grafted Guar gum with various grafting percentage: Effect of intramolecular synergism. *Corros. Sci.* **88,** 246–253 (2014).

11. Roy, P. *et al.* Graft copolymerization onto starch–I. Synthesis and optimization of starch grafted with N-tert-butylacrylamide copolymer and its hydrogels. *Carbohydr. Polym.* **44,** 103–112 (2003).

12. Gref, R., Rodrigues, J. & Couvreur, P. Polysaccharides grafted with polyesters: novel amphiphilic copolymers for biomedical applications. *Macromolecules* **35,** 9861–9867 (2002).

13. Deshpande, P. P., Jadhav, N. G., Gelling, V. J. & Sazou, D. Conducting polymers for corrosion protection: a review. *J. Coatings Technol. Res.* **11,** 473–494 (2014).

14. Galema, S. A. Microwave chemistry. *Chem. Soc. Rev.* **26,** 233–238 (1997).

15. Tizzotti, M., Charlot, A., Fleury, E., Stenzel, M. & Bernard, J. Modification of polysaccharides through controlled/living radical polymerization grafting—towards the generation of high performance hybrids. *Macromol. Rapid Commun.* **31,** 1751–1772 (2010).

16. Obermayer, D., Gutmann, B. & Kappe, C. O. Microwave chemistry in silicon carbide reaction vials: separating thermal from nonthermal effects. *Angew. Chemie* **121,** 8471–8474 (2009).

17. Singh, V., Tiwari, A., Tripathi, D. N. & Sanghi, R. Microwave assisted synthesis of guar-g-polyacrylamide. *Carbohydr. Polym.* **58,** 1–6 (2004).

18. Umoren, S. A. & Eduok, U. M. Application of carbohydrate polymers as corrosion inhibitors for metal substrates in different media: A review. *Carbohydr. Polym.* **140,** 314–341 (2016).

19. Singh, V., Sharma, A. K. & Maurya, S. Efficient cadmium (II) removal from aqueous solution using microwave synthesized guar gum-graft-poly (ethylacrylate). *Ind. Eng. Chem. Res.* **48,** 4688–4696 (2009).

20. Nayak, B. R. & Singh, R. P. Synthesis and characterization of grafted hydroxypropyl guar gum by ceric ion induced initiation. *Eur. Polym. J.* **37,** 1655–1666 (2001).

21. Ohya, Y., Maruhashi, S., Hirano, T. & Ouchi, T. Preparation of poly (lactic acid)-grafted polysaccharides as biodegradable amphiphilic materials. in *Biomedical Polymers and Polymer Therapeutics* 139–148 (Springer, 2002).

22. Loupy, A. Solvent-free microwave organic synthesis as an efficient procedure for green chemistry. *Comptes Rendus Chim.* **7,** 103–112 (2004).

23. Zhang, L.-M., Tan, Y.-B., Huang, S.-J., Chen, D.-Q. & Li, Z.-M. Water-Soluble Ampholytic Grafted Polysaccharides. 1. Grafting of the Zwitterionic Monomer 2-(2-Methacrylo-Ethyldimethylammonio) Ethanoate onto Hydroxyethyl Cellulose. (2000).

24. Dror, Y., Cohen, Y. & Yerushalmi- Rozen, R. Structure of gum arabic in aqueous solution. *J. Polym. Sci. Part B Polym. Phys.* **44,** 3265–3271 (2006).

25. Fares, M. M., El-faqeeh, A. S. & Osman, M. E. Graft copolymerization onto starch–I. Synthesis and optimization of starch grafted with N-tert-butylacrylamide copolymer and its hydrogels. *J. Polym. Res.* **10,** 119–125 (2003).

26. Gupta, G., Birbilis, N., Cook, A. B. & Khanna, A. S. Polyaniline-lignosulfonate/epoxy coating for corrosion protection of AA2024-T3. *Corros. Sci.* **67,** 256–267 (2013).

27. Raju, A. *et al.* Adduct modified nano-clay mineral dispersed polystyrene nanocomposites as advanced corrosion resistance coatings for aluminum alloys. *Appl. Clay Sci.* **126,** 81–88 (2016).

28. Silva, A. C. M., Moghadam, A. D., Singh, P. & Rohatgi, P. K. Self-healing composite coatings based on in situ micro–nanoencapsulation process for corrosion protection. *J. Coatings Technol. Res.* 1–29 (2017).

29. Thakur, V. K. & Kessler, M. R. Self-healing polymer nanocomposite materials: A review. *Polymer (Guildf).* **69,** 369–383 (2015).

30. Sun, D., Zhang, H., Tang, X.-Z. & Yang, J. Water resistant reactive microcapsules for self-healing coatings in harsh environments. *Polymer (Guildf).* **91,** 33–40 (2016).

Table Electrochemical Impedance parameters of the synthesized corrosion inhibitors.

System	Parameters		
	Uncompensated solution resistance (R_U)	**Double layer capacitence (C_f)**	**Polarization resistance (R_p)**
PAM-g-GA	9.354e3	44.41e-12	12.14e3
PAM-g-GG	9.635e3	47.05e-12	10.99e3
PAM-g-ST	29.99e3	70.49e-12	28.94e3
PAA-g-GG	538.1	13.41e-12	55.88e3
PAA-g-CS	666.9	13.51e-12	56.39e3
PMMA-g-GA	1.141e3	18.43e-12	5.419e3
PMMA-g-CL	1.145e3	18.38e-12	5.497e3
PEG-g-CS	1.099e3	18.19e-12	5.399e3
PAM-co-PAA-g-GG	6.510e3	29.00e-6	3.386e3

Table Electrochemical impedance parameters of the sulphonate doped PANi and PPy coatings

System	Parameters				
	Solution resistance R_{soln} (Ω)	**Corrosion resistance R_{cor} (Ω)**	**Pore resistance R_{po} (Ω)**	**Corrosion capacitence C_{cor} ($S•s^n$)**	**Coating capacitence C_c ($S•s^m$)**
PANi-TSA	140.4e-15	9.782e3	4.814e3	1.055e-6	104.6e-9
PANi-CSA	574.6	1.570e6	2.794e3	2.146e-6	91.91e-9
PANi-SFA	456.7	8.318e6	12.64e3	1.056e-6	820.1e-9
PANi-SSA	1.019e3	2.543e6	4.270e3	2.081e-6	360.5e-9
PPy-TSA	1.806e3	16.98e6	35.17e3	91.40e-9	88.90e-9
PPy-CSA	45.65	151.0e3	96.83	8.876e-6	1.341e-6
PPy-SFA	976.9	14.23e6	5.189e3	863.7e-9	68.90e-9
PPy-SSA	100.0	10.00e3	5.000e3	1.000e-6	100.0e-9

Table Electrochemical impedance parameters of the adduct modified clay composite coatings

System	Parameters				
	Solution resistance R_{soln} (Ω)	**Corrosion resistance R_{cor} (Ω)**	**Pore resistance R_{po} (Ω)**	**Corrosion capacitence C_{cor} ($S•s^n$)**	**Coating capacitence C_c ($S•s^m$)**
Mt-PANi		9.782e3	4.814e3	1.055e-6	104.6e-9
Bt-PANi	574.6	1.570e6	2.794e3	2.146e-6	91.91e-9
Am-PANi	456.7	8.318e6	12.64e3	1.056e-6	820.1e-9
Mt-PTH	1.019e3	2.543e6	4.270e3	2.081e-6	360.5e-9
Bt-PTH	1.806e3	16.98e6	35.17e3	91.40e-9	88.90e-9
Am-PTH	45.65	151.0e3	96.83	8.876e-6	1.341e-6

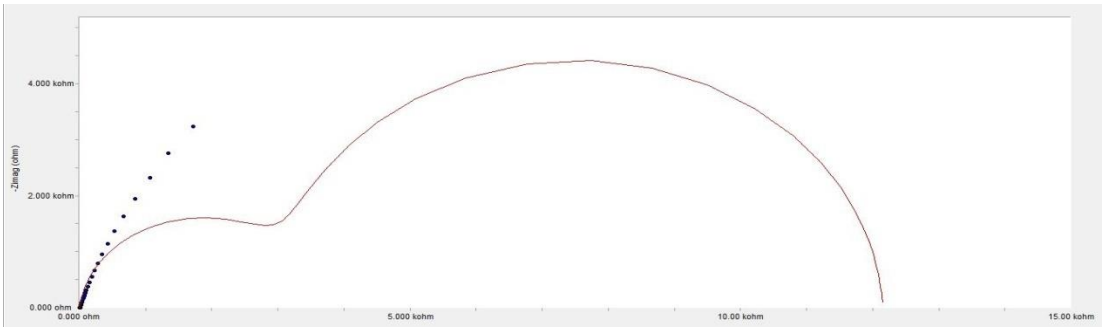

Figure. Reap2cpe fitting on nyquist plot of bare metal (SS-304)

Parameter	Value	± Error	Units
Rsoln	904.5e-18	7.185e3	ohms
Rcor	9.859e3	2.790e3	ohms
Rpo	4.883e3	4.430e3	ohms
Ccor	1.025e-6	237.7e-9	S*s^a
n	903.8e-3	20.82e-3	
Cc	106.0e-9	474.3e-9	S*s^a
m	905.5e-3	123.9e-3	
Goodness of Fit	4.280e3		
eis bare .dta			

Fig. EIS data of bare SS-304

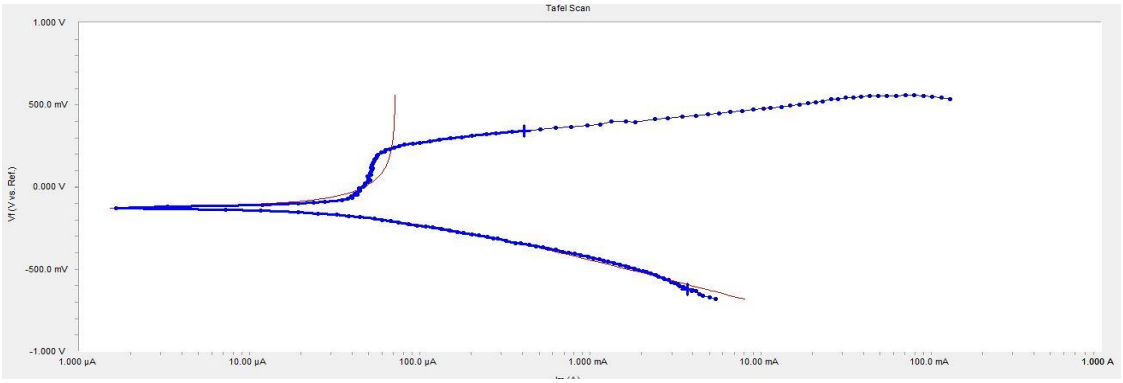

Fig. Tafel fitting on tafel curve of bare SS-304

Parameter	Value
Beta A	4.247e3 V/decade
Beta C	280.5e-3 V/decade
Icorr	74.30 µA
Ecorr	-125.0 mV
Corrosion Rate	95.69 mpy
Chi Squared	45.24
Data File	bare.dta
Fit Status	BetaA is large. This result suggests passivation control.

Fig. Tafel data after fitting on bare SS-304

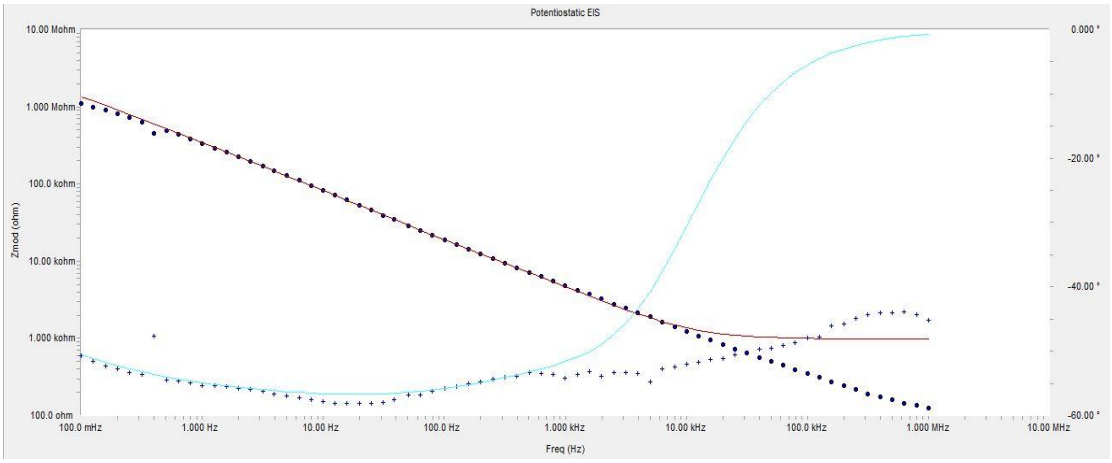

Fig. Bode plot showing Reap2cpe fitting on sulphonate doped conducting polymer coating

Parameter	Value	± Error	Units
Rsoln	976.9	11.41e3	ohms
Rcor	14.23e6	79.35e6	ohms
Rpo	5.189e3	36.50e3	ohms
Ccor	863.7e-9	1.854e-6	S*s^a
n	594.7e-3	644.1e-3	
Cc	68.90e-9	2.168e-6	S*s^a
m	892.2e-3	3.635	
Goodness of Fit	165.2e-6		
eis pp-3 .dta			

Fig. EIS data of Reap2cpe fitting on sulphonate doped conducting polymer coating

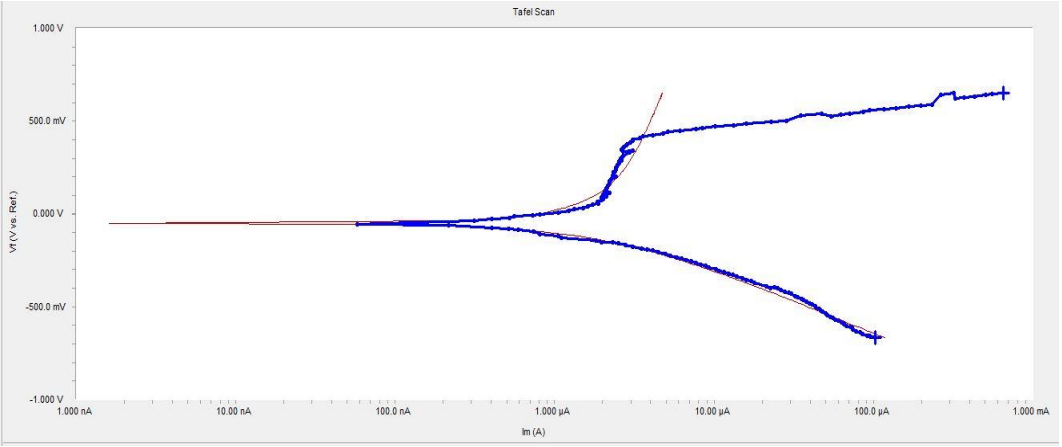

Fig. Tafel fitting on the representative sulphonate doped conducting polymer coating

Parameter	Value
Beta A	2.129 V/decade
Beta C	357.3e-3 V/decade
Icorr	2.240 µA
Ecorr	-51.70 mV
Corrosion Rate	2.877 mpy
Chi Squared	26.68
Data File	pa1.dta
Fit Status	The difference between Eoc and Ecorr is large. Your sample may have changed.

Fig. Tafel fitting data of the representative sulphonate doped conducting polymer coating

Parameter	Value	± Error	Units
Rsoln	1.889	0.000	ohms
Rcor	10.00e-3	0.000	ohms
Rpo	524.4e12	0.000	ohms
Ccor	1.592e27	0.000	S*s^a
n	998.1e-3	0.000	
Cc	2.253e-3	0.000	S*s^a
m	514.6e-3	0.000	
Goodness of Fit	566.5e-3		
eis ptfaa 09-06-2017.dta			

Fig. Reap2cpe fitting data of PTF-AA2219-T6 coating

Parameter	Value	± Error	Units
Rsoln	418.4e-3	584.5	ohms
Rcor	384.7	1.000e38	ohms
Rpo	136.2e12	1.687e22	ohms
Ccor	7.060e27	1.000e38	S*s^a
n	385.7e-3	1.000e38	
Cc	2.105e-6	287.4e-9	S*s^a
m	261.6e-3	12.36e-3	
Goodness of Fit	124.2e-3		
eis ptfss 09-06-2017.dta			

Fig. Reap2cpe fitting data of PTF-SS-304 coating

Parameter	Value
Beta A	305.8e-3 V/decade
Beta C	254.9e-3 V/decade
Icorr	28.20 nA
Ecorr	-58.50 mV
Corrosion Rate	36.35e-3 mpy
Chi Squared	15.52
Data File	tafel ptfss.dta
Fit Status	The difference between Eoc and Ecorr is large. Your sample may have changed.

Fig. Tafel fitting data of PTF coating